Characterisation of Nuclear Envelope-Associated Proteins (NEAP) in *Arabidopsis thaliana*

G. M. L. D. DETOURNE

PhD 2019

OXFORD BROOKES UNIVERSITY
UNIVERSITE CLERMONT AUVERGNE

2019

Ecole Doctorale
Sciences de la Vie, Santé, Agronomie, Environnement

Thèse

Présentée à l'Université Blaise Pascal pour l'obtention du grade de
A thesis submitted in partial fulfilment of the requirements of Oxford Brookes University for the degree of

DOCTOR OF PHILOSOPHY
DOCTEUR D'UNIVERSITE
Spécialité : Physiologie et Génétique Moléculaires

Characterisation of Nuclear Envelope-Associated Proteins (NEAPs) in *Arabidopsis thaliana*

Gwénaëlle DETOURNE

Soutenue le 29 Mai 2019

President of the Jury:
Dr Paul Fransz
Jury members:
Dr Verena Kriechbaumer
Dr Monica Pradillo
Director of Studies:
Professor David Evans
Professor Christophe Tatout

Génétique, Reproduction et Développement (GReD) – UMR CNRS 6293, INSERM U1103
Université Clermont Auvergne
28, Place Henri Dunant
63001 Clermont-Ferrand

Oxford Brookes University
Department of Biological and Medical Sciences
Headington Campus
OX3 0BP
Oxford UK

ABSTRACT

During evolution, eukaryotic cells have acquired a nuclear envelope (NE) enclosing and protecting the genome, which is organized in chromatin, a structure wrapping DNA around histone proteins. The NE is composed of two membranes: on the nucleoplasmic side, the Inner Nuclear Membrane (INM) and on the cytoplasmic side, the Outer Nuclear Membrane. The NE allows communication between both compartments through Nuclear Pore Complexes and bridges the cytoskeleton to the nucleoskeleton through the LInker of Nucleoskeleton to Cytoskeleton complex. Thus, the nucleoskeleton associated with the INM is needed to transmit signals to the nucleus and induce changes in chromatin organisation and ultimately gene expression.

A novel family of NUCLEAR ENVELOPE ASSOCIATED PROTEINS (NEAPs) proposed to be new components of the plant nucleoskeleton has been recently evidenced in the model plant *Arabidopsis thaliana*. AtNEAP proteins are encoded by a small gene family composed of three genes and are targeted through a nuclear localisation signal to the nucleus where they are anchored at the INM through their C-terminal transmembrane domain. AtNEAPs also possess several long coiled-coil domains reminiscent of the lamin structure in animals. This thesis aimed at performing a functional analysis of AtNEAPs using T-DNA insertion and CRISPR/Cas9 mutant lines. The AtNEAP interactome was investigated by molecular approaches (Yeast Two Hybrid), which indicated AtNEAP interactions with each other to form homo or hetero-dimers; as well as *in vivo* localisation and co-localisation coupled to image analyses (apFRET, acceptor photobleaching Fluorescence Resonance Energy Transfer), which confirmed interactions with the transcription factor (TF) AtbZIP18. AtNEAP specific antibodies generated during this study were used to confirm expression *in vivo*. Altogether, results indicated that AtNEAPs are part of the nucleoskeleton, with a role in anchoring TFs at the INM to maintain nuclear morphology and chromatin organisation.

Key words: Nuclear periphery, NEAP, nucleoskeleton, chromatin organisation, CRISPR/Cas9, bZIP18.

RESUME

Au cours de l'évolution, les cellules eucaryotes ont acquis une enveloppe nucléaire (NE) renfermant et protégeant le génome organisé en chromatine, une structure où l'ADN s'enroule autour de protéines histones. La NE est composé de deux membranes: du côté nucléoplasmique, la membrane nucléaire interne (INM) et du côté cytoplasmique, la membrane nucléaire externe. La NE permet la communication entre les deux compartiments par le biais des complexes de pores nucléaires et relie le cytosquelette au nucléosquelette via le complexe LINC (LInker of Nucleoskeleton to Cytoskeleton). Ainsi, le nucléosquelette associé à l'INM est nécessaire pour transmettre des signaux au noyau et induire des changements dans l'organisation de la chromatine et finalement dans l'expression des gènes.

Une nouvelle famille de protéines associées à l'enveloppe nucléaire (NEAP), proposées comme nouveaux composants du nucléosquelette de la plante, a récemment été mise en évidence dans la plante modèle *Arabidopsis thaliana*. Ces protéines sont codées par une famille de trois gènes et sont ciblées vers le noyau via un NLS où elles sont ancrées à l'INM via leur domaine transmembranaire C-terminal. Les protéines AtNEAPs possèdent également plusieurs longs domaines en spirale (coiled-coil) rappelant la structure des lamines chez les animaux. Cette thèse visait à réaliser une analyse fonctionnelle des AtNEAPs à l'aide de lignées mutantes T-DNA et CRISPR/Cas9. L'interactome AtNEAP a été étudié par des approches moléculaires (Yeast Two Hybrid), indiquant des interactions entre AtNEAPs pouvant former des homo- ou hétéro-dimères; ainsi que la localisation et la co-localisation *in vivo* couplées à de l'imagerie (apFRET), qui ont confirmé les interactions avec le facteur de transcription (TF) AtbZIP18. Les anticorps spécifiques à AtNEAP générés au cours de cette étude ont été utilisés pour confirmer l'expression *in vivo*. En outre, les résultats ont indiqué que les AtNEAPs font partie du nucléosquelette et jouent un rôle dans l'ancrage des TF à l'INM afin de maintenir la morphologie nucléaire et l'organisation de la chromatine.

Mots-clés : Périphérie nucléaire, NEAP, nucléosquelette, organisation de la chromatine, CRISPR/Cas9, bZIP18.

ACKNOWLEDGMENTS

First of all, I would like to thank Professor David Evans and Professor Christophe Tatout for having designed this PhD project in 2015 and I would like to thank the Postgraduate Research tutors who gave me the opportunity to work on this project, Dr Susan Brooks and regretted Professor Chris Hawes. I would like to thank all the members of the jury, Dr Verena Kriechbaumer, Dr Paul Fransz and Dr Monica Pradillo for having accepted to be reporters and for paying attention to the whole work achieved during this PhD.

A special thank you to all my supervisors, David, Christophe, Dr Emmanuel Vanrobays and Dr Katja Graumann, without forgetting Dr Aline Probst for everything you have done for me during this PhD. Thank you Christophe and Manu for having raised in me a huge interest in genetics and molecular biology and for the knowledge transmission through your teaching when I was a young student. Many thanks, David and Katja, for all the scientific approach but also for your warmful welcome in Oxford and for your strong personal support when I needed it the most…

Thank's to all the colleagues I worked with through all those years ; in Clermont-Ferrand, Sylvie, Sylviane, Sam, Sophie, Maxime, Lauriane, Cyril, Olivier, Simon, Aurélia and all the plant GReDins without forgetting JC, Claude, Ayhan, Cyril and Mounir for sport support, Fabrice, Rachel, Isa, Joëlle who first let me step into GReD life ; but also in Oxford, Chris, Joe, Francès, Verena, Vidya, Vanessa, John, Jirke, Sue and all the plant scientists, without forgetting Margaret, Dan and Iris. Your patience with me, kindness, support and fruitful exchanges were very helpful.

All this scientific work would not have been possible without the technical help and support of l'équipe administrative du GReD, Marie-Jo, Maryse, Nadia, Marie-Diane and the Research Degrees Team, Catherine Joyejob and Jill Organ, and his previous Administrator, Philip Voysey. So many thanks to all of them.

Un grand merci à ma famille et mes amis pour leur soutien tout au long de la thèse. Mes parents, premièrement, pour leur soutien sans faille quoiqu'il advint et leur aide dans mes nombreux déménagements entre autres (que de voyages !). Mon frère, Florian, ma grand-mère Marie-Louise qui me demandait régulièrement comment allaient mes petites plantes, mes grands-parents Denise et Jean-Claude et tous mes oncles, tantes et cousin(e)s ; ainsi que mes amis, Hélène, Carine, David, Thibaut, Aude, Léo, Marine, Géraldine et TimTim sans oublier Martin. Un merci tout particulier à Fred pour m'avoir soutenue dans les moments les plus difficiles et m'avoir ainsi permis d'aller jusqu'au bout…

A mon Papa, et mes Grands-Pères

CONTENT

ABBREVIATIONS

aa: amino acids

Ade: Adenine

apFRET: acceptor photobleaching Fluorescence Resonance Energy Transfer

APS: Ammonium Persulfate

At: *Arabidopsis thaliana*

BAF: Barrier to Autointegration Factor

BRLZ: Basic DB region leucine zipper

BSA: Bovine Serum Albumine

bZIP: basic-leucine zipper

CC: Coiled-coil

CFP: Cyan Fluorescent Protein

CHD: Chromodomain-Helicase-DNA-binding protein

ChIP: Chromatine Immuno-Precipitation

CRWN: Crowded Nuclei

C-ter: C-terminus

DBD: DNA-binding domain

DMSO: Dimethyl sulfoxide

dNTPs: desoxyribonucleotides tri-phosphates

DSB: DNA Double Strand Break

EAR: Ethylen-responsive element binding factor-associated Amphiphilic Repression

EDMD: Emery-Dreifuss Muscular Dystrophy

EF: FRET efficiency

EP: Electroporation

ER: Endoplasmic Reticulum

FAST: Fast Arabidopsis-seedlings mediated Transformation

FG: phenylalanine-glycine

F*IS*H: Fluorescence *In Situ* Hybridization

FRAP: Fluorescence Recovery After Photobleaching

GAR: Glycine-ARginine

GDP: Guanosine TriPhosphate

GFP: Green Fluorescent Protein

GTP: Guanosine DiPhosphate

HDAC: Histone DeACetylase

HGPS: Hutchinson-Gilford Progeria Syndrome

His: Histidine

HS: Heat Shock

IB: Infiltration Buffer

IF: Intermediate Filament

IP: Immunoprecipitation

INM: Inner Nuclear Membrane

Ino80: Inositol-requiring 80

ISWI: Imitation Switch

KASH: Klarsicht, ANC-1, Syne Homology

KD: Knock-Down

KO: Knock-Out

LADs: Lamin Associated Domains

LB: Luria Broth

LBR: Lamin B Receptor

LEM: LAP2, Emerin, MAN1

Leu: Leucine

LINC: LInker of Nucleoskeleton to Cytoskeleton

LINC: Little Nuclei

MARs: Matrix Attachment Regions

MS: Murashige and Skoog

MYTH: Membrane Yeast Two Hybrid

NADs: Nucleolus Associated Domains

NEAP: Nuclear Envelope-Associated Protein

NE: Nuclear Envelope

NEBD: NE BreakDown

NES: Nuclear Export Signal

NHEJ: Non-Homologous End Joining

NLS: Nuclear Localisation Signal

NMCP: Nuclear Matrix Constituent Protein

NPC: Nuclear Pore Complex

N-ter: N-terminus

NTF2: Nuclear Transport Factor 2

Nups: Nucleoporins

OD: Optical Density

ONM: Outer Nuclear Membrane

PBST: Phosphate Buffer Saline - Tween

PEG: Polyethylene Glycol

PI: Pre-Immune

PIC: Protease Inhibitor Cocktail

PTM: Post-Translational Modification

q-RT-PCR: quantitative Reverse Transcription - Polymerase Chain Reaction

RanGAP: RanGTPase Activating Protein

RanGEF: Ran Guanine nucleotide Exchange Factor

ROI: Region Of Interest

Rpm: rotations per minute

RT: Room Temperature

AtSAP18: SIN3 ASSOCIATED POLYPEPTIDE P18

SD: Synthetically Defined

SDS – PAGE: Sodium Dodecyl Sulfate Polyacrylamide Gel Electrophoresis

SINE: SUN-Interacting Nuclear Envelope

SIOX: Simple Interactive Object Extraction

SOC: Super Optimal broth with Catabolite repression

SUN: Sad1p/UNC-84

SW12/SNF2: SWItch/Sucrose NonFermentable

TCA: Trichloro-acetic acid

TE/LiAc: Tris EDTA/LithiumAcetate

TEMED: N,N,N,N-Tétraméthyléthylènediamine

TIK: Toll-Interleukin-Resistance KASH

TM: TransMembrane

TPL: TOPLESS

Trp: Tryptophan

TSI: Transcriptionally Silent Information

Y2H: Yeast Two Hybrid

YEB: Yeast Extract Broth

YNB: Yeast Nitrogen Base

YFP: Yellow Fluorescent Protein

YPD: Yeast extract Peptone Dextrose/D-glucose

WIP: WPP domain-Interacting Protein

WIT: WPP domain-Interacting Tail-anchored protein

WPP: tryptophan-proline-proline

LIST of FIGURES

LIST of TABLES

CHAPTER 1
INTRODUCTION

INTRODUCTION

One of the main differences between prokaryotes and eukaryotes is the presence of a nucleus, which allows the packaging of DNA into a specialized compartment and isolates it from the cytoplasm. Separation is made by two phospholipid bilayers forming an Inner Nuclear Membrane (INM) and an Outer Nuclear Membrane (ONM), which are the continuity of the endoplasmic reticulum (ER), an essential compartment for protein maturation.

The nucleus is mobile and its migration occurs principally through nucleo- and cytoskeleton interactions, thanks to properties of the Nuclear Envelope (NE), (Tamura and Hara-Nishimura, 2013; Zhou and Meier, 2014). During cell division, the NE is necessarily disrupted by a mechanism called NE Break Down (NEBD), a process in which NE and nucleoskeleton components are implicated (Murphy *et al*., 2010; Smoyer and Jaspersen, 2014). The nucleus structure plays fundamental roles for the cell, such as in stress responses, cell development or even reproduction and has to be dynamic in order to adopt various shapes and to regulate gene expression (Ungricht and Kutay, 2017; Yang *et al*., 2017; Zhou and Meier, 2014). This involves the interaction of structural components of the nucleus including the envelope and nucleoskeleton with specialised genomic regions (Pombo and Dillon, 2015). Thus, the main characteristics of nuclei, depending on cell type, are due to envelope and periphery components interacting with special genomic regions.

The work in this thesis was carried out to further characterize proteins localized at the nuclear periphery in *Arabidopsis thaliana* (*A. thaliana*), specifically the NUCLEAR ENVELOPE ASSOCIATED PROTEINS (AtNEAP), a protein family with suggested roles in organising nuclear shape and chromatin, being part of the nuclear periphery protein network, (Pawar *et al*., 2016). Before introducing this family in detail by describing previous work on AtNEAPs, the genomic organization of the nucleus and the properties of the nuclear envelope

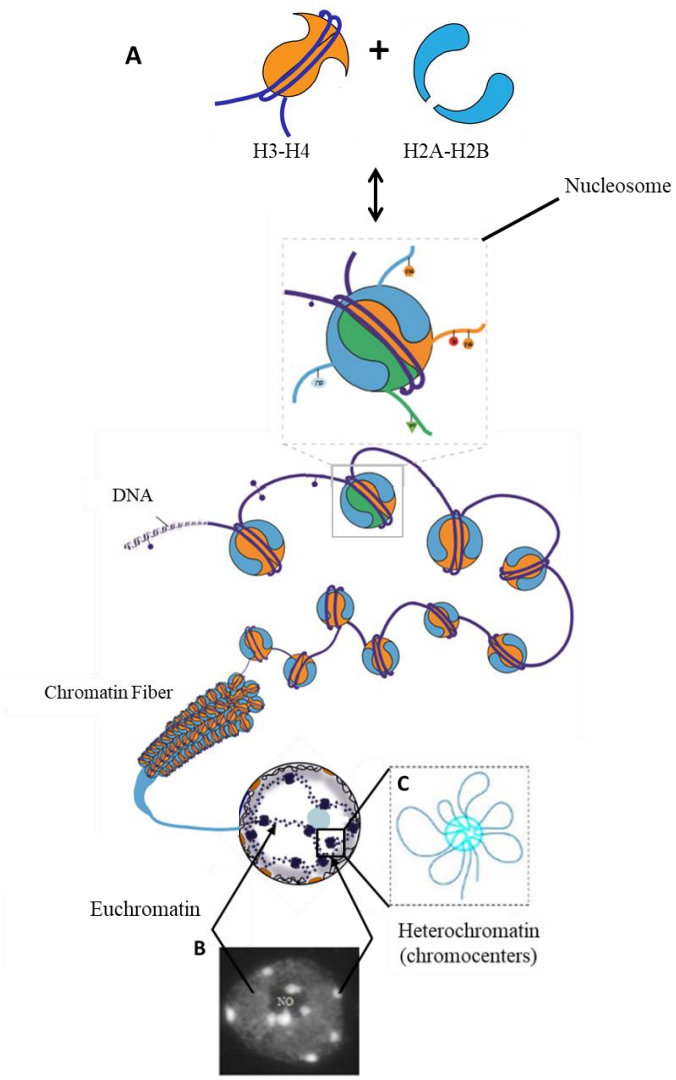

Figure 1-1: Chromatin formation and organisation (adapted from Probst et al., 2009)**. A.** The basic unit of chromatin is the nucleosome composed of histones H2A, H2B, H3, and H4 and 146bp of DNA. The beads of the string organization of nucleosomes folds into higher order chromatin structures. NO: nucleolus. **B.** Picture of an *Arabidopsis thaliana* nucleus stained with DAPI. Heterochromatin which is visible in microscopy in *A. thaliana* as bright foci called chromocentres is the most condensed chromatin state while euchromatin observed as a light grey background is the more relaxed chromatin state. **C**. Representation of the rosette organisation of chromatin. Heterochormatic sequences (in blue green) cluster together in chromocentre structures, while euchromatic sequences form chromatin loops anchored at the chromocentre, (Fransz et al., 2002, 2003, 2006; Grob et al., 2014, Feng et al., 2014).

and nuclear periphery components will be considered. Then, the aims of this PhD will be presented.

I – Chromatin formation and structure

In eukaryotes, the genomic DNA contained in the nucleus is organized into chromatin by association with histone proteins. A 146 base pair DNA sequence is wrapped around an octamer of histones forming the nucleosome, (Luger *et al*., 1997). This structure represents the basic unit of chromatin, ***Figure 1-1***.

There are five types of histones: H2A, H2B, H3, H4 and the histone linker H1. Every nucleosome is composed of a $(H3\text{-}H4)_2$ tetramer and two H2A-H2B dimers. Histone H1 allows the linkage of nucleosomes with each other for a higher level of compaction (Bharath *et al*., 2002; Rutowicz *et al*., 2018). Every type of histone belongs to a multigene family and, except for histone H4, there are one or several variants, which are non-allelic isoforms of canonical histones (Talbert *et al*., 2012). Incorporation of these variants influences nucleosome stability, DNA accessibility and, thus, gene expression. Indeed, particular variants contribute to specialized functions like centromere organization, silencing of transposable elements and repetitive sequences, X chromosome inactivation, specific gene activation or genomic stability, (Henikoff, 2008; Okada *et al*., 2005).

Post-translational modifications (PTM), mostly at the N-terminus (N-ter) of histones but also in their core domain are involved in *fine-tuning* gene expression. Histone PTMs can either directly affect the stability of the nucleosome or histone-DNA interaction or are interpreted by histone reader proteins that bind with specificity to certain histone PTMs translating this information into a more transcriptionally repressive or permissive chromatin environment.

The best-described PTMs are acetylation, methylation, phosphorylation, ubiquitinylation and sumoylation, (Bradbury, 1992; Desrosiers and Tanguay, 1986; Imhof and Becker, 2001; Maison *et al*., 2011; Probst *et al*., 2009; Strahl and Allis, 2000; Wu *et al*., 1986). The different combinations of PTMs together with the different canonical or variant histones within a nucleosome specify the epigenetic information (Jenuwein and Allis, 2001). Therefore, histone composition of nucleosomes and PTMs carried by histones modulate DNA accessibility and, in a higher scale, chromatin organization inside the nucleus.

During replication or transcription, the transcriptional machinery requires access to the underlying DNA. For that purpose, nucleosomes can slide along DNA or be fully or partially removed due to the action of chromatin remodellers. To date, four protein families are implicated in chromatin remodelling: SWITCH/SUCROSE NON FERMENTABLE (SWI/SNF), IMITATION SWITCH (ISWI), CHROMODOMAIN-HELICASE-DNA-BINDING PROTEIN (CHD), AND INOSITOL-REQUIRING 80 (INO80) (Clapier and Cairns, 2009; Henikoff, 2008; Petesch and Lis, 2012).

Classically, two different states of chromatin are distinguished according to their compaction levels (Heitz, 1928). The most condensed state is heterochromatin that shows high nucleosomal occupancy and enrichment in epigenetic marks repressive for transcription (Chodavarapu *et al*., 2010; Ricci *et al*., 2015) restricting access to DNA and limiting gene expression. The more decondensed chromatin, with lower nucleosomal occupancy, is euchromatin. It is more favourable for gene expression. However, these two principal chromatin states identified by cytological (Heitz, 1928), and molecular (Elgin and Grewal, 2003) analysis, have been further refined. Up to four main different states that result from combinations of several histone and DNA post-translational modifications, histone variants, transposable element composition and gene expression level were defined (Roudier *et al*., 2009, 2011; Sequeira-Mendes *et al*., 2014). In addition, it has been evidenced that NE and

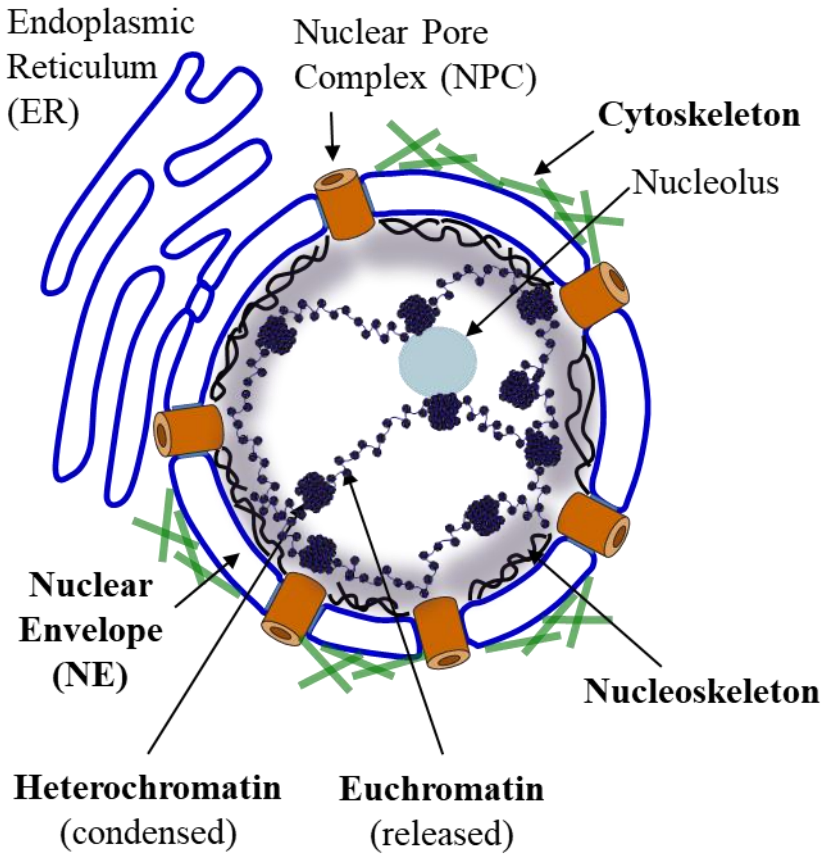

Figure 1-2: Nucleus organisation and structure. In eukaryotes, chromatin is separated from the cytoplasm by the nuclear envelope (NE) which is in continuity with the endoplasmic reticulum (ER). Throughout this membrane there are thousands of nuclear pore complexes (NPC), which allow communication between cytoplasm (outside) and nucleoplasm (inside). Also, on each side of the NE, cytoskeleton (green bars) and nucleoskeleton (black helix) made of protein complexes are responsible for keeping nucleus integrity and chromatin organisation. The two main states of chromatin (eu- and heterochromatin) are illustrated as arrays of relaxed or condensed nucleosomes (blacks beads).

nuclear periphery components have a role in structure and positioning of specific chromatin states within the nucleus, (Mattout *et al*., 2006; Murphy *et al*., 2010; Starr, 2009).

II – Nuclear envelope components

As presented previously, the NE is composed of two membranes: one on the nucleoplasmic side, INM, and another on the cytoplasmic side, ONM. The NE delimits the cytoplasm from the nucleoplasm and has many other functions, which have been well studied in animals. It allows communication between both compartments through Nuclear Pore Complexes (NPC) and bridges the cytoskeleton and the nucleoskeleton through the LInker of Nucleoskeleton to Cytoskeleton (LINC) complex, which permits nuclear migration and participates in maintaining nuclear shape and structure (Burke, 2012; Meier, 2001; Méjat and Misteli, 2010; Rose *et al*., 2004), ***Figure 1-2***.

II.1 – The Nuclear Pore Complex (NPC)

NPCs are embedded at sites of fusion between the ONM and INM and allow the NE to be permeable to a variety of macromolecules and signals. NPCs are ring-shape channels principally responsible for nucleo-cytoplasmic transport. The structure is octagonally symmetrical to its cylindrical axis and is composed of five different protein classes. The transmembrane ring is in contact with the NE, the core scaffold is made of an outer ring, an inner ring and a linker; cytoplasmic filaments, nuclear basket and central FG (hydrophobic core phenylalanine-glycine rich) are completing the complex, ***Figure 1-3*** (Alber *et al*., 2007; Brohawn *et al*., 2009; Grossman *et al*., 2012; Tamura and Hara-Nishimura, 2011, 2013). Hence, NPCs are formed by a large complex of proteins, with around 30 nucleoporins (Nups), which are highly conserved between vertebrates, yeast and plants (DeGrasse *et al*., 2009; Tamura *et al*., 2010). Despite a conserved structure, NPCs show some differences depending on the kingdom. Plant NPCs are 100 MDa in size, while vertebrates are 120 MDa and yeast

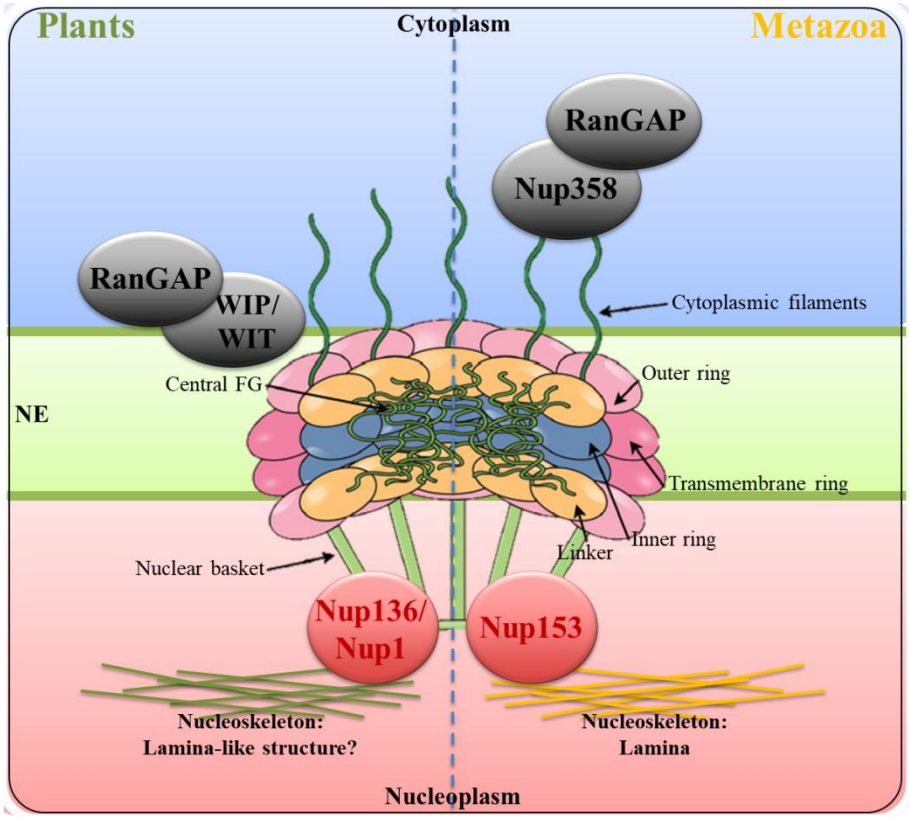

Figure 1-3: Schematic representation of the Nuclear Pore Complex (NPC) structure and main differences between plant and metazoan NPC components, (adapted from Tamura and Hara-Nishimura, 2013). The large complex of around 30 nucleoporins composing the NPC is well conserved through kingdoms. Major differences between plants and metazoan is the substitution of Nup358 by a WIT/WIP complex to anchor RanGAP close to the NPC for nucleo-cytoplasmic transport. Also, anchoring of the NPC to the nucleoskeleton here indicated as lamina-like structure / lamina by Nup153 in metazoa is replaced by Nup136/Nup1 in plants, (Zhou et al., 2012; Zhou & Meier, 2014; Tamura et al., 2010; Tamura and Hara-Nishimura, 2011).

only 50 MDa. Plants lack homologues to seven vertebrate proteins, of which one, Nup358 is important for anchoring RanGAP (RanGTPase Activating Protein, important for the nucleo-cytoplasmic transport (Ran cycle)) to the NE, (Hutten *et al*., 2008; Xu *et al*., 2007), and is substituted by a WIT/WIP complex in plants, (see ***II.2-b***), (Zhou and Meier, 2014; Zhou *et al*., 2012). Another is Nup153 anchoring the NPC to the nucleoskeleton in vertebrates, suggested to be replaced by Nup136/Nup1 in plants, which interacts dynamically with NPC at the NE, (Tamura and Hara-Nishimura, 2011; Tamura *et al*., 2010), ***Figure 1-3***.

II.1-a – Nucleo-cytoplasmic transport

Nucleo-cytoplasmic transport can be achieved by passive diffusion for small molecules like ions or small proteins below 50 kDa (Macara, 2001), but NPCs control the transit of macromolecules such as bigger proteins, ribosomes, RNA or RNA polymerases, by active transport, thanks to specific chaperones, named karyopherins, (Macara, 2001). Those chaperones are called importins or exportins depending on the direction of transport and have antagonist functions in the Ran cycle. Importins recognise a NLS (Nuclear Localization Signal) tag present on cargo proteins for transport into the nucleus and exportins recognise a NES (Nuclear Export Signal) for export from the nucleus, (Tran *et al*., 2014). The complex formed binds FG rich nucleoporins and is translocated between compartments. In the nucleoplasm, the importin-cargo complex is recognised by RanGTP, which changes importin conformation and releases cargo protein from importin. Importin-RanGTP is then translocated into the cytoplasm where RanGAP hydrolyses RanGTP in RanGDP and releases importin. To avoid any depletion of RanGTP inside the nucleus, RanGDP is brought back into the nucleus by its own import carrier, Nuclear Transport Factor 2 (NTF2), found in mammals, yeast and plants, (Macara, 2001; Zhao *et al*., 2006). RanGDP inside the nucleus is recycled to RanGTP by RanGEF (Ran Guanine nucleotide Exchange Factor) ready to disrupt new importin-cargo complexes. In this way, RanGAP and RanGDP are found only in the cytoplasm and RanGEF

and RanGTP only in the nucleoplasm, (Tran *et al*., 2014). The export mechanism is similar to import but this time RanGTP promotes and stabilizes exportin-cargo complexes. Once in the cytoplasm, RanGTP is hydrolysed to RanGDP by RanGAP and cargo protein is released from exportin. RanGDP and exportin are then brought back inside the nucleus by NTF2, (Macara, 2001; Zhao *et al*., 2006).

II.1-b – Association with INM and chromatin

Plant NPCs are non-randomly distributed over the NE. In vertebrates, NPC anchorage and position correlates with proteins of the inner nuclear periphery called lamins (see ***III.1***). This corresponds to observations in tobacco where NPC are anchored by a filamentous structure at the INM (Fiserova *et al*., 2009). Indeed, NPCs, more than acting as simple transport channels, have a role in pathogen response, (Gu *et al*., 2016), and many other functions. Among those, it has been shown that transcriptionally active and repressed genes associate with the NPC and the NE, (Dieppois and Stutz, 2010; Smith *et al*., 2015; Tran *et al*., 2014). Control of gene expression can be achieved by regulation of transcription factors or by modifying chromatin structure and accessibility to the transcriptional machinery, (see ***I***) (Capelson and Hetzer, 2009). Thus, NPCs have a transport-dependent role, for example, by importing transcription factors into the nucleus for specific gene activation, (Capelson and Hetzer, 2009), and also a transport-independent role in gene regulation, by tethering active regions of chromatin or recruiting actors of the transcription and mRNA export machineries, (Burns and Wente, 2014; Capelson and Hetzer, 2009; Tran *et al*., 2014).

Hence, NPCs are important to maintain nuclear shape, chromatin organisation, gene regulation, and together with the LINC complex (see ***II.2***), physically link the cytoskeleton to the nucleoskeleton and allow them to communicate.

II.2 – The LINC complex

The LINC complex spans the NE and bridges the cytoskeleton to the nucleoskeleton. In metazoa, this complex is composed of Sad1p/UNC-84 (SUN) domain proteins, which are localized in the INM, and of Klarsicht, ANC-1, Syne Homology (KASH) domain proteins, which are localized in the ONM. These two types of proteins interact in the periplasm via their C-terminal domains. On the nucleoplasmic side, SUN domain proteins interact with chromatin, lamins and other INM associated proteins via their N-terminal domain. On the cytoplasmic side, KASH domain proteins interact via their N-terminal domain with actin and different components of the cytoskeleton. In this way, communication between cytoplasm and chromatin is possible, which is important for many intra- and extracellular processes, (Starr, 2009). These include nuclear and chromosome positioning, cell division, and maintenance of nuclear shape, (Link *et al*., 2014). Indeed, defects in the LINC complex leads to diseases such as muscular dystrophy and progeria in humans (Burke, 2012; Méjat and Misteli, 2010; Tzur *et al*., 2006; Zhou and Meier, 2013).

The LINC complex is functionally conserved in eukaryotes, (Crisp *et al*., 2006; Graumann, 2014; Graumann *et al*., 2010; Murphy *et al*., 2010; Poulet *et al*., 2017). However, while SUN domain proteins are highly conserved across opisthokonts (a clade grouping metazoan and fungi), KASH domain proteins are more diverse in structure and function (Evans *et al*., 2014). The bridging complex has been described in humans, fly, worm, yeast and most recently in plants, (Meier, 2016; Tatout *et al*., 2014). In plants, it has been most studied in *Zea mays* (Murphy *et al*., 2010) and in *A. thaliana* (Graumann, 2014; Graumann *et al*., 2010; Meier, 2016). Further details will be presented below, concerning characteristics of SUN and KASH domain protein families, ***Figure 1-4***.

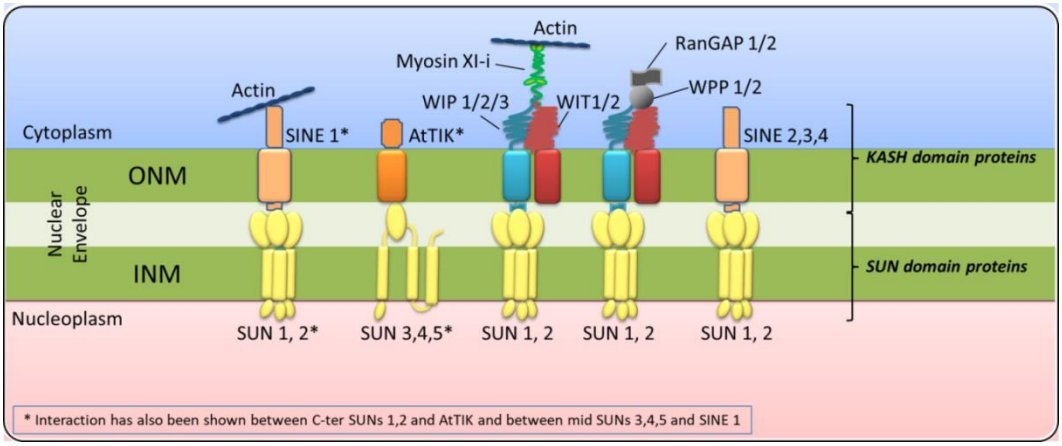

Figure 1-4: Different types of LInker of Nucleoskeleton and Cytoskeleton (LINC) complexes in *A. thaliana.* Due to a variety of Klarsicht-Anc1-Syne1 Homology (KASH) domain proteins in the Outer Nuclear Membrane (ONM) and the different Sad1-Unc84 (SUN) domain proteins in the Inner Nuclear Membrane (INM), several combinations of LINC complexes are possible and would be specific of cell types and developmental stages, (Meier, 2016).

*Interaction has also been shown between C-ter SUNs1-2 and AtTIK and between mid-SUNs3-5 and SINE1.

II.2-a – SUN domain protein family

Mammalian SUN domain proteins were found using bioinformatics analysis by comparison with SUN domain proteins found in the other kingdoms. The name comes from two proteins, which contain a C-terminal SUN domain: Sad1, a spindle pole body component described in yeast *Schizosaccharomyces pombe*, (Hagan and Yanagida, 1995) and UNC84, described in worm embryo, *Caenorhabditis elegans*, (Malone *et al*., 1999). The SUN domain proteins are highly conserved in the different kingdoms and play a crucial role in cell survival. They are involved in nuclear migration, organization and shape determination, (Oda and Fukuda, 2011), chromosome and telomere positioning, cell cycle-dependent NEBD and NE reformation and in apoptosis, (Evans *et al*., 2014).

Plant SUN domain proteins were first described in *Z. mays* by (Murphy *et al*., 2010) and in *A. thaliana* by (Graumann *et al*., 2010). Computational methods indicated that the SUN domain protein family in *A. thaliana* is composed of five different proteins (from AtSUN1 to AtSUN5) and two subfamilies have been distinguished, (Graumann *et al*., 2010; Tatout *et al*., 2014). AtSUN1 and AtSUN2 have the SUN domain at the C-terminus while AtSUN3, AtSUN4 and AtSUN5 have their SUN domain in a central position, (Graumann, 2014). Thus, there are Cter-SUN proteins (AtSUN1 and AtSUN2) and Mid-SUN proteins (AtSUN3, AtSUN4 and AtSUN5), which have been demonstrated to be conserved from yeast to plant as a monophyletic group (Graumann, 2014; Murphy *et al*., 2010; Poulet *et al*., 2017). In addition to a different SUN domain position, these two subfamilies have a different number of transmembrane domains (TMD) and coiled-coil domains (CCD). CCDs are necessary to form oligomers, as previously shown with AtSUN1 and AtSUN2, which form homo- and heterodimers, (Graumann *et al*., 2010). Also, the two Arabidopsis subfamilies localise at the NE and at the ER but the Cter-SUN proteins are enriched at the nuclear envelope compared to the ER (Graumann, 2014). Moreover, both subfamilies interact with the same KASH domain

proteins, (introduced in detail in ***II.2-b*** below), such as AtWIP1, and AtTIK, (Graumann, 2014; Zhou *et al*., 2012, 2015), but only Cter-SUN proteins are currently known to interact with SINE proteins, (Evans *et al*., 2014; Zhou *et al*., 2014).

II.2-b – KASH domain protein family

Though no sequence homologues for opisthokont KASH domain proteins exist in plants, different proteins have been identified, containing KASH domains and also having conserved binding properties for plant SUNs (Meier, 2016; Zhou and Meier, 2013, 2014; Zhou *et al*., 2015). In Arabidopsis, so far, four protein families have been evidenced, the WPP (tryptophan-proline-proline)- DOMAIN-INTERACTING PROTEINS (AtWIP1-3) and their binding partners the WPP DOMAIN-INTERACTING TAIL-ANCHORED PROTEINS (AtWITs), (Zhou and Meier, 2014; Zhou *et al*., 2012), the SUN-INTERACTING NUCLEAR ENVELOPE (AtSINE1-5, (Zhou *et al*., 2014)) and the TOLL-INTERLEUKIN-RESISTANCE KASH (AtTIK) domains proteins, (Graumann, 2014; Meier, 2016). The KASH domain is composed of a TM domain followed by a XXPT motif in C-ter position important for interacting with SUN domain proteins. On the cytoplasmic side, through AtWIT interaction, AtWIP proteins interact with RanGAP, a factor implicated in nucleo-cytoplasmic transport through NPCs, (see ***II.1***) and AtSINE proteins interact with F-actin fibers, (Zhou *et al*., 2014). AtTIK protein is the least described at the moment.

Thus, as in metazoan, (Rothballer and Kutay, 2013), in plants different types of LINC complexes are anchored at the NE combining different KASH domain proteins, AtWIP, AtSINE and AtTIK and the two-subfamilies of SUN domain proteins, AtSUN1-2 and AtSUN3-5. Some types of LINC complexes could be specific to particular cell types or certain development stages, as suggested by expression profiles like AtSUN5 that is specifically expressed in pollen, (Meier, 2016), ***Figure 1-4***.

III – Nuclear periphery components

At the nuclear periphery in metazoans, a meshwork of proteins is present on the nucleoplasmic side of the INM. This meshwork is named the lamina and is composed of type V intermediate filament (IF) proteins, lamins, and also lamin binding proteins, (Burke and Stewart, 2013).

III.1 – Lamins and their associated proteins and domains

Metazoan lamins belong to the IF family and comprise the fifth type of IFs. These proteins are separated into two classes: A-type and B-type lamins. A-type lamins are mainly composed of lamin A and lamin C, encoded by a single gene, called *LMNA* in human. B-type lamins are mainly composed of lamin B1 and lamin B2, encoded by *LMNB1* and *LMNB2* respectively (Burke and Stewart, 2013). As an IF protein, the lamin monomer is formed by a central CCD also known as an α-helical rod domain (~50nm and 350aa), a short head domain of ~30aa at N-ter and a long C-ter tail domain of ~200aa containing an Ig-fold domain of ~3.5nm in diameter (Turgay *et al*., 2017). Lamin A and lamins B1 and B2 display also a C-ter CaaX motif where “C” is cysteine, “aa” aliphatic residues and “X” any amino-acid, usually a methionine. This CaaX motif is important for PTM processes like farnesylation to target newly synthesized lamins to the NE and carboxy-methylation to realize the correct cleavage of the protein, (Burke and Stewart, 2013). A lamin dimer is formed by two parallel monomers with both Ig-fold domains on the same side and then dimers associate head-to-tail to form polymers leading to a rod-shape fibre, 3.5nm thick (Turgay *et al*., 2017). This fibre displays typical paired globular domains, distant of approximately 20nm from each other on the rod, relative to tetrameric and hexameric regions containing lamin Ig-fold domains. Globular domains can also be associated with lamin binding partners (Turgay *et al*., 2017). A- and B-

type lamins are major components of lamin filaments and form a dense meshwork underneath the INM, representing 12.5% of the ~14nm-thick lamina (Turgay *et al*., 2017).

Lamins interact with the LINC complex by binding SUN proteins (Mattout *et al*., 2006), and, with other components of the lamina, anchor chromatin domains and regulatory molecules such as transcription factors, (Burke and Stewart, 2013). Thus, this particular structure forms a scaffold at the nuclear periphery, tethers peripheral actors to the lamina and plays a crucial role for cell survival by regulating gene expression, chromatin organization, or even nuclear shape and movements, (Mattout *et al*., 2006). Mutations in lamins and also in the other components of the lamina are deleterious for the organism and generate laminopathies, such as the Hutchinson-Gilford Progeria Syndrome (HGPS) in human, (Méjat and Misteli, 2010), or Emery-Dreifuss Muscular Dystrophy (EDMD), (Ho and Hegele, 2018; Mattout *et al*., 2006; Mounkes and Stewart, 2004; Samson *et al*., 2018).

Indeed, lamins, even if major components of the lamina, are not lone actors. Some lamin-binding partners are anchored into the INM with one, two or more TM domains, such as the lamin B receptor (LBR) and the LEM domain (LAP2, Emerin, MAN1 domain) protein family, tethering lamina to the NE (Dilsaver *et al*., 2018); some others mediate interactions with chromatin, such as Barrier to Autointegration Factor (BAF) linking chromatin to the lamina, (Wilson and Foisner, 2010), ***Figure 1-5A***. LEM domain proteins play many roles in cell signalling, (Huber *et al*., 2009), and through interactions with A- and B-type lamins, transmit signals to gene expression networks and also to translational machinery in the cytoplasm, (Ma and Blenis, 2009). LEM domain proteins are also able to bind DNA directly due to specific domains or chromatin proteins, (Wilson and Foisner, 2010).

Particular chromatin domains named Lamin Associated Domains (LADs) have been evidenced using a technique termed DamID. This technique reveals by adenine methylation, the DNA regions that enter into contact with a bait lamina protein (usually Lamin B1) fused

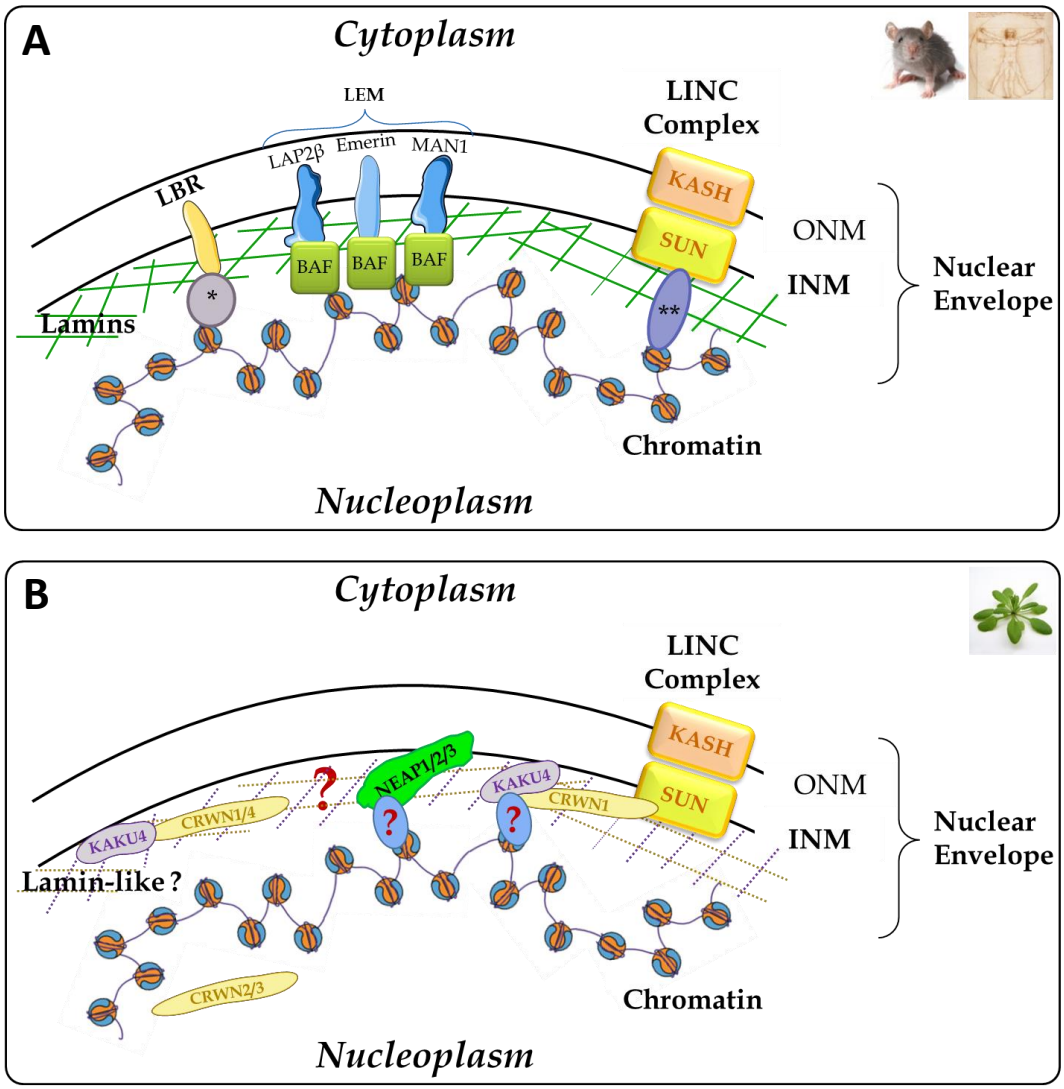

Figure 1-5: Comparison of the nuclear periphery structure and organisation in metazoan versus plants. **A.** In metazoa, the lamina is mainly composed of lamin filaments (green), which interact with proteins anchored at the INM, such as Lamin B Receptor (LBR) and LAP2β-Emerin-Man1 (LEM) proteins, and also with the LINC complex via SUN domain proteins. Thanks to intermediate proteins like Barrier of Autointegration Factor (BAF), chromatin domains are tethered at the lamina and thus at the nuclear periphery. Different proteins act as intermediate proteins and link chromatin to the lamina such as *Heterochromatic Protein 1 (HP1), **Bouquet1-2 (Bqt1-2), Silent Information Regulator 4, (Sir4) or Non-Disjunction 1 (Ndj1).
B. In plants, there is no homologue of lamins but KAKU4 and CRoWded Nuclei (CRWN) proteins are suggested as having the same role, (see *Chp1-III.2)*. Nuclear Associated Proteins (NEAP) are the most recent identified proteins and their function is investigated in this study.

to the bacterial *Dam* methylase, (van Steensel and Belmont, 2017; van Steensel and Henikoff, 2000). In differentiated human cells, LADs represent up to 30-35% of the human genome, usually harbouring repressive chromatin features, (Guelen *et al*., 2008). Two classes of LADs can be found: constitutive LADs (cLADs), that are present in all cell types, and facultative LADs (fLADs) that are LADs in a cell-type specific manner, (van Steensel and Belmont, 2017). Several studies suggest that this organization directly participates in silencing maintenance of particular chromatin regions. Indeed, localisation shift of those regions to the nuclear interior is usually related to a transcriptional gene reactivation of these regions, (Kind *et al*., 2013; Reddy *et al*., 2008). In 2010, two studies revealed the existence of other genomic regions with repressive chromatin features associated to the nucleolus, (van Koningsbruggen *et al*., 2010; Németh *et al*., 2010). These genomic regions were named NADs for Nucleolus Associated chromatin Domains. Interestingly, some NADs were already described as LADs, indicating a potential redundancy of these regions. Further studies revealed that after mitosis, some LADs are found in close association with nucleoli, demonstrating the existence of a stochastic reshuffling of a portion of LADs (possibly fLADs), (Kind *et al*., 2013).

In *A. thaliana*, NADs were identified by (Pontvianne *et al*., 2016) and genomic regions associated with the nuclear periphery were described by (Bi *et al*., 2017) using a derived Chip-seq approach (Re-ChIP-seq) with the nuclear pore protein NUP1 as bait. As in human cells, plant NADs and LADs-like are composed of genomic regions displaying heterochromatic features as the repressive histone modifications H3K9me2 and H3K9me3 (Bi *et al*., 2017; Pontvianne *et al*., 2016; van Steensel and Belmont, 2017). Importantly, genes present in these regions tend to be low expressed-genes, indicating a potential link between gene nuclear positioning and gene expression. However, unlike in human cells, plant LADs-like and NADs correspond to two mutually exclusive regions in *A. thaliana*, (Picart-Picolo *et al*., 2019).

Much less is known about the plant equivalents of the nucleoskeleton organisation and of proteins with such functions described in above paragraphs. Thus, this project aims to characterize new components of the NE and how the protein network at the nuclear periphery can possibly interact with chromatin.

In yeast, there are no lamin sequence homologues currently known, and the plant lamina or « plamina », (Fiserova *et al*., 2009), contains no lamins, LEM domain proteins or LBR homologues, (Rose *et al*., 2004). Neverthless, a meshwork of proteins is visible (Fiserova and Goldberg, 2010; Fiserova *et al*., 2009). A few plant proteins are suggested to have the same functions as mammalian lamins in controlling nuclear shape and chromatin organization, like CROWDED NUCLEI (CRWN) and KAKU4 proteins, detailed below (***III.2***), and more recently, AtNEAPs, which have the same characteristics as LEM proteins, suggesting similar functions. In addition, like LEM domain proteins, AtNEAPs may interact with chromatin. As this is the subject of the thesis, it will be described in detail in subsequent chapters, ***Figure 1-5B***.

III.2 – The plant lamina-like structure

Thus, no sequence homologues in plants have been found for metazoan lamins or lamin associated proteins. It seems likely that plants have developed their own proteins for supporting the NE and some recently identified proteins appear to have similar functions as lamins and are believed to be part of the plant nucleoskeleton.

III.2-a – Lamin-like proteins: CRWN family

(Moreno Díaz de la Espina *et al*., 1991) were the first to describe a fibrillar nuclear matrix underneath the INM in onion root cells similar to the one observed in metazoan. This matrix was isolated using specific extraction protocols from Laemmli and colleagues, (Laemmli, 1970; Lewis *et al*., 1984). Also, Matrix Attachment Regions (MARs) or Scaffold

Attachment Regions were described as DNA-nuclear matrix contact regions, (Breyne *et al*., 1994) and could be related to the current LADs and NADs, see ***III.1*** above.

Later, the first protein family to be identified was the NUCLEAR MATRIX CONSTITUENT PROTEIN (NMCP) family, which is highly conserved in plants but absent from metazoans and fungi, (Ciska *et al*., 2013). NMCP1 was the first protein of the family, identified using an antibody raised against the nuclear matrix purified from *Daucus carota* (Masuda *et al*., 1997). Although larger with a molecular mass of 134kDa, DcNMCP1 has a similar structure to metazoan lamins with a large central CCD and a putative NLS in its tail domain (Masuda *et al*., 1997). In Arabidopsis, four homologues have been identified in a genome-wide search for CCD proteins, (Rose *et al*., 2004). According to their mutant phenotypes that show "LITTLE NUCLEI", they were firstly named, AtLINC1-4 (Dittmer *et al*., 2007), but as it was confusing with the use of LINC complex for Linker of Nucleoskeleton and Cytoskeleton, they have been finally named AtCRWN1-4, (Wang *et al*., 2013), for "CROWDED NUCLEI". In the literature, all these names can be found, CRWN, LINC and NMCP, designing the same protein family in different plant species.

A mass spectrometry analysis of the Arabidopsis matrix at the nuclear periphery, (Sakamoto and Takagi, 2013) isolated about 1,600 proteins including AtCRWN1 and AtCRWN4 but not AtCRWN2 and AtCRWN3. AtCRWN1, AtCRWN2 and AtCRWN3 evolved at the same time and belong to the same monophyletic group as type 1 NMCP, and AtCRWN4 belongs to type 2 NMCP, (Wang *et al*., 2013). CRWN1 and CRWN4 are localized at the nuclear periphery, while CRWN2 and CRWN3 are preferentially localised at the nucleoplasm, (Dittmer *et al*., 2007; Sakamoto and Takagi, 2013).

It has also been shown that, like metazoan lamins, CRWN1 and CRWN4 are involved in maintenance of nuclear morphology (Dittmer *et al*., 2007; Sakamoto and Takagi, 2013; Wang *et al*., 2013). They are also involved in chromosome pairing, especially at

pericentromeric regions, evidenced by Hi-C in *crwn4* mutant plants, (Grob *et al*., 2014), and a chromocentre fusion has been observed in *crwn1crwn2* mutants that can be explained by the increased pairing at heterochromatic regions (Poulet *et al*., 2017; Wang *et al*., 2013).

The structure of the CRWN protein family, with a central CCD, similar to, but larger than the metazoan lamin CCD, is predicted to confer the ability to form filaments like lamins, (Ciska *et al*., 2013; Dittmer *et al*., 2007; Sakamoto and Takagi, 2013). Although no evidence were yet established concerning a real CRWN polymerisation, due to their similarities with metazoan lamins, CRWN proteins are not only suspected to be part of the plant lamina but also to be functional homologues of lamins, (Ciska and Moreno Díaz de la Espina, 2014; Ciska *et al*., 2013; Sakamoto and Takagi, 2013). Also, in mammals, SUN domain proteins interact with lamins; in plants, AtSUN1 and AtSUN2 are able to interact with AtCRWN1, (Graumann, 2014).

III.2-b – A CRWN-binding protein: KAKU4

AtCRWN1 and AtCRWN4 are able to interact with another nuclear periphery protein, named KAKU4, (Goto *et al*., 2014). Indeed, in a screen searching for mutants with an altered nuclear morphology, (Tamura *et al*., 2013) identified three proteins named KAKU for "nucleus" in Japanese. AtKAKU1 (see II-2-b) is a myosin XI-I known to interact with KASH domain proteins AtWIT1 and AtWIT2; AtKAKU2 is allelic to AtCRWN1, confirming the role of AtCRWN1 in nuclear morphology, (Dittmer *et al*., 2007); and AtKAKU4, a protein containing a NLS and a GAR domain with repeated glycine-arginine in C-ter position, and implicated in maintaining nuclear shape, (Goto *et al*., 2014).

KAKU4 is a CRWN-binding protein but neither CRWN nor KAKU4 seem to be responsible for the localisation at the nuclear periphery of each other, (Goto *et al*., 2014). Indeed AtKAKU4 has no paralogue and in an *Atkaku4* mutant AtCRWNs are well localised. On the contrary, the possible dependency on AtCRWN proteins for AtKAKU4 localisation

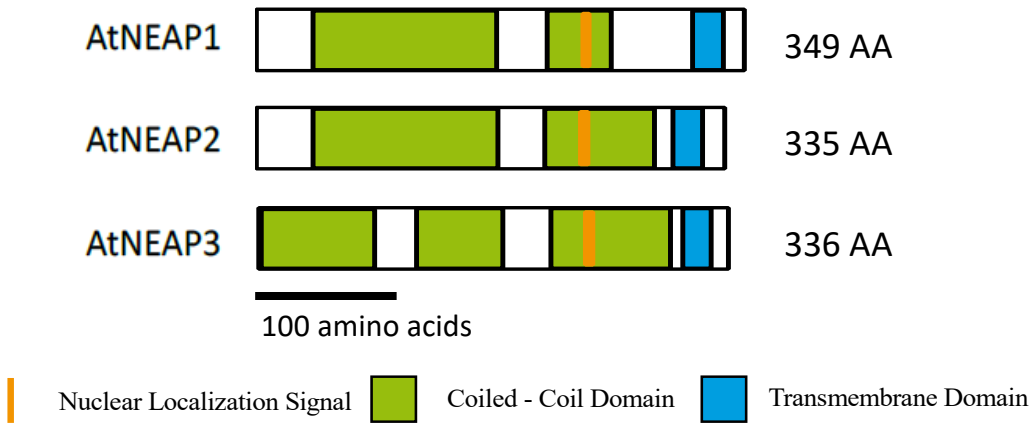

Figure 1-6: ***Arabidopsis thaliana*** **Nuclear Envelope-Associated Protein (NEAP) family** is composed of three proteins of about 350 amino acids (AA) containing coiled-coil (CC) domains, nuclear localisation signal (NLS) and a transmembrane (TM) domain at the C-terminus.

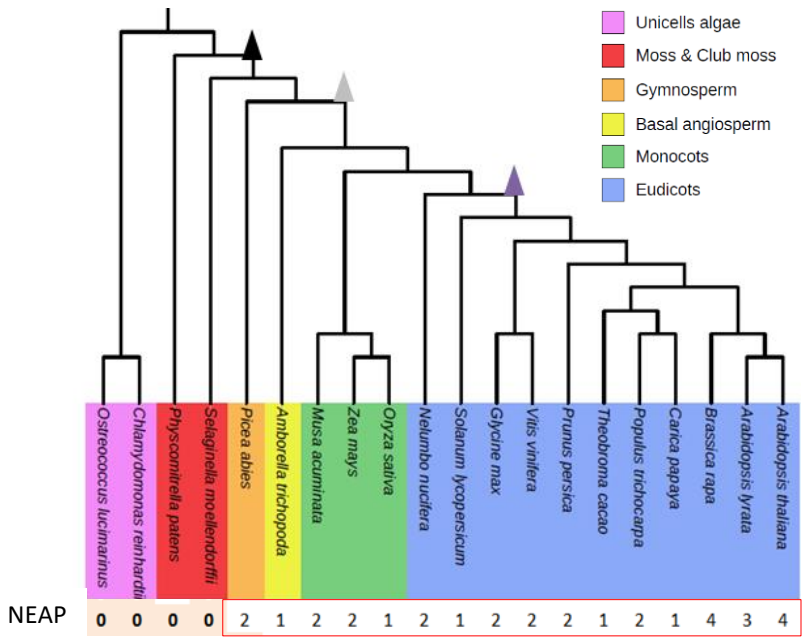

Figure 1-7: NEAP proteins during Plant Kingdom evolution. NEAP proteins are present in gymnosperms, basal angiosperms, monocots and eudicots but are absent from the most primitive species like moss and unicellular algae. Number of NEAP proteins in each studied species is indicated in the line above the phylogenic tree. Triangles indicate whole genome duplication events; adapted from Poulet et al., 2016.

has to be confirmed as the experiment was carried out only with an *Atcrwn1* single mutant and AtCRWN2, AtCRWN3 or AtCRWN4 could complement *Atcrwn1* loss-of-function. Also, AtKAKU4 could be localized at the INM even if no TM domain is present on the protein, (Goto *et al*., 2014). Interestingly, when AtKAKU4 as well as AtCRWN1 were over-expressed in plants, growth and deformation of the NE as well as intra-nuclear vesicle like NE invaginations have been observed in a dose-dependent manner, (Goto *et al*., 2014). This may indicate a function related to nuclear envelope assembly.

Thus, KAKU4, with CRWN1 and CRWN4, and to a lesser extent with CRWN2 and CRWN3 would form a protein network "lamina-like" at the nuclear periphery in plants. Their interaction with chromatin and the existence of LADs in plants is still a matter of intense investigations.

IV – The NUCLEAR ENVELOPE-ASSOCIATED PROTEINS

IV.1 – A new family of Inner nuclear membrane associated proteins

Based on a bioinformatic screen for new nuclear membrane proteins with KASH-like characteristics, and containing CCD and NLS, AtNEAP proteins were found and shown to possess a TM domain, (Pawar *et al*., 2016), ***Figure 1-6***. Phylogenetic analysis and sequence alignment tools (Poulet *et al*., 2016) revealed that the *NEAP* gene family first appeared in gymnosperms and are absent from archaic species as unicellular algae, ***Figure 1-7***. The monocots and the eudicots form monophyletic groups with specific-to-species gene duplication. Thus, during speciation of the *Brassicaceae* of which *A. thaliana* is a member, a duplication event resulted in three genes, *NEAP1*, *NEAP2*, *NEAP3*, (Poulet *et al*., 2016). As *AtNEAP4* is specific to Arabidopsis, truncated and transcribed at very low level, it has been considered as a pseudogene, (Poulet *et al*., 2016).

The first investigation to characterize AtNEAPs explored their localization. For that purpose, transient infiltration in *Nicotiana benthamiana* plants was used. These studies used constructs of transiently over-expressed AtNEAP proteins fused to a fluorescent label. Localization was assessed by confocal microscopy. All three proteins localized to the nuclear periphery and fluorescence recovery after photobleaching (FRAP) experiments showed that AtNEAP1 and AtNEAP2 are more tightly bound to the nuclear periphery than AtNEAP3. Moreover, mobile fractions of AtNEAP1 and AtNEAP2 are comparable to other NE or NE-associated proteins like AtSUN proteins. Studies of the different protein domains of AtNEAP3 indicated that the first CCD and TM domain are required for localization at the nuclear periphery rather than in the nucleoplasm. The NLS was shown to be required to target the protein to the nucleus instead of cytoplasm, (Pawar *et al*., 2016).

A second investigation explored whether AtNEAPs were able to form homo- or heterodimers by carrying out an acceptor photobleaching Fluorescence Resonance Energy Transfer (apFRET) experiment after co-infiltrating two AtNEAP proteins fused either with yellow or cyan fluorescent protein (YFP/CFP) in *Nicotiana benthamiana* leaves (see Methods section III-E). Results obtained indicated that AtNEAP1, AtNEAP2 and AtNEAP3 can interact with each other and with themselves. As these studies were performed with transiently over-expressed proteins, complementary studies were also carried out using the Membrane Yeast Two Hybrid (MYTH) system. These confirmed AtNEAP1-AtNEAP1, AtNEAP1-AtNEAP2 and AtNEAP1-AtNEAP3 interactions although these interactions were weak in MYTH, (Pawar *et al*., 2016). Other protein partners for AtNEAPs have been identified by Pawar *et al*, 2016. Indeed, apFRET and MYTH experiments showed that all three AtNEAPs interact with LINC complex components AtSUN1 and AtSUN2, (Pawar *et al*., 2016).

IV.2 – AtNEAP-interacting partner: AtbZIP18, a link with chromatin?

A MYTH screening using AtNEAP1 as bait, also revealed among others a basic-LEUCINE ZIPPER (AtbZIP18) protein as an interacting partner, which is a transcription factor (TF), (Gibalová *et al*., 2017; Pawar *et al*., 2016). Localization and co-localization studies show AtbZIP18 localized to the nucleus and the cytoplasm. When AtNEAP1 is co-expressed with AtbZIP18, AtNEAP1 fails to localize at the nuclear periphery and co-localizes with AtbZIP18 in the nucleoplasm (Pawar *et al*., 2016), indicating a potential *in-vivo* interaction for AtbZIP18 and AtNEAP1.

Thus, the transcription factor AtbZIP18 (Pawar *et al*., 2016) could be an interactor of AtNEAP1. AtbZIP18 belongs to a large family of transcription factors, named bZIP, implicated in a broad range of mechanisms (Dröge-Laser *et al*., 2018). In *A. thaliana* the protein family is composed of 78 members divided in 13 groups (A-M), (Dröge-Laser *et al*., 2018). The main characteristic is the presence of a BRLZ domain for a basic DNA-binding region followed by a leucine zipper allowing bZIP dimerization. AtbZIP18 belongs to group I, which is related to stress response, cell cycle regulation and various developmental aspects, (Dröge-Laser *et al*., 2018). It is implicated in pollen development and has been further characterized by (Gibalová *et al*., 2017). AtbZIP18 localizes to the ER and also in the nucleus, but is excluded from the nucleolus, (Gibalová *et al*., 2017). It has a rather ubiquitous expression pattern with higher levels of expression in mature pollen grains, embryo nuclei and roots. AtbZIP18 is thought to be redundant with AtbZIP34, one of its binding partners, and they both have a role in the male gametophyte. AtbZIP18 and AtbZIP34 could be repressors as in each single mutant there are more upregulated genes than downregulated. Moreover, AtbZIP18 has an Ethylene-responsive element binding factor-associated Amphiphilic Repression (EAR) motif, which is implicated in transcriptional inhibition through chromatin modification, (Gibalová *et al*., 2017; Kagale and Rozwadowski, 2010). Indeed, the EAR motif

is a common active transcriptional repression motif recruiting co-repressors such as AtSIN3, AtSAP18 (SIN3 ASSOCIATED POLYPEPTIDE P18) or TOPLESS (TPL), which interact with AtHDA19 to proceed to histone deacetylation and thus gene repression, (Kagale and Rozwadowski, 2011).

Through yeast two-hybrid (Y2H) experiments it has been shown that AtbZIP18 can also interact with AtbZIP61 and AtbZIP52, which also possesses an EAR motif; increasing the number of possible heterodimers, (Gibalová *et al*., 2017) and thereby different targeted genes.

Thus, it is of particular interest to investigate the interaction of AtbZIP18 with AtNEAP protein family in order to establish a link between chromatin and the nuclear periphery. Also, as AtbZIP18 would be a negative regulator of gene expression, this could help to better picture why and how heterochromatin is recruited at the nuclear periphery.

IV.3 – Aims of the research project

To be able to fully characterize AtNEAP proteins, reverse genetics is needed and different single mutants for all three genes have been selected and then crossed to obtain double and triple mutants, (Pawar-Menon, PhD thesis, 2015). The first set of mutants available included a single *Atneap1* KO, a single *Atneap3* KO, a double *Atneap1Atneap3* KO (Pawar *et al*., 2016) and a single *Atneap2* "leaky" probable knock-down (KD), see ***Results Chapter 3-I***.

The aim of the work presented in this thesis was to characterise the role, function and interactions of the AtNEAP protein family, building on previous work (Pawar-Menon, PhD thesis, 2015; Pawar *et al*., 2016), which indicated a location at the nuclear periphery and suggested a role in the interaction of chromatin with the nuclear envelope and nucleoskeleton through the LINC complex.

During this PhD, attempts were made to generate a triple *Atneap* mutant and this was achieved using CRISPR/Cas9 technology to generate a new single *Atneap2* KO mutant, which was crossed with the double *Atneap1Atneap3* KO mutant already available. Finally, the triple KO *Atneap1Atneap2Atneap3* and all the combinations of single and double mutants from this crossing were identified and selected. Study and characterisation of the mutants is described in section ***Results Chapter 3***.

New interaction partners of AtNEAP were explored using classical Y2H and confirmation of location and interaction with AtbZIP18 using high-resolution confocal microscopy (apFRET) was obtained. In addition, localisation *in-vivo* in *A. thaliana* was confirmed using a transient expression method called the FAST technique. Finally a number of tools were developed for future work, including antibodies specific to AtNEAPs, a complementation vector for mutant lines and protein extraction protocols for immunoprecipitation.

The results of the work will be discussed in the context of current knowledge of plant nuclear structure and constituents of the NE, nucleoskeleton and chromatin. Finally, possible future work will be discussed in order to more fully determine the role of this protein family in the nuclear periphery protein network; and its implication in the regulation of gene expression through interaction with the transcription factor AtbZIP18.

CHAPTER 2
MATERIALS and METHODS

Table 2.1: Amino-acid concentrations for Yeast media

Amino Acid	Abbreviation	Concentration (mg/ml)
Methionine	MET	20
Lysine	LYS	30
Uracile	URA	20
Histidine	HIS	20
Adenine	*ADE	20
Leucine	LEU	60
Tryptophane	TRP	20

*Add 4ml NaOH 5M to dissolve

MATERIALS and METHODS

I – Yeast

I.1 – Yeast strains

In this study, two *Saccharomyces cerevisiae* strains were used; **Y187**, *MATα, ura3-52, his3-200, ade2-101, trp1-901, leu2-3, 112, gal4Δ, gal80Δ, met–, URA3::GAL1*$_{UAS}$*-GAL1*$_{TATA}$*-LacZ, MEL1* for transformations with prey plasmids and **AH109**, *MATa, ura3-52, his3-200, trp1-901, leu2-3, 112, gal4Δ, gal80Δ, GAL2-ADE2, LYS2::GAL1-HIS3, URA3::MEL1-LacZ* for transformation with bait plasmids.

I.2 – Yeast growth and media

Yeasts were grown at 30°C for at least 3 days in different media, either liquid or solidified by adding agar 2%.

In order to start a fresh culture, a rich medium, Yeast extract Peptone Dextrose/D-glucose (YPD, 1% yeast extract, 2% peptone, 2% glucose/dextrose) was used.

In order to select yeasts transformants, a synthetically defined (SD, 2% glucose, 6.9g/l Yeast Nitrogen Base (YNB) medium) was used. SD medium was a minimal medium supplemented with essential amino acids (aa), some of which were omitted for selection of some plasmids and/or activated reporters. See ***Table 2.1***.

I.3 – Yeast transformation

Cells of either Y187 or AH109 strains grown on YPD were collected with a pipette tip and diluted in 1mL of 1X TE/LiAc and centrifuged at 13000g for 1min. This washing step was repeated with 1mL of 1X TE/LiAc and the pellet was resuspended in 500µL of 1X

TE/LiAc. For one transformation, 40µL of yeast was needed. DNA carrier was denatured at 95°C for 5min and put on ice.

Transformation was carried out with 300µL TE/LiAc/PEG 40%, 5µL DNA carrier, 200-500ng of plasmid (see ***IV.8***) and 40µL yeast prepared as above. The mix was incubated at 30°C for 30min, then 12µL DMSO was added and tubes were incubated at 42°C in a water bath for 15min in order to apply a heat shock. Finally, cells were plated on SD medium depleted for the selective amino-acids and incubated at 30°C for 3 to 5 days.

For screening a high number of proteins, cells of Y187 strain were transformed with a cDNA library of prey plasmids (Clontech, "Mate & Plate™ Library - Universal Arabidopsis (Normalized)") made from mRNA isolated from 11 Arabidopsis tissues.

I.4 – Yeast-Two-Hybrid (Y2H) screening

SD supplemented with all aa required but depleted in leucine and tryptophan (SD –Leu–Trp) was used to select diploid yeast containing bait and prey plasmids encoding tryptophan and leucine biosynthesis genes, respectively, that are otherwise absent from the cell. Thus, SD –Leu is used to select yeast containing prey plasmids and SD –Trp to select yeast containing bait plasmids.

When interaction occurs between bait and prey, the Gal4 transcription factor is reformed and activates the responsive *HIS3* and *ADE2* genes. Thus, diploid yeast containing bait and prey plasmids with interacting bait and prey proteins is able to grow on a SD medium depleted in leucine, tryptophan, histidine and adenine (SD/–Ade/–His/–Leu/–Trp).

Table 2.2: Antibiotic concentration and organism used for bacterial and plant selection

Antibiotic	Concentration (µg/ml)	Organism used on
Ampicillin	50	*E. coli / A. tumefaciens*
Gentamicin	25	*A. tumefaciens*
Kanamycin	50	*E. coli / A. tumefaciens*
Rifampicin	50	*A. tumefaciens*
Spectinomycin	50	*E. coli / A. tumefaciens*
Zeomycin	25	*E. coli*
Basta	10	*Arabidopsis thaliana*

II – Bacteria

II.1 – Bacterial strains

All cloning was performed in *Escherichia coli* (*E. coli*) using a chemically competent high efficiency DH5α strain. The DB3.1 strain was used to amplify empty gateway vectors containing the lethal *ccdB* gene (Bernard and Couturier, 1992).

For sub-cloning of binary vectors, the chemically competent *Agrobacterium tumefaciens* (*A. tumefasciens*) GV3101 strain was used, followed by plant transformation. GV3101 strain (C58 background) contains a rifampicin resistant gene (RIF) for selection during transformation, a nopaline type Ti plasmid pMP90 without its transport function (pTiC58DT-DNA) and a plasmid containing *vir* gene. The VIR T-DNA gene was inserted into the plant genome with essential elements (pTiC58DT-DNA, pMP90). Its T-DNA transfer function is damaged but can be transferred to the binary vector T-DNA to help smooth transfer. PMP90 (pTiC58DT-DNA) Ti plasmid contains screening tags: streptomycin and gentamycin for selection upon plant transformation such as Arabidopsis, tobacco, maize and potatoes.

II.2 – Bacterial growth and media

E. coli were grown O/N at 37°C in Luria Broth (LB) medium, either solidified by adding 1% agar or liquid, containing specific antibiotics depending on the vector transformed in the bacteria, see ***Table 2.2***.

A. tumefaciens were grown at 28°C in LB medium or Yeast Extract Broth (YEB), either solidified by adding 1% agar or liquid. Overnight shaking cultures (150rpm) were used for infiltration; otherwise cells were cultivated on plates for 48 hours, always at 28°C.

Rifampicin and gentamicin for helper plasmid T1 were required to select the GV3101 strain, plus additional antibiotic for selection of the plasmid of interest, see ***Table 2.2***.

II.3 – Transformation of E. coli

For electroporation (EP), the chemically competent *E. coli* DH5α strain was used. Cuvettes were cooled on ice and 50µL aliquots of cells were then thawed also on ice. Then 50-200ng of plasmid (see *IV.8*) were added to the cells and transferred to the cooled cuvettes. Samples were incubated for 30sec before electroporation at 1.8kV. Immediately, 450µL of Super Optimal broth with Catabolite repression (SOC, LB medium supplemented with 20mM glucose) was added and transferred to 2mL tubes for incubation at 37°C with shaking for 1h. Finally, 50µL were plated on LB Agar with specific antibiotics (see ***II.2***) and incubated at 37°C overnight.

For heat shock (HS) transformation, the following kits and cells were used; Agilent, "Ultracompetent cells XL-10" and NEB, "HiFi competent cells" and "5-alpha Competent *E. coli*". The respective reagents and protocols were used as indicated by the manufacturers. Refer to *IV.1* – List of primers for plasmid isolation procedure.

II.4 – Transformation of A. tumefaciens

Chemically competent *A. tumefaciens* GV3101 strain was used for transformations. Two different but similar techniques were used depending on the laboratory.

For EP, cuvettes were cooled on ice and 40µL aliquots of cells were thawed on ice. Then 50-200ng of plasmid were added to the cells and transferred to cooled tubes. Samples were incubated for 30sec before applying an electroporation of 1.8kV. Immediately, 1mL SOC was added and transferred to 2mL tubes for incubation at 28°C for 3h. Finally, 5µL were plated on LB Agar with specific antibiotics (see ***II.2*** and ***Table 2.2***) and incubated at 28°C for 48h.

For HS, 100µL of cells were thawed on ice and 0.5-1µg of plasmid was added to the cells and incubated on ice for 5min, then 5min in liquid nitrogen and 5min at 37°C. After heat

Table 2.3: Details of Arabidopsis lines used in this study

Arabidopsis lines used in this study							
Usual name		***First neap2***	***neap1***	***neap3***	***neap2 CRISPR***		
Official name		*Atneap2*	*Atneap1.1*	*Atneap3.1*	*Atneap2.1*		
Mutations	**Type**	T-DNA	T-DNA	T-DNA	CRISPR		
	Reference	GABI_589B02	Sail_846B07	WiscDsLoxHs086_02C	N/A		
Gene accession number		At5g26770	At3g05830	At1g09470	At5g26770		
Antibiotic resistance		Sulphadiazine	Basta	Kanamycine	N/A		
		X	X	X		***First triple neap***	**Combinations of mutants**
			X	X		***neap1neap3***	
			X		X	***neap1neap2***	
				X	X	***neap2neap3***	
			X	X	X	***triple neap***	

shock, 1mL YEB or LB was added and cells shaken at 28°C for 3h. Finally, 200µL were plated on YEB Agar with specific antibiotics (see ***II.2*** and ***Table 2.2***) and incubated at 28°C for 48h.

III – Plant

III.1 – Seed Stock

The wild type *Arabidopsis thaliana* (*A. thaliana*) *Columbia* (Col-0) and different mutant lines used in this study are listed in ***Tables 2.3 and 2.4***.

Wild type *Nicotiana benthamiana* (*N. benthamiana*) plants were used for *A. tumefaciens* infiltrations and transient protein expression (see ***III.5***).

III.2 – Seed germination and plant growth

For all plants, temperature and light conditions were 23°C and 8h dark/16h light. They were grown either in sterile soil or *in vitro* on plates with MS medium (Murashing and Skoog (Caisson Laboratories), 0.8% agar, 1% sucrose, pH5.7). In order to synchronise seed germination, all the seeds sown were left at 4°C for 48h before being transferred into growth chambers (Aralab).

For *in vitro A. thaliana* cultures, seeds were previously sterilized with 70% ethanol and 0.05% SDS and then rinsed with 95% ethanol and left to dry before sowing.

III.3 – Crossing lines

In order to obtain multiple T-DNA insertion mutants, homozygous single or double T-DNA insertion mutants were crossed by directed pollination. *A. thaliana* plants to be crossed were grown as detailed above in ***III.2***. The mother plant was grown to a stage where it had a single floral stalk and few young flower buds. All open flowers, buds with white tips, immature budding meristems and mature siliques were removed with a pair of forceps so that

Table 2.4: List of constructs stably transformed into Arabidopsis lines

CDS transformed	Plant Background	Antibiotic resistance
YFP_NEAP1	Wild type Col-0	Basta
YFP_NEAP2		Basta
YFP_NEAP3		Basta
CFP_NEAP1		Basta
CFP_NEAP2		Basta
CFP_NEAP3		Basta
CRISPR_E1N2		Basta
CRISPR_E3N2		Basta

three to four buds remained for emasculation. The remaining flower buds were emasculated by first splitting the petals and sepals and then picking them out carefully along with all anthers. The mother plant was then pollinated using a mature flower from the father plant, by tapping the anthers on the style with the pollen visibly covering the stigma. This was repeated for all floral buds. Crossed buds were marked by tying coloured threads around them for identification. Once mature, a small paper bag was tied around individual siliques and they were allowed to dry inside the bag before collection. Hybrid seeds, expected to be heterozygous for both mutations from their homozygous parents were allowed to self-pollinate and their progeny was genotyped for identification of the homozygous double or triple mutant lines.

III.4 – Phenotype analysis

Root Assay was performed on wild type Col-0 and mutant lines sown on MS medium according to growth conditions, see ***III.2***. Square plates were used for this experiment, and kept vertical to let the primary root grow vertically at the medium surface. Seedlings were grown for 10 days after germination (dag) and primary root growth was assessed at different time points, 3, 5, 7 and 10 dag. Measures of root length were carried out with *ImageJ* software (see ***VIII.1***) on 45 independent seedlings per genotype and statistical analysis conducted as described in ***VII***.

Silique size was measured on 36 siliques at the same stage from 12 plants per genotype and statistical analysis carried out as described in ***VII***.

Seed number per half silique was scored from 36 siliques measured previously from 12 plants per genotype and statistical analysis carried out as described in ***VII***.

Staining of live cotyledon nuclei and fixation. Experiments were done in darkness. In this study, PicoGreen® solution (Molecular Probes) an ultra-sensitive fluorescent nucleic acid stain was used instead of DAPI as a DNA intercalating agent. From aliquots of Picogreen,

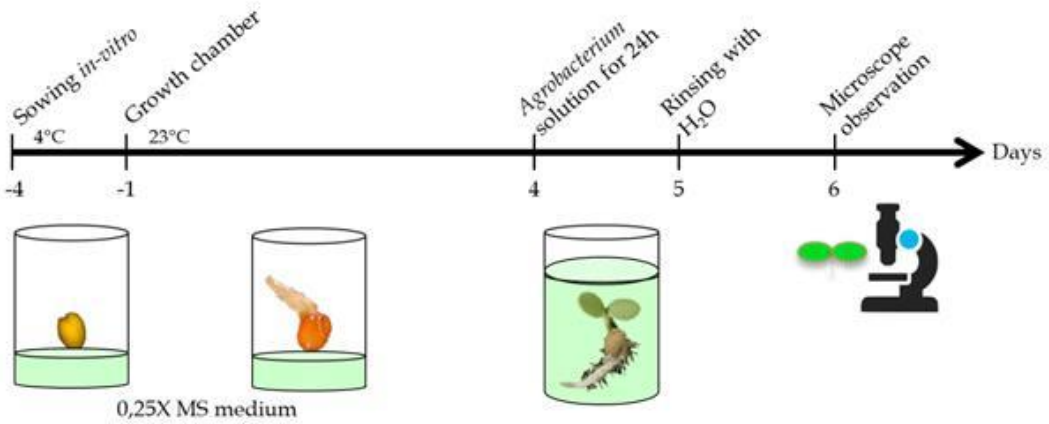

Figure 2-1: Main steps of adapted FAST protocol from Li and Nebenfuhr, 2010.

diluted in DMSO (1:10) and stored at -20°C, a solution of Picogreen diluted 1 in 200 with PBS 1X 0.01% Triton X-100 was prepared. Three to four 10 or 14 dag seedlings per line were taken and placed in water until all seedlings were harvested. Then, samples were placed in Picogreen solution and incubated for 15min at RT, 5min under vacuum and 30min more at RT. Next, samples were fixed with formaldehyde (formaldehyde 1%, PBS 1X, DMSO, H_2O) for 25min at RT and 5min under vacuum. Afterwards, fixative solution was replaced by methanol for a quick rinse followed by three washes of 5-10min with methanol and then for three washes of 5-10min with ethanol until the green colour disappeared. Samples were rehydrated with PBS 1X and then with 3 times 10min into PBS:glycerol 20:80 and left in this solution until slide mounting.

III.5 – Transient transformation

Transient transformation of A. thaliana was performed with an adapted protocol from (Li and Nebenführ, 2010) named Fast Agro-mediated Seedling Transformation (FAST) ***Figure 2-1***. In an ELISA plate (96 well), 110µL 0.25X MS medium (see ***III.2***) was poured into every well except those at the periphery, where 200µL H_2O was poured into the wells to keep the plate moisturized. Two seeds per well were sown for a total of 60 wells per plate and left for 48h at 4°C before placing plates in growth cabinets. On the day of seedling transformation (4dag), the transformed *A. tumefaciens* of interest (see ***II.4***) was resuspended from the plate on which it was growing to washing solution (10mM $MgCl_2$, 100µM acetosyringone) and OD measured. Seedlings were submitted to 100µL of co-cultivation medium (1.13g/l MS, 1% sucrose, 100µM acetosyringone, pH6.0 and just before use 0.005% (v/v; 50µl/l) Silwet L-77) in the presence of the transformed *A. tumefaciens* of interest at the OD required. Plates were wrapped in aluminium foil to keep them dark and then put back into the growth cabinet for 24h shaking at 75rpm. At 5dag, wells were washed with sterile H_2O,

the first time quickly and then three more times for 10min, keeping the last wash until microscope observation, with a maximum of 48h.

Transient transformation of N. benthamiana was performed using four to six week-old plants by infiltration with *A. tumefaciens*. Bacterial cultures (see ***II.4***) were removed from the incubator and 1mL from each sample was centrifuged at 8000rpm for 3min. The supernatant was removed and the pellets were gently resuspended in 1mL of Infiltration Buffer (IB, 0.5% D-Glucose, 0.5M MES, 0.02M $Na_3PO_4.12H_2O$, 0.0001% acetosyringone, H_2O) and centrifuged at 8000rpm for 3min. Supernatant was removed and 1mL IB was added to resuspend the pellet. Optical Density (OD) was measured by a Nanodrop spectrophotometer and was adjusted to 0.05 for p19 (a RNAi silencing suppressor) and 0.1 for other constructs. A 1mL syringe was used to push the resuspended bacteria into the leaf through a small hole pierced previously (Omarov *et al*., 2006). The plants were incubated at least for 2 days before checking protein expression by confocal imaging (see ***VI.3***) or harvesting plant tissue for protein extraction (see ***V.1***).

III.6 – Stable transformation – Deep floral transformation

A first overnight pre-culture was carried out with 200mL of the transformed *A. tumefaciens* cells in 15mL of LB containing the three antibiotics necessary for these cells. The day after, an overnight culture was prepared with 200mL of LB, 10mM $MgSO_4$ and with gentamycin and antibiotic corresponding to the vector of interest, but not rifampicin. The following morning, the OD_{600} was measured and the solution diluted until OD_{600} = 0.2. Incubation then was continued until it achieved an OD_{600} = 0.6-0.8. The solution was then centrifuged at 4000g for 10min, then the pellet was resuspended in 100mL of IB (5% sucrose, 0.1M $MgCl_2$, 0.02% Silwett). Then, all floral buds of a plant were immersed for 20s in this

solution. Afterwards, trays of plant pots were covered for 48h and finally transferred to the green house to be dried out.

IV – Nucleic Acids

IV.1 – List of primers

A list of primers is provided as supplemental tables at the end of this thesis (***Appendix I*** and ***Appendix II***).

IV.2 – Extraction of genomic DNA

Small pieces of young leaves were incubated in 8 tube PCR strips with DNA extraction buffer (0.2M Tris-HCl pH7.5, 0.25M NaCl, 0.025M EDTA pH8, 0.5% SDS, H_2O) for 10min at 99°C and spun down at 13500rpm for 8min. Then, supernatants were mixed with equal volumes of isopropanol, incubated for 15min at RT and spun down at 13500rpm for 15min. DNA pellets were washed with 70% ethanol, dried at 55°C and resuspended in H_2O.

IV.3 – RNA extraction

For RNA extraction, 8 to 12 seedlings of 14dag per sample were ground into powder with liquid nitrogen and were submitted to a number of different extraction protocols. Different kits used were “NucleoSpin RNA plant” from Macherey-Nagel and the “RNAeasy Plant Minikit” from Quiagen, both following the manufacturers’ protocol. A protocol using Trizol, Phenol, Chlororoform, and Isoamylic Alcohol was also used. This technique will be described in detail.

After a 5min-incubation at RT in 1mL Trizol (Tri-Reagent, Euromedex) and centrifugation at 4°C, 5min, 13200rpm, 200µl chloroform were added to the supernatants and samples incubated for 5min at RT and then centrifuged at 4°C, 15min, 13200rpm. The aqueous phase was taken and RNA precipitated with 600µL isopropanol. Samples were

incubated at least 30min at -20°C, then centrifuged at 4°C, 10min, 13200rpm and the final RNA pellet was washed with 1mL 70% ethanol. Pellets were resuspended in 50µl RNase-free H_2O.

Residual DNA present in the samples was removed by treatment with 4U DNaseI (1U/µL, RQ1 DNaseI, Promega) and 1X DnaseI buffer. DNase was then removed by Phenol-Chloroform-Isoamylic Alcohol Extraction (25:24:1) and RNAs were washed with Chlororoform-Isoamylic Alcohol (24:1). Finally, RNAs were precipitated overnight at -20°C, in 63% ethanol and 0.1M NaOAc pH5.2, and then washed with 1mL of 70% ethanol. The RNA pellet was dried out and resuspended in 32µl of sterile water and quantified using a NanoDrop-1000 Spectrophotometer (Thermo Fischer Scientific).

IV.4 – cDNA synthesis

Reverse transcription for semi-quantitative and quantitative PCR (qPCR) was carried out with 1.5µg of RNA heated for 5min at 70°C with 0.04µg/mL of oligodT. The reverse transcription (RT+) was then carried out by adding 200units of M-MLV Reverse Transcriptase (Promega, 200U/µL) for 1h at 42°C, 1X M-MLV RT buffer, RNasin buffer (40U/µL) and 0.5mM dNTPs. A negative control of reverse transcription (RT-) was performed under the same conditions without the enzyme. Finally, the cDNAs were diluted in sterile water (1:3) and 4µl used as a template for the semi-quantitative PCR (see ***Appendix I*** for primers).

IV.5 – PCR

Genotyping was carried out by PCR amplification using the GoTaq G2 Flexi polymerase (Promega) and 1 to 2µl of DNA template with the specific primers of the gene of interest or of the T-DNA insertion for the mutant lines. The list of primers used is given in ***Appendix I***. General PCR conditions were a first step of DNA denaturation at 95°C for 3min,

then a cycle repeated 36 times composed of one step of DNA denaturation at 95°C for 30sec, one step of annealing for primers at 52°C for 30sec and one step of DNA elongation at 72°C with 1min per Kb depending on the fragment size amplified. Afterwards, a final elongation at 72°C for 10min and a cooling until 20°C were applied.

IV.6 – Agarose gel electrophoresis

PCR products, gDNA and linearised plasmids were separated on 1.5 to 2% agarose gels prepared in 1X Tris Acetate EDTA buffer (TAE: 40mM Tris, 20mM acetic acid and 1mM EDTA). The agarose solution was heated in a microwave until it polymerised and was allowed to cool to 50°C, before addition of 0.625µg/mL of ethidium bromide (Thermoscientific) and pouring into a gel cast. If use of the GoTaq buffer without dye, 5 to 10µl of PCR product was diluted in 6X gel loading dye (NEB) and loaded into the agarose gel wells submerged in 1X TAE buffer. Alongside DNA samples, 6µL of Quickload® 100bp or 1kb+ DNA ladder (NEB) was also loaded. Gels were run at 100V until the dye front reached the end of the gels. DNA bands were imaged using a UV transilluminator (Ultra-Violet Products Ltd., Cambridge, UK) and Uvisave gel documentation camera (UVItec Ltd., Cambridge, UK).

IV.7 – List of vectors

A list of vectors is provided as supplemental tables at the end of this thesis, (***Appendix III, Appendix IV*** and ***Appendix V***).

IV.8 – Gateway cloning

Most of the constructs in this study were generated using Gateway technology (Marsischky and LaBaer, 2004). The first reaction of the Gateway system involves a plasmid pDONR which contains attB1 and attB2 recombination sites, an insertion zone for the DNA

fragment to be cloned, as well as antibiotic resistance allowing the selection of the transformed bacteria. All vectors used for this study are detailed in section ***IV.7*** and ***Appendix III.***

Fragments of interest were amplified by PCR under standard conditions using specific primers containing the Gateway attB1 and attB2 sequences at 5' and 3' ends of the fragments (see ***Appendix II*** for primer sequences). Sequences of interest were then integrated into the pDONR-vector by a BP reaction. For this, 200ng of PCR products flanked at each end by the attB regions were mixed with 1µl BP clonase ™ II enzyme mix and 150ng of the pDONR-vector in a final volume of 5µl. The reaction mixture was incubated at 25°C for at least 1h and then 1µL of proteinase K (2µg/µL) was added to the mixture for 10min at 37°C to remove the recombinase. This first step yielded the pDONR plasmid containing the gene-of-interest associated with the specific antibiotic resistance cassette. Plasmids were then transformed into DH5α *E. coli* (see ***II.3***) grown on specific plates (see ***II.2***).

pDONR plasmids amplified by well-transformed DH5α *E. coli* were extracted as described below (see ***IV.9***), and submitted to a LR reaction after having been validated by sequencing. For that, 200ng of pDONR clones were mixed with 1µL LR clonase enzyme and 150ng of the destination vector, pDEST (see ***IV.8*** and ***Appendix IV***) in a final volume of 5µL. The reaction mixture was treated and inactivated as described above and pDEST plasmids transformed into DH5α *E. coli* (see ***II.3***) grown on specific plates (see ***II.2***).

pDEST plasmids amplified by well-transformed DH5α *E. coli* were extracted as described below (see ***IV.9***) and quality controlled by sequencing. When validated, they were either transformed into *A. tumefaciens* (see ***II.4***) for plant transformation (see ***III.5*** and ***III.6***) or into *S. pombe* (see ***I.3***) for Y2H (see ***I.4***).

IV.9 – Plasmid DNA extraction

"NucleoSpin Plasmid – Plasmid DNA Purification" from Macherey-Nagel and "Monarch Plasmid Miniprep Kit" from NEB were used for plasmid DNA extraction according to the manufacturer's protocol.

V – Protein

V.1 – Protein extraction

For controls in Y2H experiments (see ***I***), but also to test antibodies (see ***V.4*** and ***Chapter 4-III***), protein extracts were obtained from yeast colonies by resuspending them in 300µL of TCA Buffer (10mM Tris-HCl pH8, 20% TCA, 25mM NH_4OAc and 1mM EDTA) followed by an addition of about 100µL of glass microbeads and an incubation of 5min at -80°C. Solution was then vortexed for 1min and incubated on ice for 3min. This step was repeated three times. Lysate was transferred in a new tube (without beads) and washed 2 times with 100µL of TCA Buffer in order to isolate a maximum of proteins. Lysate was centrifuged for 10min at 4°C at 16000g and pellet resuspended in 150µL of Resuspension Buffer (100mM Tris-HCl pH11, 3% SDS). Finally, 150µL of 2X Laemmli buffer was added and samples denatured at 65°C for 10min before loading supernatants on a gel.

Total protein was extracted from non-infiltrated and transiently expressing *N. benthamiana* leaves for western blot analysis (see ***III.5***). Weighed empty 15mL tubes were placed in liquid nitrogen together with a mortar, pestle and spatula to precool. Two to four leaves per sample were cut and veins and midrib were removed. Leaves were ground to a fine powder in liquid nitrogen; the powder was then transferred into the cold 15mL tubes.

A first extraction buffer, developed to extract highly insoluble proteins, was used (0.1M Tris-HCl (pH 6.8), 4.5M Urea, 1M Thiourea, 2% CHAPS, 0.5% Triton X-100, 0.01M DTT, 1% Protein Inhibitor Cocktail (PIC, Sigma P9599-IML), Benzonase, 1.10^{-6}M PMSF).

For each 1g of plant material, 1mL extraction buffer was added. Samples were incubated at 4°C for 1h on a rotating mixer, then centrifuged at 13300rpm, 4°C for 10min. Supernatants were stored at -80°C before proceeding to protein precipitation with 10% of protein extract, 80% ice cold acetone and 10% TCA. Samples were left overnight at -20°C, then centrifuged at 4°C, 13000rpm for 15min. Pellets were washed twice with ice cold acetone and the centrifugation repeated (1mL acetone then 0.5mL in 2mL tubes). Afterwards, all acetone was removed and pellets were resuspended in SDS gel loading buffer (0.0625M Tris-HCl (pH 6.8), 25% Glycerol, 2% SDS, 0.05% Bromophenol blue, 8M Urea, 0.35M DTT; with the DTT stored at -20°C and added just before use). Samples were stored at -20°C.

A second extraction buffer was used in order to enrich protein extracts in nuclei. As previously, proteins were extracted from non-infiltrated and transiently expressing *N. benthamiana* leaves and also from three-week-old *A. thaliana* seedlings grown on plates (see *III-B.*). This buffer was adapted from Xia *et al*, 1997, named "Honda buffer" and composed of 2.5% Ficoll 400, 5% Dextran T40, 0.4M Sucrose, 0.035M Tris-HCl pH7.4, 10mM $MgCl_2$, 2.5mM DTT, 0.5mM PMSF, 0.1% Protease Inhibitor Cocktail (PIC). Once tissue was ground into powder, it was resuspended with 10mL of ice-cold Honda buffer per 1g of plant material. The mixture obtained was filtered through two layers of Miracloth (Calbiochem) and 0.5% (final concentration) Triton X-100 was added to the filtrate. Samples were incubated for 15min at 4°C on a rotating wheel (with head to tail rotation) and then centrifuged at 1500g at 4°C for 5min. Pellets were washed in 1mL Honda buffer to which Triton X-100 had been added to a final concentration of 0.1%, then centrifuged at 1500g, 4°C for 5min and finally washed with 1mL Honda buffer without Triton X-100 before the centrifugation step was repeated. Nuclei pellets were resuspended with 300µL SDS loading buffer or Laemmli 2X (Laemmli buffer (BIORAD) + β-mercaptoethanol 0.7M) and then stored at -20°C.

In order to prepare a protein extract enriched in nuclei and ready for an immunoprecipitation (IP) protocol, an adapted Honda protocol and buffer were used. Honda buffer 2 was made up with 0.02M Tris-HCl pH7.4, 0.44M Sucrose, 1.25% Ficoll 400, 2.5% Dextran T40, 0.01M $MgCl_2$, 0.5% Triton X-100, 0.005M DTT, 0.1% PIC (Roche, cOmplete and cOmplete Mini). Once tissue was ground into powder, resuspension was made with 30mL of ice-cold Honda buffer 2 per 4g of plant material. The mixture obtained was filtered through two layers of Miracloth (Calbiochem) and centrifuged at 2000g, 4°C for 15min. Nuclei pellets were transferred into 1.5mL tubes and washed from one to three times with 1mL Honda buffer 2 and centrifuged at 13000rpm, 4°C for 10min and resuspended in IP buffer (Law *et al*., 2010).

V.2 – Sodium Dodecyl Sulfate Polyacrylamide gel electrophoresis (SDS-PAGE)

Fresh 8% and 10% SDS gels were prepared (resolving gel: H_2O, 8% or 10% Acrylamide, 0.375M Tris-HCl (pH 8.8), 0.1% SDS, 0.05% APS, TEMED; stacking gel: H_2O, 4% Acrylamide, 0.125M Tris-HCl (pH 6.8), 0.1% SDS, 0.05% APS, TEMED). Precast gels from BIO-RAD were also used (8-16% and 10% Mini-PROTEAN TGX Precast Protein Gels).

For PAGE and blotting (see ***V.3***), the BIO-RAD miniprotean system was used. The gels were submerged in 1X Tris-Glycine electrophoresis buffer (5X (1L): 15.1g Tris Base, 94g Glycine, 10% SDS, H2O). Before loading on a gel, samples were boiled at 90°C for 5min or incubated at 37°C for 30min and centrifuged at 16000g for 5min. Gels were run at 150V for 15min and then at 100V for approximately 90min or until the samples had migrated through the gel. The “Precision Plus Protein™ Dual Color Standards” molecular mass marker ladder from Bio-Rad was used for every gel.

Table 2.5: Dilutions of antibodies used in this study

Antibodies & Fluorescent dyes		WB immunostaining
Primary Antibodies	Anti-GFP	1 in 3000 in 3% skimmed milk PBST
	Anti-NEAP1/2	1 in 250 in 3% skimmed milk PBST
	Anti-NEAP wobble	1 in 50 in 3% skimmed milk PBST
Secondary Antibodies	Goat anti-rabbit Cy5	1 in 400 in 3% skimmed milk PBST
	Goat anti-rabbit HRP	1 in 1000 in 3% skimmed milk PBST

V.3 – Western blotting and immunostaining

Three types of membrane were used for blotting including nitrile, PVDF or nitrocellulose membranes. Gels were transferred for 1h at 100V at RT in a BioRad Mini-protean II gel tank with an ice pack and 1X transfer buffer (10% 10X stock [1L: 144g Glycine, 30g Tris-Base, H_2O], 20% methanol, 70% H_2O ice-cold). Some gel transfers were also been carried out with the Trans-Blot Turbo^{TM} Transfer System from BIO-RAD, using BIO-RAD reagents for western blotting.

After transfer, membranes were placed for a few minutes in Ponceau S Staining Solution (0.1% (w/v) Ponceau S in 5% (v/v) acetic acid) to stain total proteins, then rinsed in Phosphate Buffer Saline (PBS). Membranes were blocked with 5% skimmed milk in PBST (0.5% Tween-20 in 1X PBS) for 1h on rotator. Then, blocking solution was replaced by primary antibody (IAb) solution (diluted in PBST-3% skimmed milk, see ***Table 2.5***), and left to incubate O/N rotating at 4°C and 10min at RT. Next, IAb was removed (and stored at -20°C for further use) and the membrane was washed 3 times quickly and 3 times for 10min with PBST. A secondary antibody (IIAb, diluted in PBST-3% skimmed milk, see ***Table 2.5***) was incubated for 1h in the dark at RT. Lastly, membranes were washed 3 times quickly and 3 times for 10min with PBST and stored in PBS at 4°C until imaging (in the dark).

V.4 – Antibody design

Peptides were designed to be highly specific to AtNEAP protein sequences (Eurogentec, Ltd, Southampton, UK). The first peptide (-QLDDKTRSLRE-) was specific to AtNEAP1 and AtNEAP2, including splicing variants, and antibodies generated for this study were named “anti-NEAP1/2”. The other peptide, (-H-DL-D/G-E/H-KK-E/H-SFRRNVVS-C-NH_2-), was specific to all three AtNEAPs but only for a small part of the peptide, the other part being a “wobble” version of the three sequences and antibodies generated with this

sequence were named anti-NEAP wobble. (See ***Figure 4-8***). Before rabbit immunization, pre-immune sera were tested and the results are detailed in ***Chapter 4-III*** and ***Figure 4-9***. Two rabbits were selected and immunized by Eurogentec with the two different peptides according to their "p28 day speedy protocol". At the end of the immunization program, Eurogentec evaluated the antibody titre by ELISA before affinity purification on a peptide column. Final volume before purification was about 30mL and quantity received for purified antibodies from one of the two rabbits were 3.4mL for anti-NEAP1/ 2 (2265µg/mL) and 3.2mL for anti-wobble (406µg/mL). Once the purified polyclonal antibodies received from the company, experiments were carried out to further test and optimize their use.

VI – Microscopy

VI.1 – Wide field microscopy

A MAAF DM 6000 (Leica-microsystems) wide field microscope was used with an Optigrid module for structured illumination and a sCMOS camera (ORCA FLASH 4.0 Hamamatsu) to capture large images of 6.5µm² with 2048x2048pixels containing up to 20-100 nuclei (XY= 0.103µm, Z= 0.2µm). The Optigrid module allowed an automatic deconvolution of the image.

VI.2 – Nuclear and chromatin organization measurements

From 3D image stacks acquired with the wide field microscope (see ***VI.1***), nuclear organization (nuclear morphology and chromatin organization) was quantified using an *ImageJ* plugin named *NucleusJ* (Desset *et al*., 2018; Poulet *et al*., 2014). It included all the necessary steps to process images of nuclei, to perform various analyses and to provide several quantitative parameters to describe the original image. *NucleusJ* then provided a set of

parameters including shape and size of nuclei, size and number of chromocentres as well as their position inside the nucleus relative to the nuclear periphery.

VI.3 – Confocal Imaging

At least two days post-infiltration of *N.benthamiana* leaves (see ***III.5***), transient protein expression was visualised and assessed by a Zeiss LSM 880 confocal microscope and with associated software (ZenLite 2012).

For ***live cell imaging***, an approximate 0.5cm^2 piece of infiltrated leaf was cut out and mounted in water on a microscope slide. A cover slip and a drop of oil were added. The x63 oil immersion lens with x2 zoom factor and CFP laser (10%) and YFP laser (1%) were used to excite, respectively, CFP at 458nm and YFP at 514nm. Emission of CFP was captured by a channel between 463-494nm and YFP emission was captured by second channel between 520-568nm. The pin hole was set at 0.9µm section to avoid cross-channel bleed (1.35 Airy Unit).

VI.4 – apFRET

Acceptor photobleaching Fluorescence Resonance Energy Transfer (apFRET) is based on CFP and YFP fluorophores. As the spectrum of CFP emission and YFP excitation overlap, CFP has the potential to transfer its emission energy to excite YFP. CFP is thus the "Donor" and YFP the "Acceptor". Energy absorption by YFP is possible only if the two fluorophores are close enough to each other (<100Å). By bleaching YFP, there is no further energy absorption of CFP emission and a resulting rise in CFP emission. FRET efficiency (EF) is then calculated, defining the percentage of energy transferred between the two fluorophores. This is the percentage of rise of CFP emission between pre-bleach and post-bleach images.

To adapt this system for studying protein-protein interactions, one protein is fused to CFP and the other to YFP. If a rise in CFP fluorescence is observed, it indicates that CFP and

YFP were close enough to each other for energy transfer and suggests binding interactions for proteins of interest, (Karpova and McNally, 2006; Karpova *et al*., 2003). All apFRET experiments were performed by adapting the methods described by Graumann *et al*., 2010 using the Zeiss LSM 880 confocal microscope and settings as described above (see ***VI.4***). YFP emission was also measured as a control of YFP bleaching.

A rectangular region of interest (ROI) of 177µm^2 was drawn over a focussed region of NE that was then bleached with 40 iterations of the 514 nm laser at 100%. A total of 50 images were taken at the scan speed of 1 scan per second, 5 before bleaching and 45 post-bleach for a total of 100 constant sized ROI using independent nuclei for every combination of constructs tested.

EF was calculated by subtracting the first post-bleach value from the last pre-bleach value. For control CFP fluorescence values, each pre-bleach fluorescence was subtracted from the previous pre-bleach fluorescence value. The mean of these differences was set as the control EF value and reflected the normal change in CFP fluorescence during imaging.

EF was calculated using the formula $EF = I_t/I_{pre} \times 100$, where I_t is the difference of CFP fluorescence between post- and pre-bleach images, and I_{pre} is the average of pre-bleach CFP fluorescence. EF was expressed as its mean + standard error of the mean (SEM) and was compared to a non-bleached control (control CFP fluorescence before bleaching).

VII – Statistical analysis

The first step of the statistical analysis, carried out in Excel, was to test the equality of variances with an F-test. When the p-value obtained was <0.05, a t-test for unequal variances was carried out. When a p-value of >0.05 was obtained, a t-test for equal variances was carried out. For both t-test, when the p-value was <0.05, the difference between variances was

considered as significant and when the p-value was >0.05, it was determined to be not significant.

VIII – Bioinformatics

VIII.1 – ImageJ

Two main plugins of *ImageJ* (https://imagej.nih.gov/ij/) were used: *NucleusJ* to quantify Nuclear morphology (see ***VI.2***) and SIOX (Simple Interactive Object Extraction) to quantify leaf surfaces during phenotypic analysis of plant material. To measure root growth, the « straight line » tool in *ImageJ* was used.

VIII.2 – Software/Websites

Software used during this study was principally the Microsoft Office package and Adobe Illustrator. For designing primers, cloning *in silico* and sequencing analysis, the Primer3 website (https://primer3.org/), GenePalette (http://www.genepalette.org/), Serial Cloner (http://serialbasics.free.fr/Serial_Cloner-Download.html) and CodonCodeAligner (https://www.codoncode.com/aligner/download.htm) software were used. For image analysis, *ImageJ* (see above paragraph *VIII.B*), and ZenLite 2012 from Zeiss were used (https://www.zeiss.com/microscopy/int/products/microscope-software/zen-lite.html. Finally, for graphs, RStudio (https://www.rstudio.com) and StatGraph (www.statgraphics.com) were used.

RESULTS

CHAPTER 3

Characterization of the AtNEAP protein family

CHAPTER 3
Characterization of the AtNEAP protein family

The function of the AtNEAP protein family at the nuclear periphery remains to be elucidated. In order to investigate the potential role of these proteins in *A. thaliana*, a range of phenotypic analyses have been performed on different combinations of *Atneap* single, double and triple mutants.

In the first instance, only the single mutants *Atneap1* and *Atneap3* and the double *Atneap1Atneap3* mutant were available, with the *Atneap1Atneap3* knock-out (KO) mutant showing reduced primary root growth, (Pawar *et al*., 2016). Before obtaining a triple *neap* KO mutant, an *Atneap2* KO mutant was created using the CRIPSR/Cas9 technique and subsequently crossed with an *Atneap1Atneap3* double mutant. Phenotypic analysis and assessment by *NucleusJ* software, (Poulet *et al*., 2014), of nuclear morphology and chromatin organization changes have been undertaken on two types of leaf epidermal cell populations, pavement and guard cells.

I – Characterization of the triple neap mutant obtained from T-DNA insertion alleles

T-DNA insertion alleles for the three *AtNEAP* genes have been obtained from NASC and crossed to obtain double and triple mutants (Pawar-Menon, PhD thesis, 2015). In order to define if these mutants were loss-of-function, *AtNEAP* transcript levels were assessed by designing specific primer pairs, surrounding the T-DNA insertion sites (pair n°1) or located downstream the T-DNA insertion sites (pair n°2), (Pawar *et al*., 2016).

Plants used were three week-old *Atneap1Atneap2Atneap3* triple mutant (called *first triple*, see ***Methods III.1***) and wild type Col-0 as a control. Total transcript level was assessed

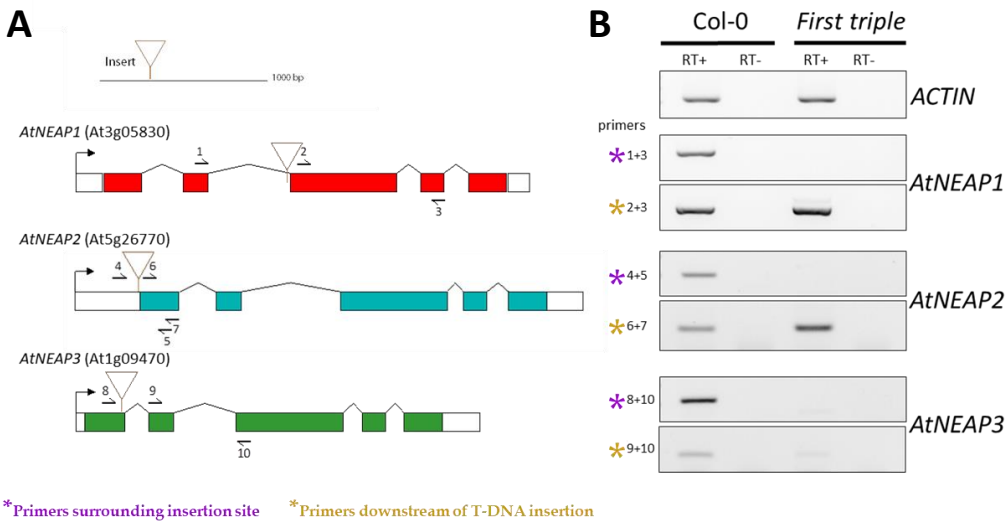

Figure 3-1: Transcript analysis of the *first triple* mutant. **A.** Representation of DNA structures of every *AtNEAP* gene, T-DNA insertions and primer positioning (arrow + number). Exons are indicated as coloured boxes and introns with lines. **B**. Expression of *AtNEAP* genes was assessed by RT-PCR using primers described in A (asterix + primer combination on the left) in wild type (Col-0) and *first triple neap* mutant. Primer pair n°1 surrounding the insertion site (purple), primer pair n°2 downstream of the insertion site (orange). *ACTIN* gene (*ACT2*, At3g18780) was used as a control. RT+ and RT-: with or without reverse transcriptase.

by comparison with *ACTIN* as a reference gene (***Figure 3-1***) using semi-quantitative RT-PCR.

First, the results from the RT-PCR confirmed the T-DNA insertions sites as no bands were detected in the *first triple* mutant with primer pair n°1 for all three *AtNEAP* genes (***Figure 3-1B***). For *AtNEAP1*, a transcript 3' of the T-DNA insertion is visible with primer pair n°2 but given the results from primer pair n°1, this is only a partial transcript potentially initiating in the T-DNA. For *AtNEAP3*, only a phantom band corresponding to a transcript in 3' of the T-DNA insertion was visible with primer pair n°2. It is quite common with T-DNA insertion in plants to observe partial transcripts initiated 3' of the T-DNA insertion although these transcripts are usually not functional. Hence, the *Atneap1* and *Atneap3* alleles are likely loss-of-function, *i.e.* Knock-Out (KO) alleles or at least Knock-Down (KD), (***Appendix VII***, Fig.7H-I in Pawar *et al*., 2016). For *AtNEAP2*, a transcript 3' to the T-DNA insertion is also visible with primer pair n°2 but this time considering the position of these primers next to the beginning of exon 1, the transcript could be similar to the full length and functional. So, *Atneap2* is likely a functional allele of *AtNEAP2*.

Thus, these results indicated that the *first triple* mutant although containing three T-DNA insertions in each of the *AtNEAP* genes cannot be considered as a complete *AtNEAP* loss-of-function. As no specific antibody was available at that stage of the work to confirm the absence of AtNEAP proteins, it was decided to create a new *Atneap2* KO mutant using the CRISPR/Cas9 technique.

II – Generation of an Atneap2 KO mutant using CRISPR/Cas9 technology

The Cas9 enzyme is able to make a DNA double strand break at specific sites of the genome recognised by a small guide RNA (sgRNA), which recruits the Cas9 enzyme. This system can be adapted in order to choose a specific site where a break is wanted. Due to repair

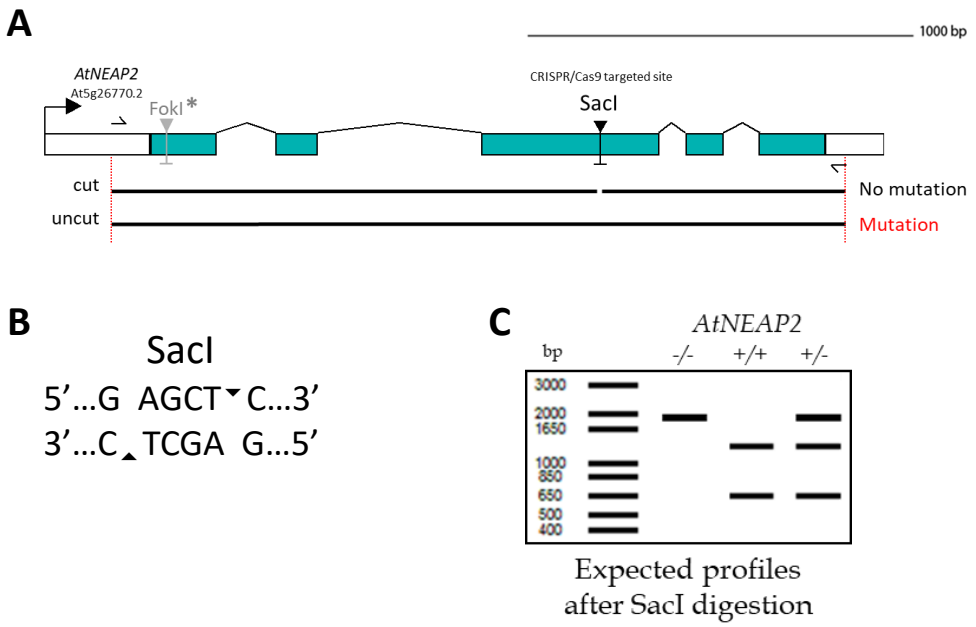

Figure 3-2: Details of *AtNEAP2* targeted site for CRISPR/Cas9. **A.** *AtNEAP2* gene sequence with the targeted site chosen in exon 3 with SacI enzyme restriction site. Primer position used for PCR amplification and expected PCR products are indicated below the gene structure. **B.** Target motif of SacI restriction enzyme. **C.** Expected profile of a mutant for exon 3 targeted site. *FokI restriction site was another CRISPR/Cas9 target site but no mutants were obtained.

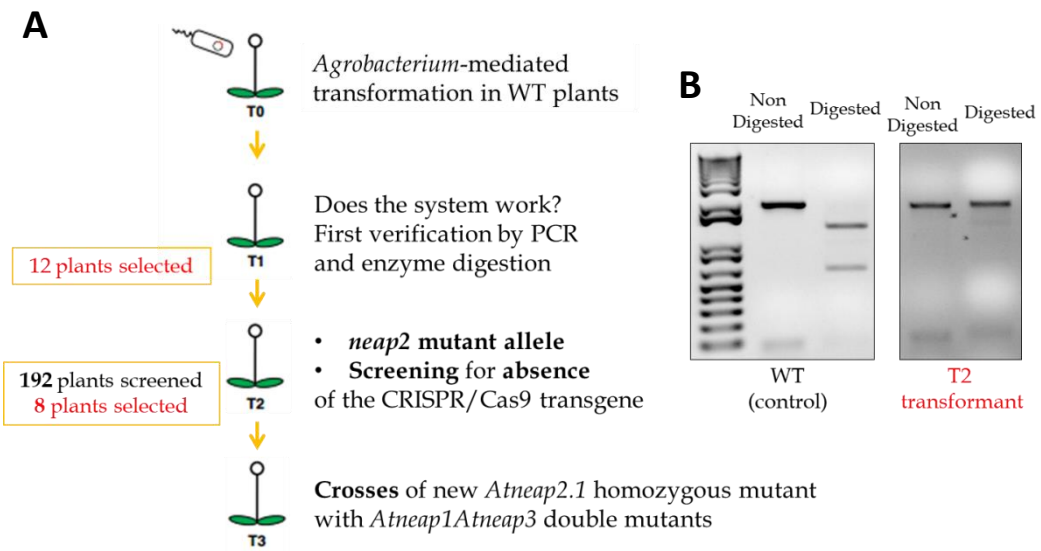

Figure 3-3: Detailed procedure for selection of CRISPR/Cas9 mutants. (adapted from Fauser et al., 2014). **A.** Steps towards the mutant selection. **B.** Typical result after SacI digestion of a wild type (left) and mutant plant (right).

of this DNA double strand break (DSB) by the cellular machinery, mainly through non-homologous-end-joining (NHEJ) in plants (Schiml *et al*., 2017). Different mutations will be created in the gene by addition or deletion of one or more bases.

For the *AtNEAP2* gene, two different target sites were chosen (***Figure 3-2***), and two special Destination vectors were created using Gateway technology, containing the sgRNA sequence specific to one or the other site chosen and also containing the Cas9 gene sequence, (Schiml and Puchta, 2016). Then, plants were transformed via *Agrobacterium tumefaciens* bacteria previously transformed with the cloned vectors.

Target sites chosen were in the first and in the third exons (or second and fourth exons depending on the splicing variant) due to the presence of a restriction site to facilitate screening of mutant plants. When a mutation is present at the target site, the restriction site is destroyed, giving loss-of ability for the restriction enzyme to recognize its site and to cut. In this way, it was possible to screen plants more easily, which have mutations in the *AtNEAP2* gene, (***Figure 3-2***).

Before obtaining a new homozygous mutant for *AtNEAP2*, selections over several generations were required. The first generation (T1) of transformed plants was treated with BASTA antibiotic to select plants, which had incorporated the T-DNA present in the cloned destination vector. Selected plants were left to grow until next generation, as mainly somatic mutations are expected since the Cas9 enzyme is expressed under the Ubiquitin promoter. Then, T2 plants were screened for two different parameters: presence or absence of the CRISPR/Cas9 transgene by PCR with specific transgene primers; and presence of a mutation in the *AtNEAP2* gene by PCR followed by an enzyme digestion of PCR products (***Figure 3-3***).

Plants, which had lost the CRISPR/Cas9 transgene and presenting a full-length band for the *AtNEAP2* gene after digestion, *i.e.* resistant DNA to digestion by restriction enzyme,

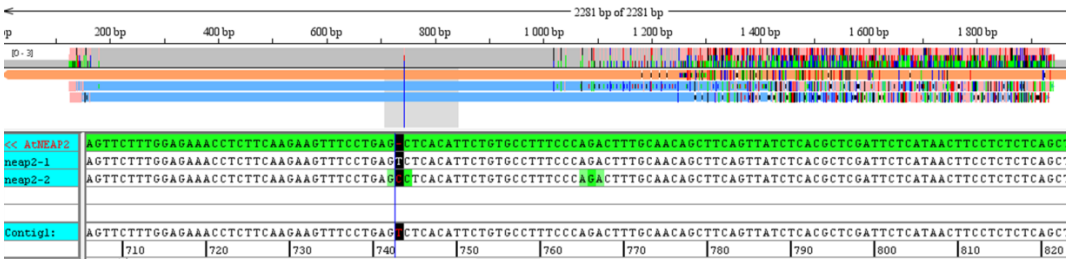

Figure 3-4: Alignment of sequences of *Atneap2-1* and *Atneap2-2* mutants after *AtNEAP2* full length amplification by PCR and sequencing. Software: CodonCodeAligner.

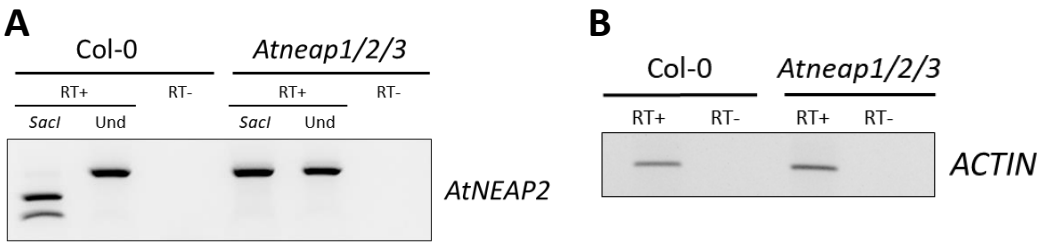

Figure 3-5: Transcript analysis of the *Atneap1/2/3* triple mutant.
A. Transcript accumulation of *AtNEAP2* in wild type (Col-0) and in *Atneap1/2/3*. A transcript is still produced in the *Atneap1/2/3* mutant but presence of the mutation is confirmed as the mutant transcript is resistant to SacI digestion. **B.** Transcript accumulation of the *ACTIN* gene (*ACT2*, At3g18780) is used as a control.

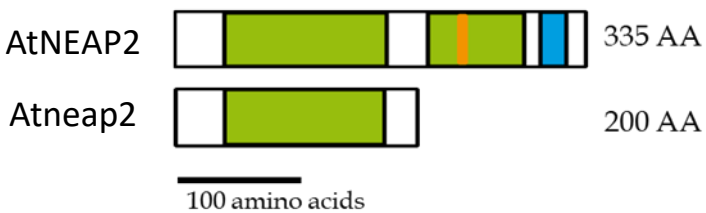

Figure 3-6: Schematic representation of wild type and putative mutant forms of AtNEAP2 proteins. Putative AtNEAP2 would be only 200 amino-acids long and miss one Coiled-Coil domain (green), the Nuclear Localisation Signal (orange) and the Transmembrane Domain (blue).

signifying mutation in the sequence, were grown to the next generation. At that step, only mutations in the fourth exon were obtained, so no further experiments have been carried out to obtain a mutant allele on the second exon as this did not work at the first attempt. T3 plants were then subjected to the same form of selection as for T2, potential homozygous mutants being expected at this stage. Finally, selection was carried out on the next generation (T4) and two different mutant alleles on the fourth exon were obtained for *AtNEAP2*, respectively named *Atneap2-1* and *Atneap2-2*. These two mutants have a single nucleotide insertion in the central exon, a T in position 743 for *Atneap2-1*, and *Atneap2-2* was a probable transheterozygous, e.g two different versions of the insertion at the same position, (***Figure 3-4***).

Each *Atneap2* mutant was then crossed with the *Atneap1Atneap3* double mutant and T2 generations were genotyped in order to find the triple *Atneap* mutant. The probability was only 1/64 to find it in this generation, so plants homozygous mutant for two genes and heterozygous for the third gene were selected in order to obtain the triple mutant easily in the next generation (1/4), and also to be able to see if the triple *neap* mutant was lethal.

Three triple *neap* mutant plants were finally obtained with the *Atneap2.1* allele and the further studies carried out were with the single *Atneap2.1* and triple *Atneap1Atneap2.1Atneap3* (named *Atneap1/2/3*) mutants.

In the meantime, further characterization of the *Atneap2.1* mutant was carried out with RT-PCR analysis and revealed that a transcript was still produced but contained the mutated SacI site, which is easy to follow by using this specific restriction enzyme. (***Figure 3-5***). *In-silico* studies indicated that an early stop codon appears after the insertion site, potentially leading to a truncated protein missing its NLS, one CC domain and the TM domain, (***Figure 3-6***, ***Appendix V***). *In vivo* studies with transient expression in *N. benthamiana* plants of a similar AtNEAP2 truncated protein (missing NLS, one CC and TM domains) fused to a GFP

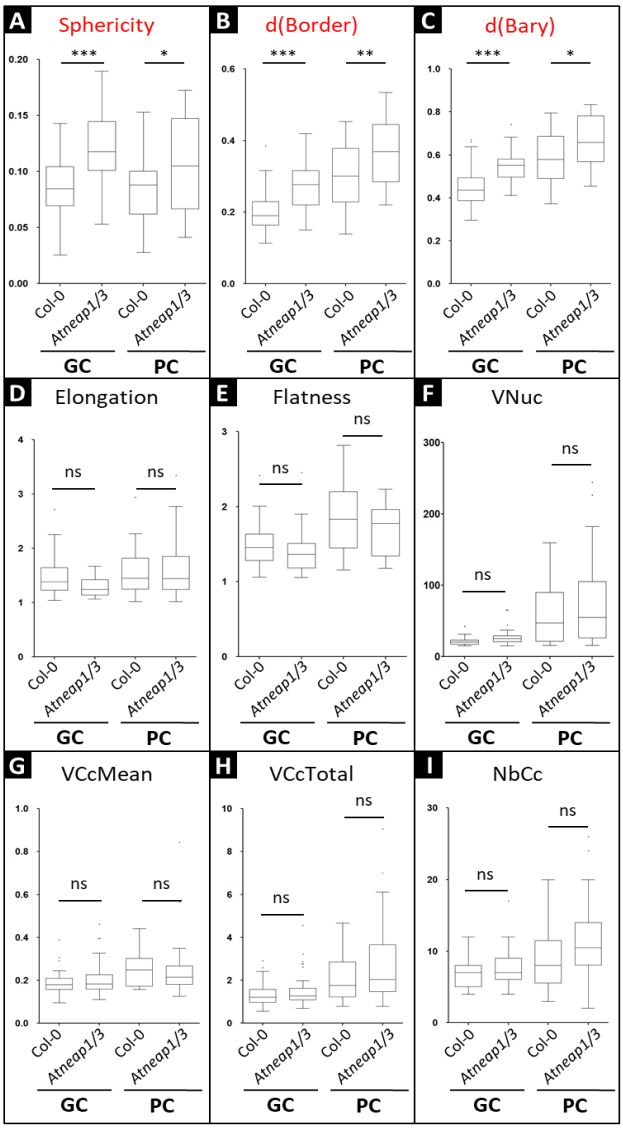

Figure 3-7: Nuclear morphology parameters in *Atneap1Atneap3* double mutant (*Atneap1/3*) and a wild type Col-0 as a control. Plantlets of 14 dag were grown on MS medium. For the guard cell population (GC), a total of 54 nuclei for Col-0 and 63 nuclei for *Atneap1/3,* and for the pavement cell population, a total of 21 nuclei for Col-0 and 36 nuclei for *Atneap1/3* were assessed by *NucleusJ* software. ns: non significant; Nine parameters are shown: sphericity (**A**), distance from chromocentre border (**B**, d(Border)) or barycentre (**C**, d(Bary)) to the NE, elongation **(D),** flatness **(E),** volume of the nucleus (**F**, VNuc), mean of the chromocentre volume (**G**, VCcMean), total volume of chromocentres (**H**, VCcTotal) and number of chromocentres (**I**, NbCc).
ns: non significant; *p< 0.05 ; ** p<0.01 ; *** p<0.001.

tag indicated that the truncated protein is not localised in the nucleus and displays a weak and diffuse GFP staining of the tobacco cells suggesting an unstable protein with a rapid turn-over, (data not shown).

Thus, it seems that the truncated AtNEAP2 protein is no longer nuclear and that the CRISPR/Cas9 induced mutation created a new KO *Atneap2* allele named *Atneap2.1*.

III – Phenotyping and studying nuclear organisation of neap mutants

As mutants of NE proteins often lead to alteration of nuclear shape and/or size, as a first attempt, nuclear morphology of single and double *Atneap* mutants was investigated in root hair cells containing elongated nuclei. However, this assay did not show obvious differences to wild type plants (Pawar *et al*., 2016). In order to establish if there are changes in nuclear morphology or chromatin organisation in a more quantitative manner, calculations from 3D images were carried out, using *NucleuJ* plugin into *ImageJ* software, this time on epidermis cells.

The first experiment used three week old seedlings and was carried out in triplicate with the *Atneap1Atneap3* double mutant (*Atneap1/3*) and a wild type (WT) Col-0 as a control. Results showed that two parameters were significantly modified in the mutant compared to WT; nuclear sphericity and the distances of chromocentre border or barycentre to the nuclear periphery, which were increased in both cell populations studied, namely pavement and guard cells, (***Figure 3-7A-C***). Other parameters, elongation, flatness, nuclear volume, chromocentre volume and number of chromocentres remained constant in the mutant compared to WT, (***Figure 3-7D-I***).

Although no specific phenotype had been observed for single *Atneap1* and *Atneap3*, phenotypic analysis was carried out on the new *Atneap2.1* mutant obtained as well as on the triple *Atneap1/2/3* mutant once available, ***Figure 3-8***. Different growth phenotypes were

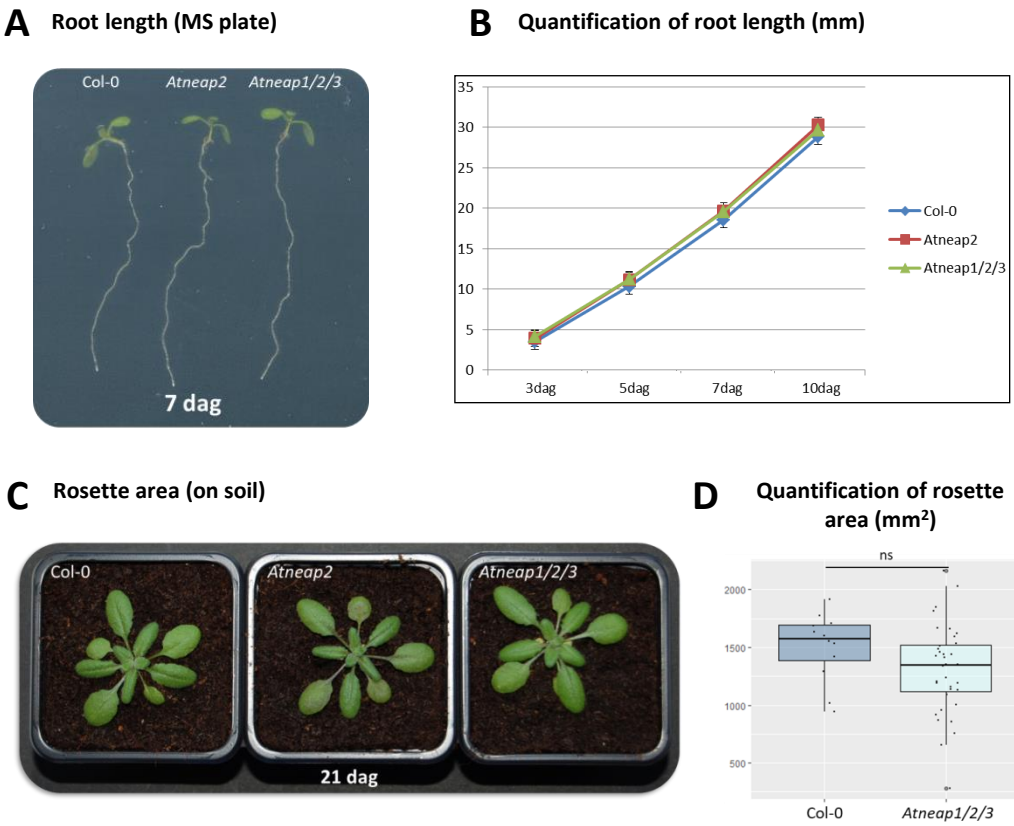

Figure 3-8: General growth phenotype of *Atneap2.1*, *Atneap1/2/3* compared to a wild type Col-0. A. Plantlets of 7dag grown on MS medium. **B.** Quantification of root length (mm) at four time points 3, 5, 7 and 10dag. **C.** Rosette of 21dag plants grown on soil. **D.** Quantification of rosette area (mm^2) of 22dag plants. ns: non significant; * $p< 0.05$; ** $p<0.01$; *** $p<0.001$.

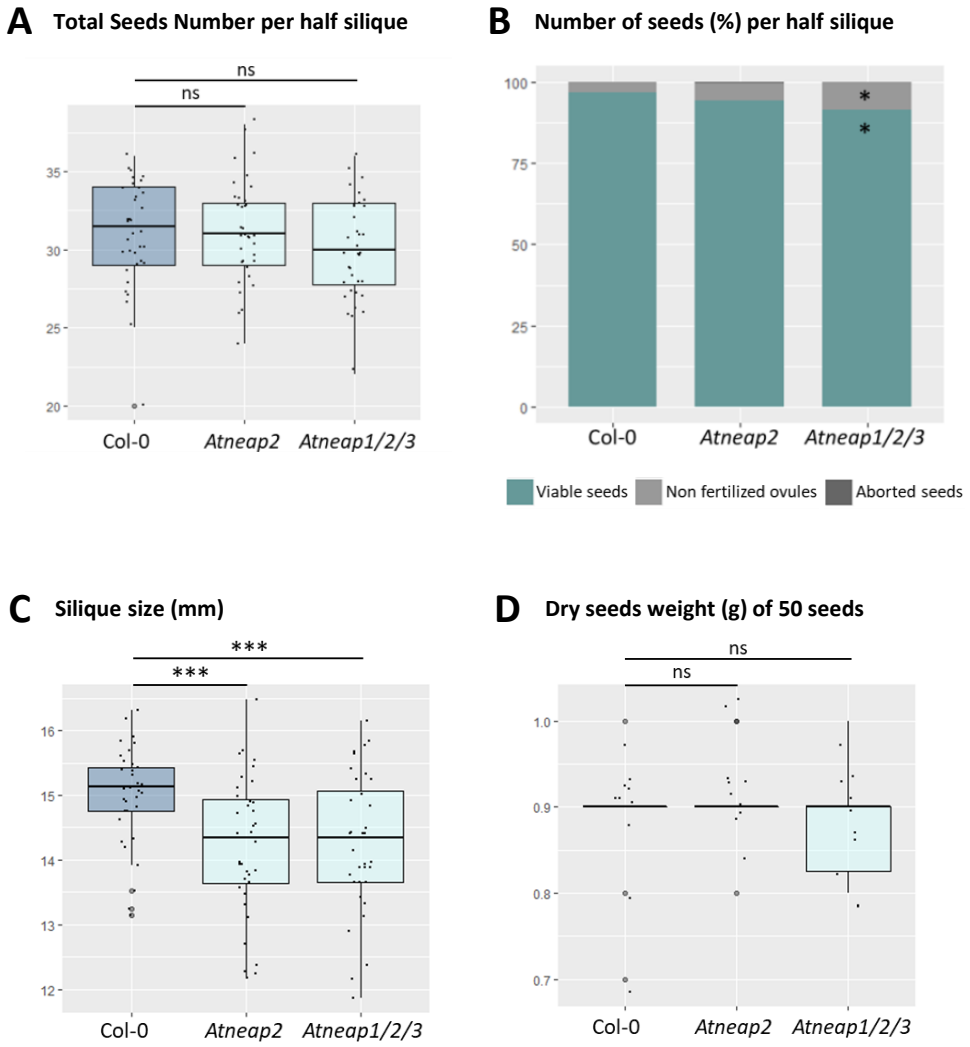

Figure 3-9: Phenotypic analysis of *Atneap2.1*, *Atneap1/2/3* compared to a wild type Col-0. A. Total seeds number per half silique, n=30. **B.** Number of seeds (%) per half silique, n=30. **C.** Silique size (mm), n=30. **A, B, C.** All the plants were grown on soil for a total of 12 plants per genotype. **D.** Dry seeds weight (g) of 50 seeds, n=500.

ns: non significant; * $p< 0.05$; ** $p<0.01$; *** $p<0.001$.

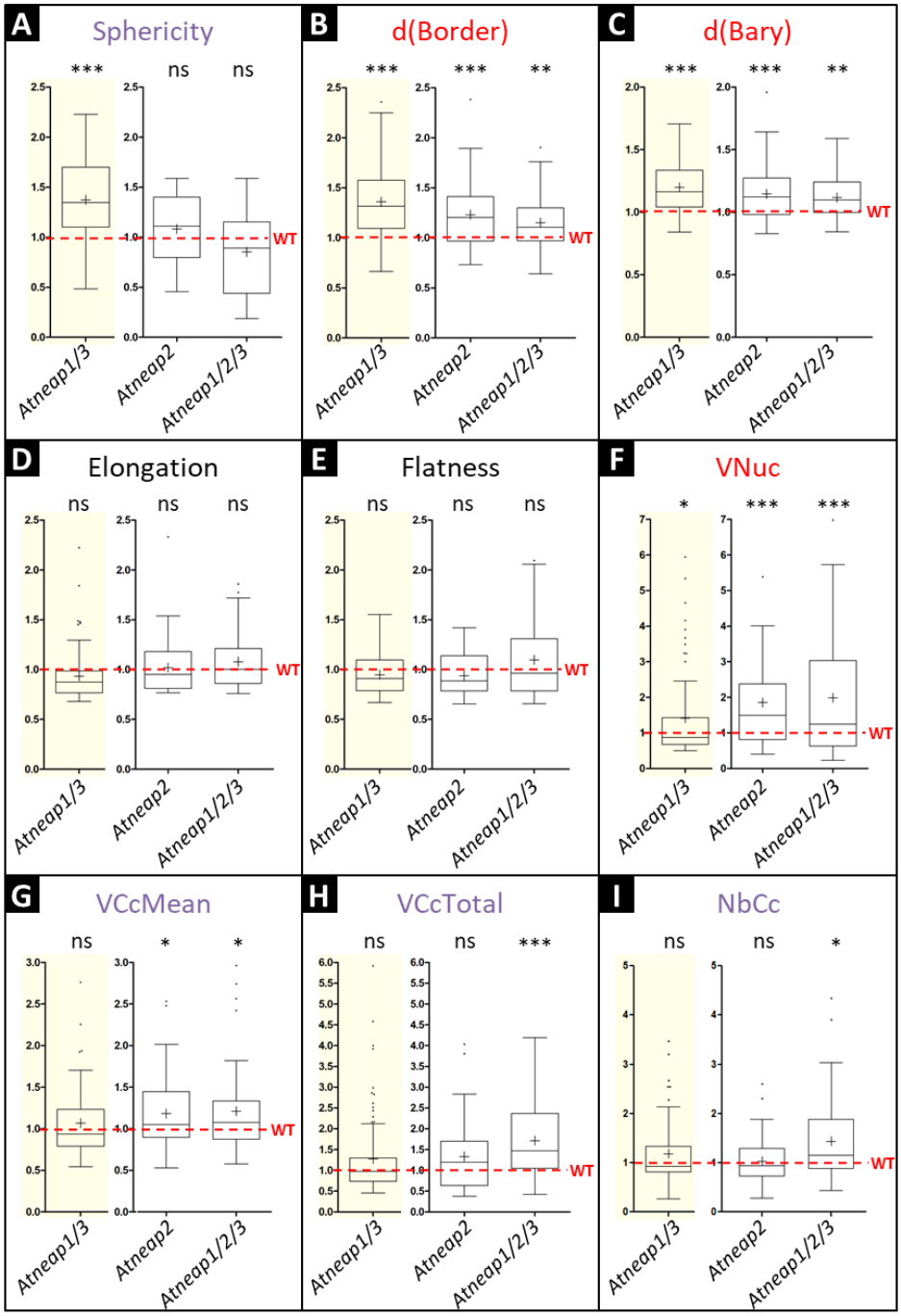

Figure 3-10: Nuclear morphology parameters in *Atneap1/3*, *Atneap2.1*, *Atneap1/2/3* normalized to a wild type Col-0. Plantlets used were 14 dag grown on MS medium. Nuclei were assessed by *NucleusJ* plugin in *ImageJ* software. Yellow parts represent data from the first experiment shown in detail in *Figure 3-7*. Data were normalized with specific WT (Col-0) from every independent experiment. The same nine parameters shown in *Figure 3-7* were studied.
ns: non significant; * p< 0.05 ; ** p<0.01 ; *** p<0.001.

assessed as the root growth kinetics until 10dag on a total of 48 independent seedlings (***Figure 3-8A, B***), leaf surface area at 21dag and the time point of the vegetative/reproductive switch on a total of 12 independent plants (***Figure 3-8C, D***). No difference was observed for those parameters, ***Figure 3-8A-D***.

Then, reproductive tissues were studied for silique size and number and weight of seeds, (***Figure 3-8E-H***). A total of 30 half-siliques from 12 independent plants (***Figure 3-8E, F, G***), and 500 dried seeds (***Figure 3-8H***) were assessed in these experiments. A weak but significantly reduced size of siliques was observed for single *Atneap2.1* and triple *Atneap1/2/3* mutants compared to WT. Also, the triple *Atneap1/2/3* mutant showed less viable seeds, more non-fertilized ovules, but a similar seed weight, indicating a potential defect in meiosis or embryo formation. This is currently being investigated in collaboration with Monica Pradillo, Complutense University of Madrid.

Then, nine nuclear morphology parameters were measured using *NucleusJ* as previously for the *first triple* mutant (***Figure 3-7***). Six independent cotyledon pairs from 21dag seedlings for each genotype, *Atneap2.1*, *Atneap1/2/3* and a WT Col-0 as a control were assessed for a total of 42 to 50 nuclei analysed, ***Figure 3-9***. Results are presented as ratio, normalized to the WT of reference for this experiment. On the left of each panel, in yellow, the results from the first experiment with the double *Atneap1/3* are shown normalized with the WT of reference for the respective experiment. As previously observed for *Atneap1/3*, the distance of the chromocentre border or barycentre, to the nuclear periphery is increased also in *Atneap2.1* and *Atnepa1/2/3* compared to the WT, ***Figure 3-9B, C***. Surprisingly, the increased sphericity observed in *Atneap1/3* was not found in *Atneap2.1* and *Atnepa1/2/3*, with no significant difference compared to the WT, and even a tendency to a lower sphericity for the *triple neap* mutant, ***Figure 3-9A***. Also, nuclear volume is increased in all mutants, ***Figure 3-9F***, and correlates with an increase of the mean of the chromocentre volume in *Atneap2.1*

and *Atnepa1/2/3*, ***Figure 3-9G***. Only the triple *neap* mutant showed an increased total chromocentre volume and number of chromocentres compared to WT, ***Figure 3-9H, I***. Elongation and flatness of the nuclei were not modified ***Figure 3-9D, E***, consistently with the previous experiment.

Thus, in absence of the AtNEAP proteins, nuclei and chromocentres are larger, and chromocentres are at a greater distance from the nuclear periphery, suggesting their tethering to the nuclear periphery is altered.

Conclusion

Using the CRISPR/Cas9 technology, generation of a triple KO mutant for the AtNEAP family was long but successful. Analysis of the general growth phenotype under optimal conditions did not reveal any effect of loss-of-function of *AtNEAP2* only, nor *AtNEAP1*, *AtNEAP2* and *AtNEAP3* simultaneously. Defects in the mutants were only observed when looking at reproductive tissues, being a reduced silique size and a reduced number of viable seeds. These results indicate firstly that major defects could arise during gamete synthesis and fecundation steps. That is why meiosis and embryo formation are being investigated in collaboration. Secondly, while no growth defects were observed under optimal growth conditions, it remains to be investigated how *Atneap* mutant plants respond to different stress conditions.

Results from these studies indicate that the entire removal of this protein family doesn't have a large effect on general phenotype for plants growing in optimal conditions. Further study of nuclear architecture and chromatin organisation showed that chromocentre position was affected. To investigate whether these changes in chromocentre position impact transcriptional silencing of repetitive sequences organized in chromocentre, analysis is being carried out on the expression of 180bp satellite repeats, the Transcriptional Silent Information (TSI) as well as three euchromatic genes (*UBC28, UEV1C* and *HXK1*) in WT Col-0 and triple

mutant *Atneap1/2/3*. This will help us to decide the best strategy to apply before proceeeding to a complete transcriptome analysis at the genome level (RNA-seq) in order to investigate the role of AtNEAP proteins on gene transcription and chromatin organisation, to establish whether this occurs in a site-specific manner or not.

In parallel, a complementation vector, pAtNEAP1::4xc-Myc-AtNEAP1, for *Atneap* mutant lines, was designed, is being synthesized and planned to be transformed into Col-0 and triple *Atneap1/2/3* mutant lines via *A. tumefaciens* (see ***Methods III.6***). Nuclei measurements will be assessed following same procedures see ***Chapter 3-III*** above. The complemented lines could also be interesting tools for the future to explore possible interacting partners by IP using anti-Myc antibody followed by mass spectrometry sequencing.

CHAPTER 4

AtNEAP protein interactome

CHAPTER 4
AtNEAP protein interactome

A second research objective was to identify novel protein partners of AtNEAP proteins to get new insights into their possible function at the nuclear periphery. Three aspects were explored: Y2H screens, characterization of a known interactor of AtNEAP protein AtbZIP18 and the design of antibodies against AtNEAP proteins.

As detailed in (Meng *et al*., 2005), several methods exist in order to investigate protein-protein interactions using yeast in the Y2H and MYTH systems (MYTH tests interactions at a cellular membrane and is particularly suited for membrane proteins) or by using fluorescent imaging-based biophysical techniques such as apFRET, or BiFC. (Pawar *et al*., 2016) showed that AtNEAP proteins were able to form homo- and hetero-dimers through apFRET experiments. In this study, interactions were explored using the classical Y2H system that tests interaction of proteins in the nucleus (Fields and Song, 1989). Experiments were carried out between AtNEAP proteins and known proteins localised at the nuclear periphery, or between AtNEAP proteins and an *A. thaliana* cDNA library to look for novel interactors through new screens.

A previous MYTH screening, using AtNEAP1 as bait (Pawar *et al*., 2016), revealed one interacting protein, a basic-leucine zipper (AtbZIP18), which is a transcription factor, (Gibalová *et al*., 2017). This study showed a co-localisation for AtNEAP1 and AtbZIP18 in the nucleoplasm, (Pawar *et al*., 2016). Thus, apFRET experiments were carried out in order to confirm this suggested interaction as well as bZIP18 domain deletion constructs to characterize the specific interaction site with AtNEAPs by Y2H experiments.

Finally, in order to study the AtNEAP interactome, specific antibodies against AtNEAPs were required for pull-down assays followed by mass spectrometry analysis. Thus,

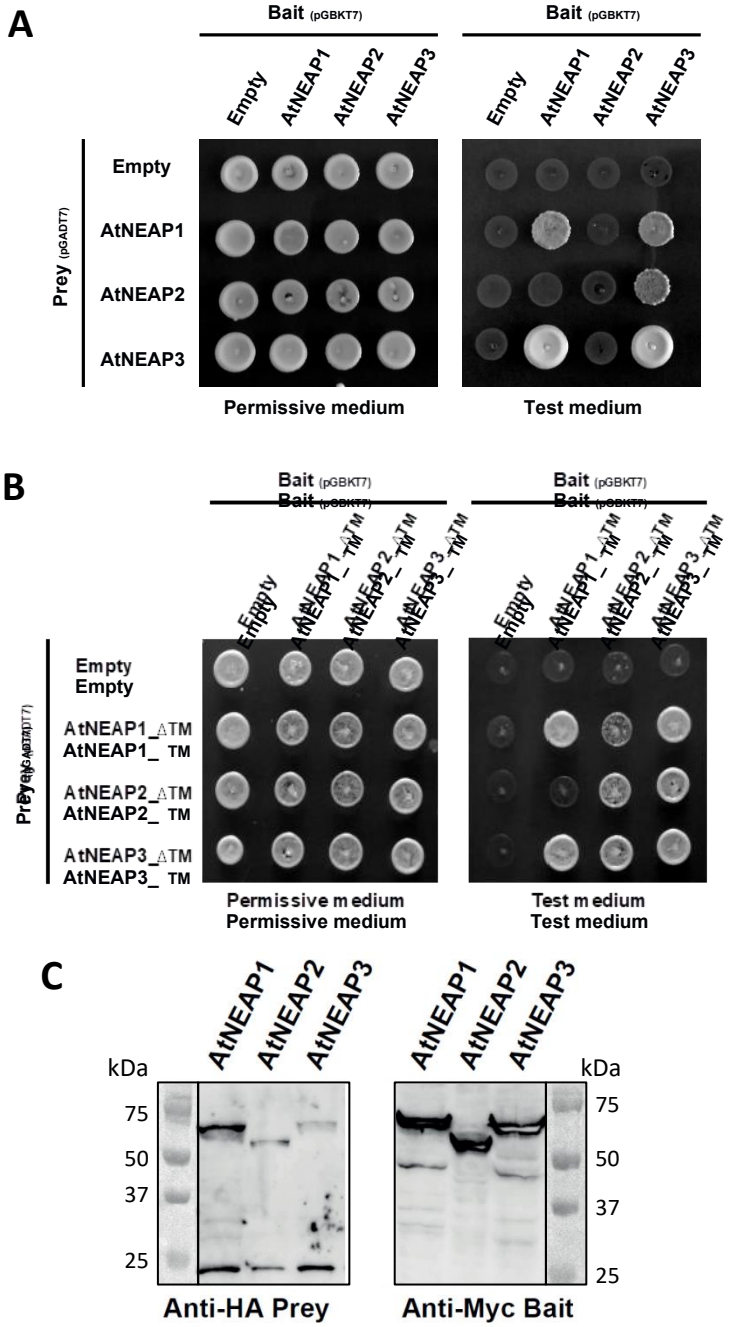

Figure 4-1: Interaction between AtNEAPs and AtNEAPs_ΔTM proteins with each other respectively. Yeast strains were tested on permissive medium (left) depleted in leucine and tryptophan to select diploids only and on test medium (right) depleted in leucine, tryptophan, histidine and adenine to select diploids with interacting proteins. **C.** WB to confirm expression of AtNEAP proteins as baits (c-Myc antibody) and preys (HA antibody).

antibodies were designed, produced in rabbits, verified and tested on different protein extracts.

I – Classic Yeast Two Hybrid (Y2H)

Only the classical Y2H system was used during this study. In the first instance, drop tests were undertaken with known baits and preys. Yeast strains containing prey or bait vectors were mated, and zygotes grown on permissive medium. Interaction with bait and prey was then tested on selective medium depleted in Trp, Leu, His and Ade. The first experiment, (***Figure 4-1A***), testing interaction of full length AtNEAP proteins with each other (baits and preys) confirmed homodimerization for AtNEAP1 and AtNEAP3 and heterodimerization for AtNEAP1-AtNEAP3 and AtNEAP2-AtNEAP3. As the TM may sequester the AtNEAP proteins at the membranes (nuclear, plasma or ER) and could impair the transcriptional activation of the reporter genes in Y2H, the same experiment was repeated with AtNEAPs depleted of the TM domain, (***Figure 4-1B***). The results showed the same interactions as previously observed ***Figure 4-1A***, *i.e.* AtNEAP1 and AtNEAP3 homodimerization and AtNEAP1-AtNEAP3, AtNEAP2-AtNEAP3 heterodimers. Results also showed AtNEAP2-AtNEAP1 heterodimer and AtNEAP2 homodimer. These results in Y2H are consistent with the ones observed by (Pawar *et al*., 2016) by apFRET and MYTH (Pawar-Menon, PhD thesis, 2015), with every AtNEAP homodimer and every combination of heterodimers. They indicate that although the TM domain does not block transcriptional activation of the reporter genes, some interactions were revealed only when the TM domain is deleted.

In the experiment shown in ***Figure 4-1C***, bait and prey fusion proteins were extracted from yeast (see ***Methods V.1***) in order to confirm the synthesis of those proteins in the yeast system. Prey constructs have a HA tag and bait constructs have a c-Myc tag allowing detection on a blot with specific tag antibodies.

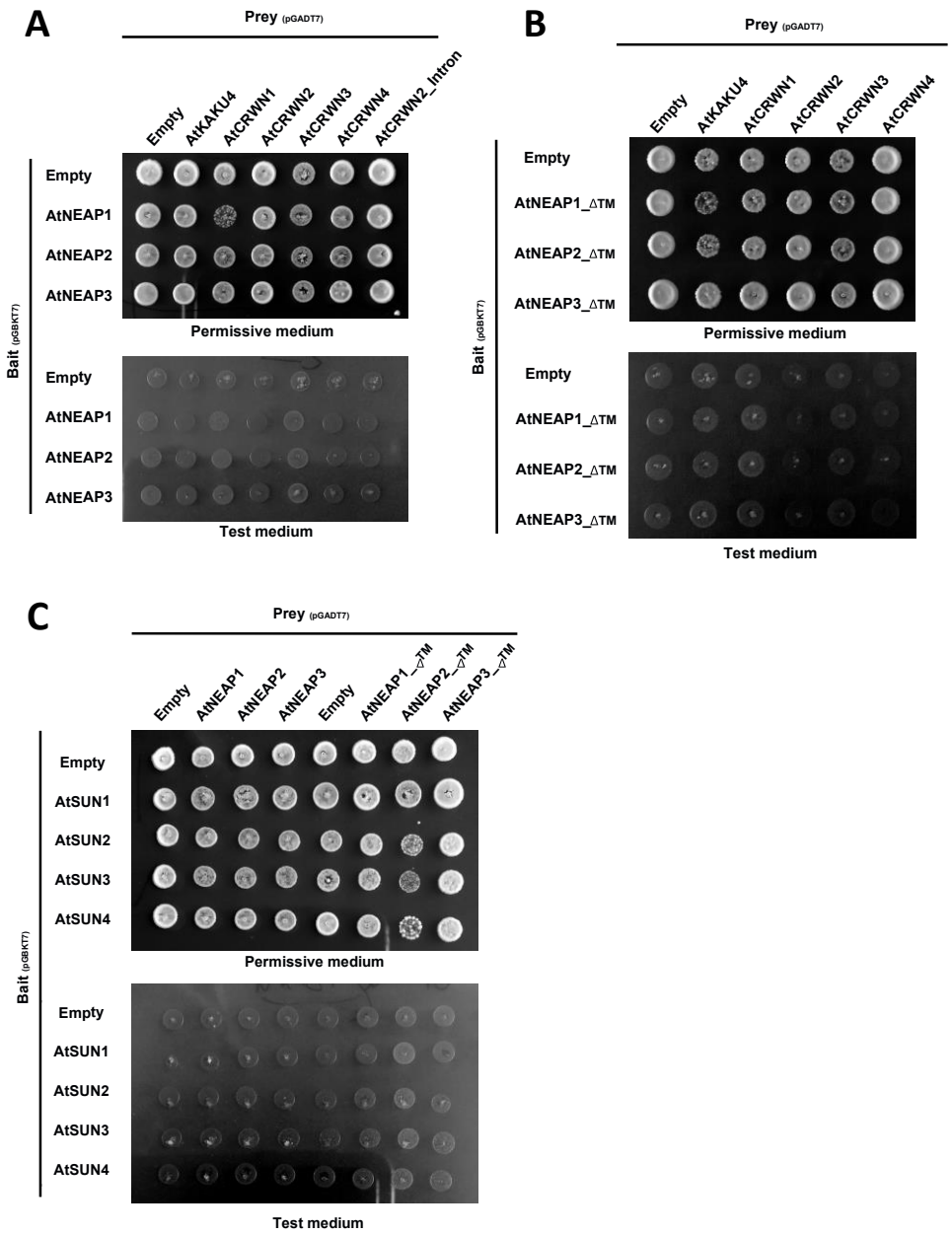

Figure 4-2: Interaction between AtNEAP proteins and known nuclear periphery and INM proteins. Yeast strains were tested on permissive medium (left) depleted in leucine and tryptophan to select diploids only and on test medium (right) depleted in leucine, tryptophan, histidine and adenine to select diploids with interacting proteins. Bait AtNEAPs (**A**) and AtNEAPs_ΔTM (**B**) vs prey AtCRWN1-4 and AtKAKU4. **C.** Bait AtSUN1-4 vs prey AtNEAPs and AtNEAPs_ΔTM.

Next, AtNEAP protein interactions were tested with other known proteins situated at the nuclear periphery (AtKAKU4 and AtCRWNs) or from the INM (AtSUN domain proteins). AtKAKU4 and AtCRWN1-4 as preys were tested against AtNEAPs as baits, either full length or without the TM domain ***Figure 4-2A, B***. The same experiment was carried out with AtSUN1-4 as baits and AtNEAPs as preys, ***Figure 4-2C***. For these drop tests, no interaction at all was detected on selective medium.

In order to look for new interactors without any *a priori* using Y2H, library screenings were carried out with each full length AtNEAP as bait. The prey library was composed of 2 million independent cDNA clones, number determined thanks to serial dilutions made from the mated culture and a count of the number of diploïds obtained on plates with permissive medium. The mating efficiency was 9.4% for the prey library crossed with bait AtNEAP1, 12.8% for the prey library crossed with bait AtNEAP2 and 18.9% for the prey library crossed with bait AtNEAP3. As the minimum for mating efficiency is 5%, this experiment was validated, but, unfortunately, on the selective medium, very few clones were recovered from these screens. Each of them was tested to avoid false positive or contamination. After those tests, only one clone for AtNEAP1 (AT1G45474), none for AtNEAP2 and two for AtNEAP3 (AT2G22360 and AT1G51510) corresponded to potential interacting proteins. As the cDNA library was constructed by cloning the cDNAs in three possible frames, sequencing of these clones was performed to define if the expressed proteins were in the correct frame. Finally, it appeared that none of the candidate clones were in the +1 frame. This whole Y2H screen experiment was repeated at another time with similar results and for that reason the Y2H investigation with the cDNA library was stopped at this stage.

In summary, AtNEAP proteins interact with each other as homo- or heterodimers but despite quite significant efforts to evaluate their interactions with known proteins of the INM

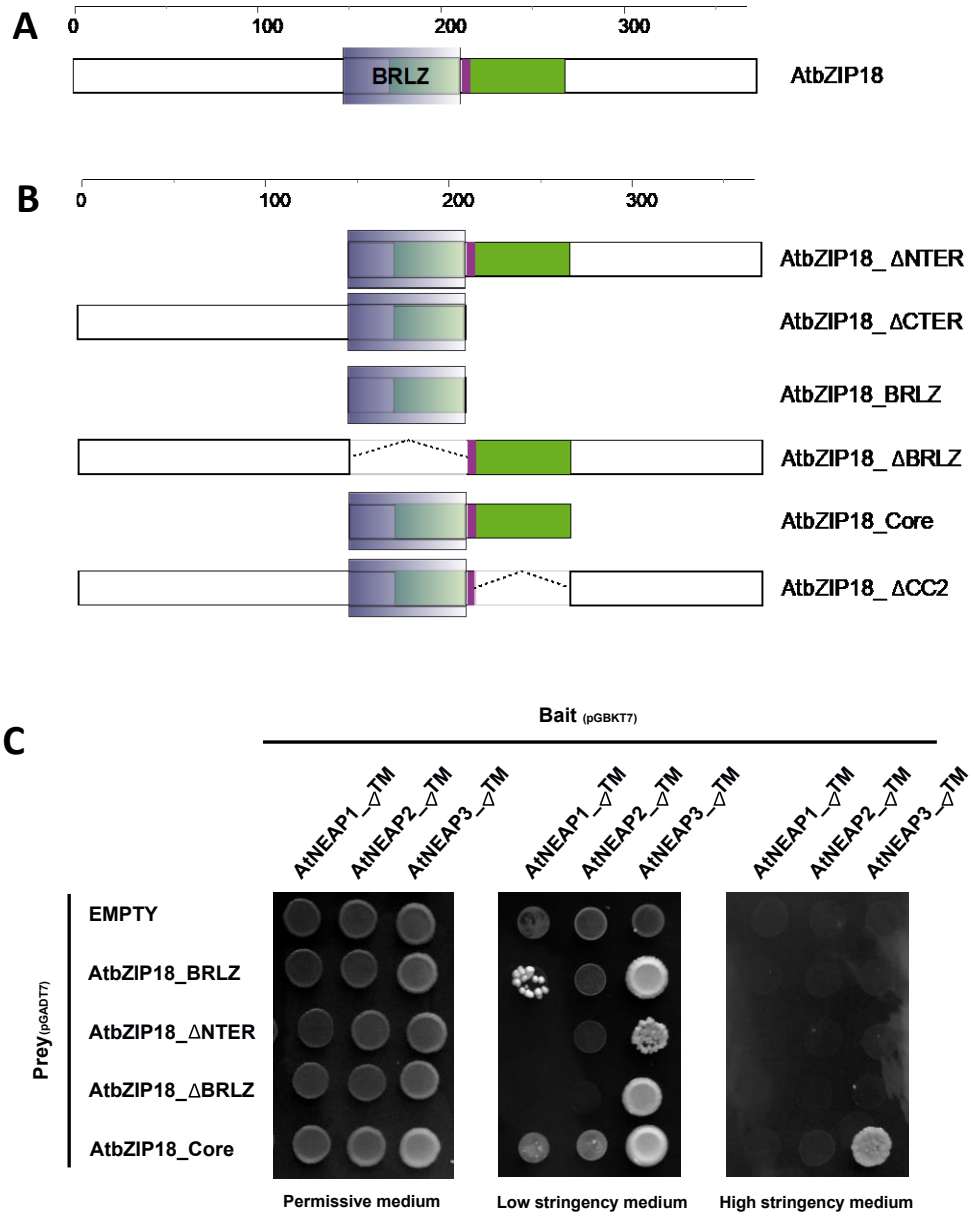

Figure 4-3: AtbZIP18 domain deletion constructs and Y2H experiments. A. Schematic representation of AtbZIP18 full length with BRLZ for basic DNA-binding domain leucine-zipper (blue), coiled-coil domains in green and EAR motif in purple. **B.** Domain deletion constructs. **C.** Y2H drop tests with 4 on 6 AtbZIP18 deletion constructs and AtNEAPs_ΔTM. Permissive medium is depleted in leucine and tryptophan; Low stringency medium is depleted in leucine, tryptophan and histidine; High stringency medium is depleted in leucine, tryptophan, histidine and adenine.

and the nuclear periphery (AtSUN domain proteins, AtKAKU4 and AtCRWNs) as well as the search of new interactors (cDNA library screenings) no new protein partners were identified.

Thus, focusing on the interaction partner previously evidenced by (Pawar *et al*., 2016), AtbZIP18 as bait was crossed with AtSUN1-4, AtKAKU4 and AtCRWN1-4 as preys to investigate their possible interaction with AtbZIP18. Unfortunately, first attempts of Y2H experiments revealed that AtbZIP18 as prey was really slow to grow and AtbZIP18 as bait was auto-activating, consistent with the observations of (Gibalová *et al*., 2017) who removed the auto-activation domain located in the N-ter of the protein, before the BRLZ domain, ***Figure 4-3A***. In the meantime, domain deletions of AtbZIP18 were designed and constructed, as shown in ***Figure 4-3B***, in order to better characterize the specific interaction domain with AtNEAPs. Some of the domain deletion constructs were missing the N-ter auto-activating domain, so normal Y2H experiments were carried out with them, ***Figure 4-3C***. The constructs AtbZIP18_BRLZ, AtbZIP18_ΔNTER, AtbZIP18_ΔBRLZ and AtbZIP18_Core as preys were crossed with AtNEAP1_ΔTM, AtNEAP2_ΔTM and AtNEAP3_ΔTM as baits. Diploïds were grown on permissive, low and high stringency media. Results showed that on high stringency medium, only AtNEAP3_ΔTM interacted with the core of AtbZIP18 containing the BRLZ domain, the EAR motif, and CC domains, ***Figure 4-3B, C***. On the low stringency medium, interactions were observed for AtNEAP3_ΔTM with every domain deletion construct. Also, the core of AtbZIP18 interacted with AtNEAP1_ΔTM and AtNEAP2_ΔTM; and the BRLZ domain of AtbZIP18 interacted with AtNEAP1_ΔTM. This full experiment was repeated with full length AtNEAPs but no interaction was observed (data not shown).

The constructs AtbZIP18_BRLZ, AtbZIP18_ΔNTER, AtbZIP18_ΔBRLZ and AtbZIP18_Core as full length AtbZIP18 were fused to GFP and transformed in *N. benthamiana* showing a nucleoplasmic localisation (data not shown).

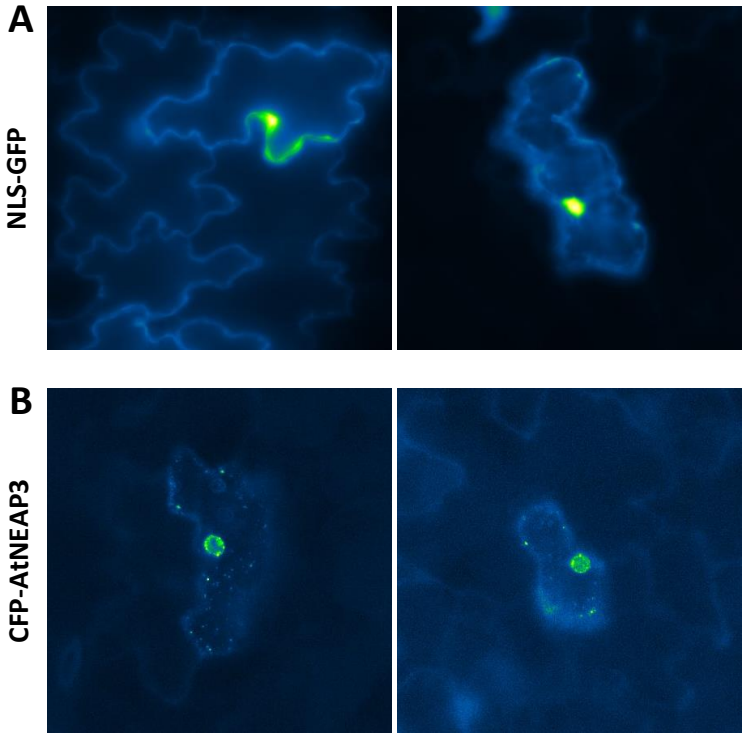

Figure 4-4: Transient transformation of *A. thaliana* cotyledon epidermal cells. Plantlets of 6 dag expressing (**A**) NLS-GFP construct or (**B**) CFP-AtNEAP3 construct. Observation were performed 48h after co-cultivation with *A. tumefaciens* at OD_{600} = 0.5 (**A)** and OD_{600} = 1 (**B**). MMAF microscope, objective X63.

In previous MYTH experiments performed by Maxime Voisin, a former PhD student of the GReD team, another transcription factor, AtMaMYB (At5G45420), identified as an AtSUN3 interactor also interacted with AtbZIP18, ***Appendix VII***. Furthermore, a preliminary MYTH experiment suggested that AtNEAP1 also interacts with AtMaMYB, work achieved by Maxime Voisin. These new interactions will have to be confirmed and extended to AtNEAP2 and AtNEAP3 but already suggest that AtNEAP1 may interact with at least two transcription factors at the nuclear periphery and that a potential network with transcription factors, which would be anchored at the nuclear periphery, is emerging, ***Appendix VII***.

II – Localisation, Co-localisation and apFRET

Transient expression in tobacco is a frequently used technique for Arabidopsis research projects as an alternative to transient expression in Arabidopsis cell culture lines which are not as well developed as an experimental system as cell culture in animals. Hence, the tobacco transient expression assay is a technique of choice when Arabidopsis is the model of study but it remains a heterologous system. In order to observe protein localisation *in vivo* but in Arabidopsis, the FAST technique of (Li and Nebenführ, 2010) was developed for Clermont-Ferrand laboratory conditions. The main aim was to study the localisation of the AtNEAP proteins in WT plants and also to visualise any change of localisation of AtNEAP proteins in the available collection of NE protein mutants when transiently expressed in Arabidopsis.

The protocol was first tested with a chimeric fusion protein, NLS-GFP, used as a positive control for nuclear localisation. As shown in ***Figure 4-4A***, NLS-GFP is located in nuclei and confirmed that the protocol was working. Then, AtNEAP proteins fused with CFP in the N-ter were transiently transformed into Arabidopsis seedlings. Positively transformed cells were observed only for the CFP-AtNEAP3 construct and confirmed the nuclear

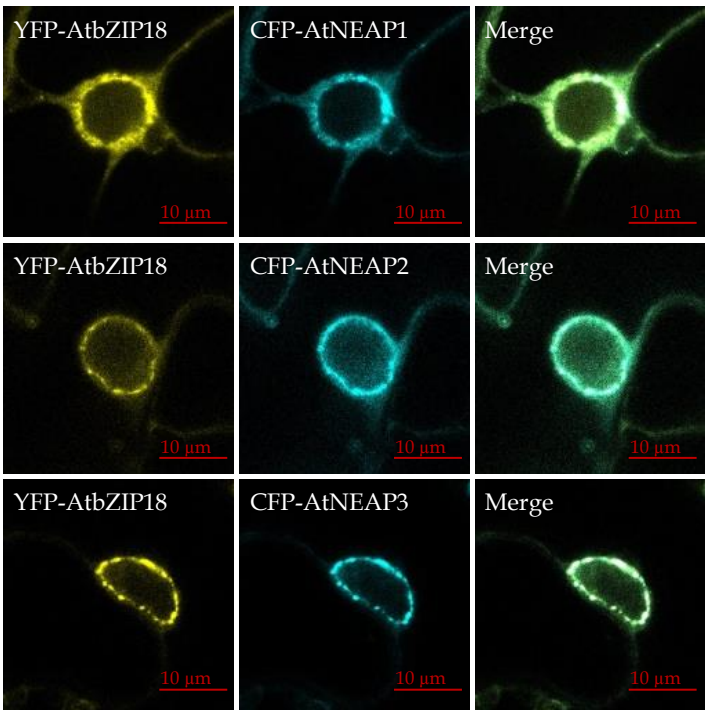

Figure 4-5: Transient expression in leaf epidermal cells of *N. benthamiana*. Three week old plants were co-infiltrated with *A. tumefaciens* containing p19 at DO_{600} = 0.5, YFP-AtbZIP18 construct at DO_{600} = 1 and depending on the condition, CFP-AtNEAP1, CFP-AtNEAP2 or CFP-AtNEAP3 construct at DO_{600} = 1. Images were obtained using a Zeiss LSM800 confocal microscope using a X63water-immersion objective. Scale bar = 10µm.

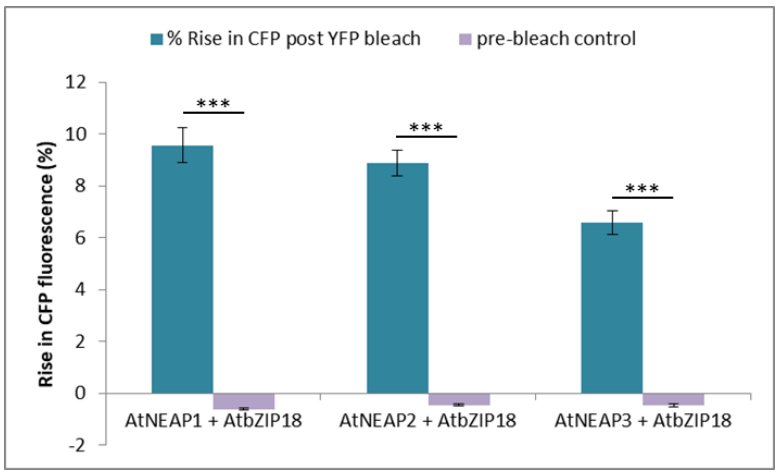

Figure 4-6: AtbZIP18 interact with AtNEAPs. apFRET was performed using 105 nuclei for AtNEAP1+AtbZIP18, 100 nuclei for AtNEAP2+AtbZIP18 and 97 nuclei for AtNEAP3+AtbZIP18. *** $p<0.001$

periphery localisation of AtNEAP3 *in vivo* in *A. thaliana*, ***Figure 4-4B***. Unfortunately, this protocol was not efficient: whilst if in most of the replicates 5 to 6 out of 8 seedlings were expressing the NLS-GFP construct, some of the replicates did not express AtNEAP and in the best experiments only 3 out of 6 seedlings expressed the CFP-AtNEAP3 construct. Given the difficulties to set up the protocol in WT, it was decided not to investigate mutant backgrounds or the co-infiltration of two constructs to observe co-localisation. Therefore, all the subsequent experiments of transient expression were performed in *N. benthamiana*.

Infiltrations of *N. benthamiana* leaves were carried out to study co-localisation and interactions with the apFRET technique. As shown in ***Figure 4-5***, in each case, both AtbZIP18 and one of the AtNEAPs co-localised at the nuclear periphery. Note that this is significantly different to previous data (Pawar *et al*., 2016) where AtbZIP18 was nucleoplasmic and not only restricted to the nuclear periphery when co-expressed with one of the AtNEAPs. Co-localisation indicates that two proteins localise in the same area but in order to prove interactions, *i.e.* a close proximity <100Å, apFRET experiments were carried out on YFP-AtbZIP18 and every CFP-AtNEAP fusion protein. Two independent replicates were carried out per combination with apFRET on 43 and 44 nuclei respectively for AtNEAP1+AtbZIP18 (N1 combination), 45 and 44 nuclei for AtNEAP2+AtbZIP18 (N2 combination), 45 and 52 nuclei for AtNEAP3+AtbZIP18 (N3 combination). An additional replicate was done for N1 and N2 combinations with 18 and 11 nuclei assessed respectively. The percentage of rise in CFP emission post YFP bleach for every condition was then calculated on a total population of 105 nuclei for N1, 100 nuclei for N2 and 97 nuclei for N3. Results shown in ***Figure 4-6*** confirmed interaction between AtbZIP18 and all three AtNEAP proteins with a p-value < 0.001 and suggest that the transcription factor AtbZIP18 can be tethered at the nuclear periphery maybe through its interaction with AtNEAP proteins. Further

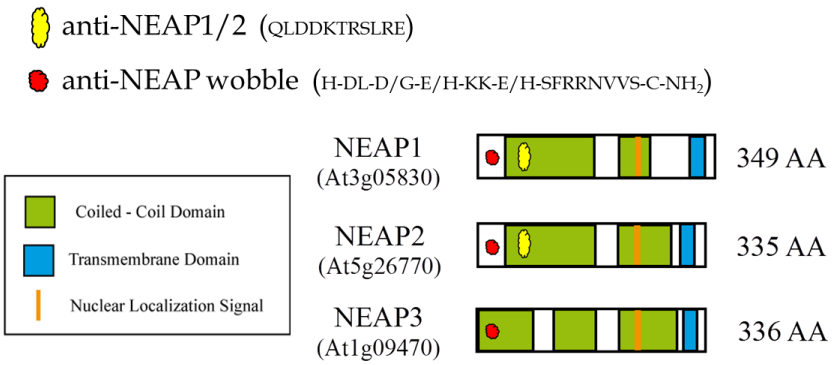

Figure 4-7: Schematic representation of target sites of specific antibodies.

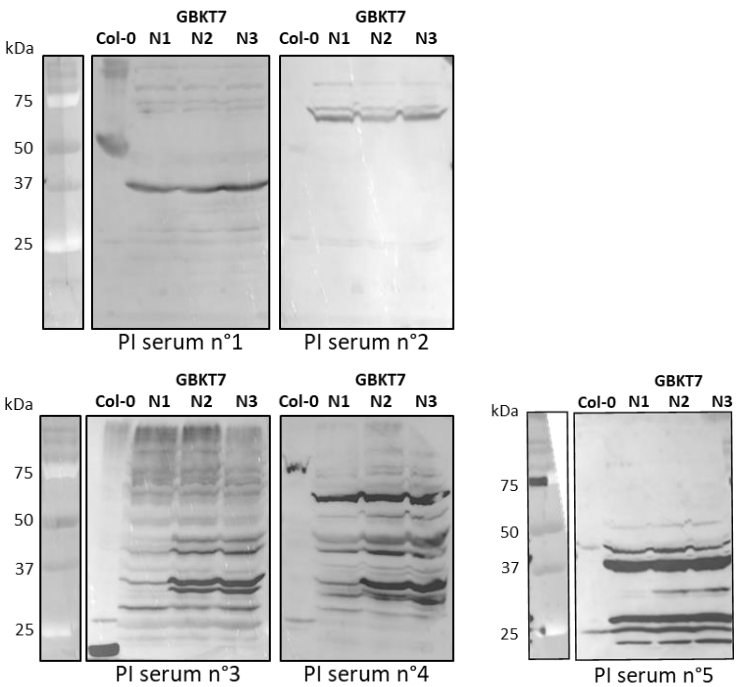

Figure 4-8: Test of Pre-immune (PI) sera on yeast extracts containing bait AtNEAP fusion proteins* and a WT Col-0 plant extract. Pre-immune sera were diluted at 1/1000 in 3% PBST-milk, and interaction revealed by a secondary goat anti-rabbit-HRP diluted at 1/50 000. *Bait AtNEAP fusion proteins are the ones used in Y2H experiments, *i.e.* pGBKT7-AtNEAPs construct and revealed previously with anti-Myc antibody (see *Figure 4-1C*).

experiments using deletion mutants and *in vivo* studies in mutant backgrounds will be needed to confirm this hypothesis.

III – Generation of AtNEAP antibodies

Specific AtNEAP antibodies were not available at the beginning of the project and were required for several reasons. Firstly to better characterize different *Atneap* mutants, via Western blotting. Secondly to investigate protein-protein interaction via immunoprecipitation (IP) and co-IP; thirdly for immunohistochemistry of *A. thaliana* tissues.

In order to produce antibodies, two different peptides were designed in collaboration with Eurogentec to be highly specific to AtNEAP protein sequences (See ***Methods V.4***). The first peptide of 11 aa is located in the N-terminal part of the AtNEAP proteins within the first CC domain and is specific to AtNEAP1 and AtNEAP2, splicing variants included (used to produce "*anti-NEAP1/2*" antibody). The second peptide is also of 11 aa and situated before the CC domain of AtNEAP1 and AtNEAP2 and at the beginning of the first CC domain of AtNEAP3. This peptide is designed to recognize all three AtNEAPs and includes a wobble version of the three sequences (used to produce "*anti-NEAP wobble*" antibody), (***Figure 4-7***). Before inoculating rabbits, pre-immune (PI) sera from five different rabbits were tested on yeast extracts containing AtNEAP fusion proteins and a total protein extract of a WT Col-0 plant, ***Figure 4-8***. The five pre-immune sera revealed a non-specific band around 25kDa for every sample. In Col-0 plant extract, a band around 50kDa was detected in PI n°1 and n°2; and PI n°4 revealed a band around 75kDa. Also, for yeast extract, PI n°5 did not detect any band above 50kDa, ***Figure 4-8***. Thus of five rabbits, only two were kept, n°3 and n°5, as they did not detect a band of similar size to the AtNEAP fusion proteins (60-70kDa) or similar to native proteins (30-40 kDa). The two selected rabbits were immunised by Eurogentec with the two different peptides according to a "p28 day speedy protocol" (immunization in 28 days), See ***Methods V.4***.

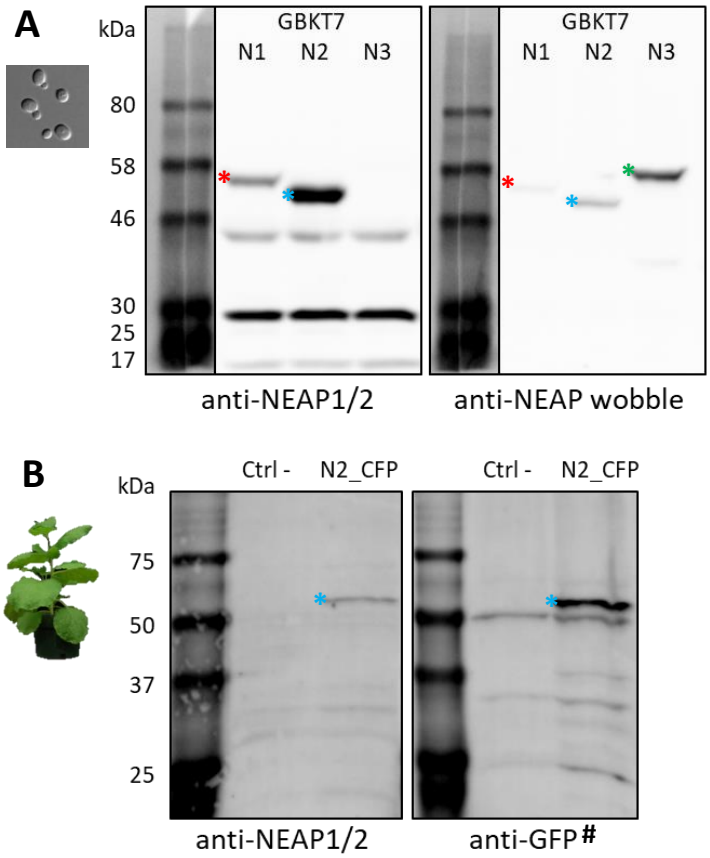

Figure 4-9: Test of anti-NEAP1/2 and anti-NEAP wobble antibodies on different protein extracts. A. Proteins were extracted from yeast (*S. cerevisiae*) containing over-expressed bait fusion AtNEAP proteins used in Y2H experiments. From left to right: pGBKT7-AtNEAP1, pGBKT7-AtNEAP2, pGBKT7-AtNEAP3. *expected bands. **B.** Proteins were extracted from infiltrated *N. benthamiana* plants with AtNEAP2-CFP. A non-infiltrated plant was used as a negative control (Ctrl -). Red, blue or green asterisks showing bands representing AtNEAP1, AtNEAP2 or AtNEAP3 respectively. Antibody dilutions were 1 in 250 for anti-NEAP1/2 and 1 in 50 for anti-NEAP wobble, and are available in ***Methods Table 2.5*** for more details. **#**. As CFP and GFP have similar protein sequences, anti-GFP antibody is able to recognize either GFP or CFP.

Once the purified polyclonal antibodies received, they were tested on several protein extracts from different organisms. Firstly, same protein extracts used in the tests of the PI sera were used, containing AtNEAP fusion proteins over-expressed in yeast (***Figure 4-9A***). Proteins synthesised from yeast were rather soluble and easy to run on SDS-PAGE. As observed in ***Figure 4-8*** with PI sera (n°3 and n°5), some bands were visible around 30 and 40kDa but at a different expected size compared to AtNEAP fusion proteins and for that reason are considered as non-specific bands. Indeed, according to *in-silico* predictions with Serial Cloner software, expected bands for pGBKT7-AtNEAP1 construct should be around 57kDa, pGBKT7-AtNEAP2 around 54kDa and pGBKT7-AtNEAP3 around 55kDa (as estimated molecular weight (MW) of Gal4 DNA-binding domain (GalDBD) from the pGBKT7 construct is 16kDa; AtNEAP1: 41kDa; AtNEAP2: 38kDa; AtNEAP3: 39kDa). In ***Figure 4-9A***, on both left and right panels, with anti-NEAP1/2 and anti-NEAP wobble respectively, bands of approximately 55kDa for AtNEAP1 and 50kDa for AtNEAP2 fusion proteins were detected. Only with anti-NEAP wobble a band was visible around 56kDa for AtNEAP3 fusion protein. Bands were approximately at the expected MW even though AtNEAP1 and AtNEAP2 fusion proteins appeared at a lower MW and AtNEAP3 fusion protein at a bigger MW. These results are consistent with the ones presented in ***Figure 4-1C*** and also in Pawar-Menon, PhD thesis, 2015, with observed bands at 61, 60 and 65 kDa for AtNEAP1, AtNEAP2 and AtNEAP3 respectively for NEAPs fused to YFP when revealed with an anti-GFP antibody (YFP being around 27kDa). Thus, using fusion proteins expressed in yeast, the anti-NEAP1/2 antibody detected AtNEAP1 and AtNEAP2 while the anti-NEAP wobble detected all the AtNEAPs, showing higher affinity for AtNEAP3. This result was not expected from the initial design of the peptides but offers the advantage of two antibodies with different specificities. Finally, the anti-NEAP wobble shows a lower efficiency and requires to be used at a lower dilution.

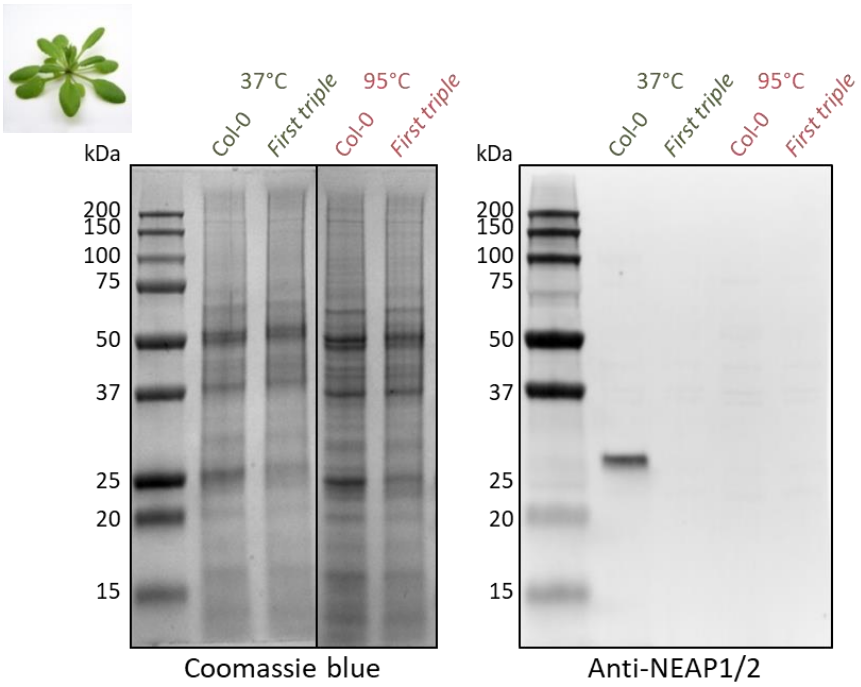

Figure 4-10: Test of anti-NEAP1/2 antibody on native AtNEAP proteins in *A. thaliana*. Proteins were extracted from 3 week-old WT Col-0, or *first triple neap* mutant plants. Same loaded gel was stained with Coomassie blue to attest the loading (left panel). Antibody dilution was 1 in 250 for anti-NEAP1/2 and more details are available in ***Methods Table 2.5***.

Then, tests were carried out on transiently over-expressed AtNEAP2-CFP fusion proteins in *N. benthamiana*, using an extraction protocol specific for membrane proteins optimized by (Pawar *et al*., 2016), ***Figure 4-9B***. Negative control was a non-infiltrated *N. benthamiana* plant. On the left panel of ***Figure 4-9B***, anti-NEAP1/2 antibody revealed a band around 56kDa for the plants infiltrated with AtNEAP2-CFP. A band with the same MW was also revealed with anti-GFP antibody for the same plant. No band around 56kDa was observed for the negative control plant for both antibodies. The predicted MW for AtNEAP2-CFP fusion protein was around 60kDa as CFP is 22kDa and AtNEAP2 is 38kDa. Then, MW observed was slightly lower than expected but this result was consistent with data previously observed by Pawar-Menon, PhD thesis, 2015. Attempts to use the anti-NEAP wobble on plant extracts failed and this antibody seems to be weaker and also needs to be used at a low dilution (a least 1 in 50). Thus, AtNEAP2-CFP was revealed by both anti-NEAP1/2 and anti-GFP antibodies and confirmed the ability of anti-NEAP2 antibody to recognize AtNEAP2, when fusion proteins are over-expressed in *N. benthamiana*.

Finally, antibodies were also tested on *A. thaliana* extracts, but additional protein extraction protocols were required for enriching extracts in nuclear proteins, (***Methods V.1***; ***Figure 4-10***). Some difficulties became apparent for extracting AtNEAP native proteins from *A. thaliana* plants, so adjustments in the protocol were made. One of those was to incubate protein lysate at 37°C for 30min instead of the classical incubation at 95°C for 5min before a loading on a SDS-gel. Avoiding the boiling step prevents those particular proteins with TM and CC domains from aggregation, limiting their migration into the SDS-PAGE. Three-week-old *A. thaliana* plants grown on MS medium, either wild-type (Col-0) or *first triple neap* mutant (*First triple*) were used. Results shown in ***Figure 4-10*** revealed only one clear band around 30kDa for Col-0 incubated at 37°C before loading. So, firstly, it seems that replacing the boiling step should be recommended for enriching the soluble lysate in AtNEAP proteins.

However, as previously observed, the detected band containing possibly AtNEAP1 and AtNEAP2 proteins had a MW of 30kDa, *i.e.* lower than the estimated MW of 41 and 38kDa respectively. After deduction of the estimated MW of the Gal4DBD and CFP tags, AtNEAP1 shows an apparent MW of 39kDa and AtNEAP2 of 34kDa on the previous blots. No band was detected for the *First triple* mutant.

Before drawing conclusions on the ability of the anti-NEAP1/2 antibody to recognize AtNEAP1 and AtNEAP2 native proteins specifically in Arabidopsis, this experiment should be repeated as this positive result has been obtained twice on two independent western blotting experiments but using the same protein extract. Also, no band was observed for the *first triple* mutant, but as the *Atneap2* mutant allele with T-DNA insertion was not a KO, a band for AtNEAP2 was expected. Then, either, something went wrong during the protein extraction, or these results indicate that no AtNEAP2 protein is synthesised in the *Atneap2* mutant allele with T-DNA insertion, or that expression levels are too low for detection, or the protein is more rapidly degraded.

Altogether, the results of antibody tests on different protein extracts demonstrated that the anti-NEAP1/2 antibody was able to recognize AtNEAP1 and AtNEAP2 expressed and extracted from yeast and tobacco. Also, this antibody would be able to recognize native proteins in Arabidopsis nuclei extracts. Thus, it would be the first time that *AtNEAP* expression has been shown in native tissues using an antibody. The anti-NEAP wobble antibody seemed to be weaker as it was tested on plant extracts with no success (data not shown) but it was able to recognize at least each AtNEAP in yeast extracts, with a higher affinity for AtNEAP3, which would be complementary to the other antibody.

Conclusion

After several attempts with Y2H looking for AtNEAP partners, no new relevant partner was identified and previous MYTH studies identifying AtbZIP18 and AtMaMYB

were not confirmed. However, this is likely to be a result of the differences in the properties of the Y2H and MYTH systems. The apFRET experiments carried out confirmed the physical interaction between AtbZIP18 and AtNEAPs, suggested by MYTH for AtbZIP18+AtNEAP1 in Pawar *et al*, 2016.

The results obtained also showed that AtbZIP18 is localised at the nuclear periphery in transient expression in *N. benthamiana* when co-infiltrated with AtNEAPs, while those proteins were suggested to be localised in the nucleoplasm in Pawar *et al*., 2016. In addition, Gibalová *et al*., 2017, showed AtbZIP18 alone to be in the nucleoplasm and in the perinuclear region. Thus, this observation could indicate that AtNEAPs and AtbZIP18 influence localisation of each other. A recent analysis of the putative domains contained in AtbZIP18 protein sequence revealed the presence of CC domains close to the BRLZ domain, which could be responsible for interaction with AtNEAPs. Further investigation is now required on specific function of AtbZIP18 with AtNEAPs at the nuclear periphery. Concerning AtMaMYB, only preliminary evidence from MYTH suggests the existence of a small network of interaction between AtSUN3, AtNEAP1, AtMaMYB and AtbZIP18 proteins, ***Appendix VII***. More experiments performed by Bisa Andov, PhD student at Oxford Brookes University, focused on AtMaMYB, are ongoing and will assess *in vivo* the relevance of this network.

In addition, specific anti-AtNEAP antibodies were obtained and proof of specificity has been demonstrated using over-expressed fusion proteins from yeast and tobacco (and possibly on native proteins extract from *A. thaliana*). To explore other molecular approaches to investigate the AtNEAPs interactome, preliminary experiments have been recently undertaken to explore the use of these new antibodies for IP and co-IP from *A. thaliana* extract. Some difficulties appeared at first steps in extracting native AtNEAP proteins and for enriching lysates in non-soluble NE proteins. Recently, a protocol was set-up by Frances Tolmie (Oxford Brookes University), using a method based on one from the group of Hank

Bass, Florida State University, who recently succeeded to immunoprecipitate SUN2 and who co-immunoprecipitated many nuclear envelope and nuclear periphery proteins (Gumber *et al*., 2019). Protein extraction protocols with enrichment in nuclear proteins have to be applied to AtNEAP proteins to produce plant materials for IP and mass spectrometry. Other approaches include (i) the construction of 6xHis-ATNEAPs and GST-AtNEAPs, respectively for nickel and GST pull-down experiments and (ii) the establishment of new transgenic lines expressing pAtNEAP1::4xc-Myc-AtNEAP1 (see ***Chapter 3 Conclusion***) in a *triple neap* mutant background for complementation and for IP using anti-Myc antibody followed by mass spectrometry sequencing, which will open new possibilities in the future.

DISCUSSION

DISCUSSION

Through different approaches adopted in this thesis, the AtNEAP protein function and interaction network at the nuclear periphery has been further characterised. Reverse genetics using CRISPR/Cas9 technology gave the opportunity to obtain a new triple KO *Atneap1 Atneap2 Atneap3* (*Atneap1/2/3*) mutant. In these plants lacking functional versions of the three AtNEAP paralogues, several phenotypic characteristics have been observed: at the whole plant level, phenotypic alterations were observed in reproductive tissues suggesting a functional role in meiosis or embryo formation. At the cellular level, changes in nuclear organisation compared to WT Col-0 plants were recorded and suggest a role for AtNEAP proteins in the localisation and possible anchoring of chromocentres at the nuclear periphery. In parallel, molecular approaches including Y2H and *in vivo* localisation and co-localisation associated with apFRET confirmed the ability of AtNEAP proteins to form homo- and heterodimers, and to interact with domains of the TF AtbZIP18. A biochemical approach including the generation of specific AtNEAP antibodies confirmed expression *in-vivo* and revealed the strong hydrophobic properties of AtNEAP resulting in difficulties in protein extraction procedures. Altogether, the results support the role of AtNEAP proteins in anchoring AtbZIP18 TF at the INM to maintain nuclear morphology and chromatin organisation. In this general discussion, firstly, short-term approaches will be suggested to demonstrate the functional role of AtNEAP proteins at the nuclear periphery. Secondly, a potential mechanism of action of AtNEAP proteins in tethering chromocentres at the nuclear periphery and a role through interaction with AtbZIP18 in gene repression will be discussed. Finally, future work (long-term approaches) and hypothesis will be suggested.

I – Role of AtNEAPs in tethering chromocentres to the nuclear periphery

In order to study AtNEAP protein function in *A. thaliana*, reverse genetics has been used. It was important to generate a triple KO mutant including a loss-of-function allele of *AtNEAP2*. This allele was not available at the beginning of this study, and two years were required to create a new *Atneap2* mutant via the CRISPR/Cas9 technique in wild type plants and to introgress the new mutant allele into the double *Atneap1Atneap3* mutant already available. No mutant plants could be recovered for the first CRISPR/Cas9 target site, ideally located at the beginning of *AtNEAP2* in the first exon. This could be explained by the fact that Cas9 mutations randomly happen so does the reparation mechanism in Arabidopsis which is preferentially NHEJ, (Schiml *et al*., 2017). Nevertheless, a mutation in the second CRISPR/Cas9 target site was obtained located in the third exon before the NLS and TM domain and it was decided to continue the work using this mutant allele. This single nucleotide insertion introduces an early stop codon and would lead to a truncated protein with neither NLS nor TM domain. A transient expression experiment of the truncated AtNEAP2 protein confirmed that this mutant protein is not targeted to the nucleus and weakly expressed suggesting some instability (rapid turnover). Then, preliminary phenotyping screens were performed on the triple *Atneap1/2/3* mutant.

A first analysis revealed an impact on the siliques, which are significantly reduced in size, and also contained a reduced number of viable seeds correlated with a higher number of non-fertilized ovules, as the total number of seeds is not affected. This result seems consistent with the higher level of transcription of *AtNEAPs* in seeds, especially in embryo, (Pawar *et al*., 2016). It also raised the question of a potential effect on meiosis or embryo formation in the *Atneap* mutants which is currently being investigated in collaboration with Monica Pradillo's group in Spain.

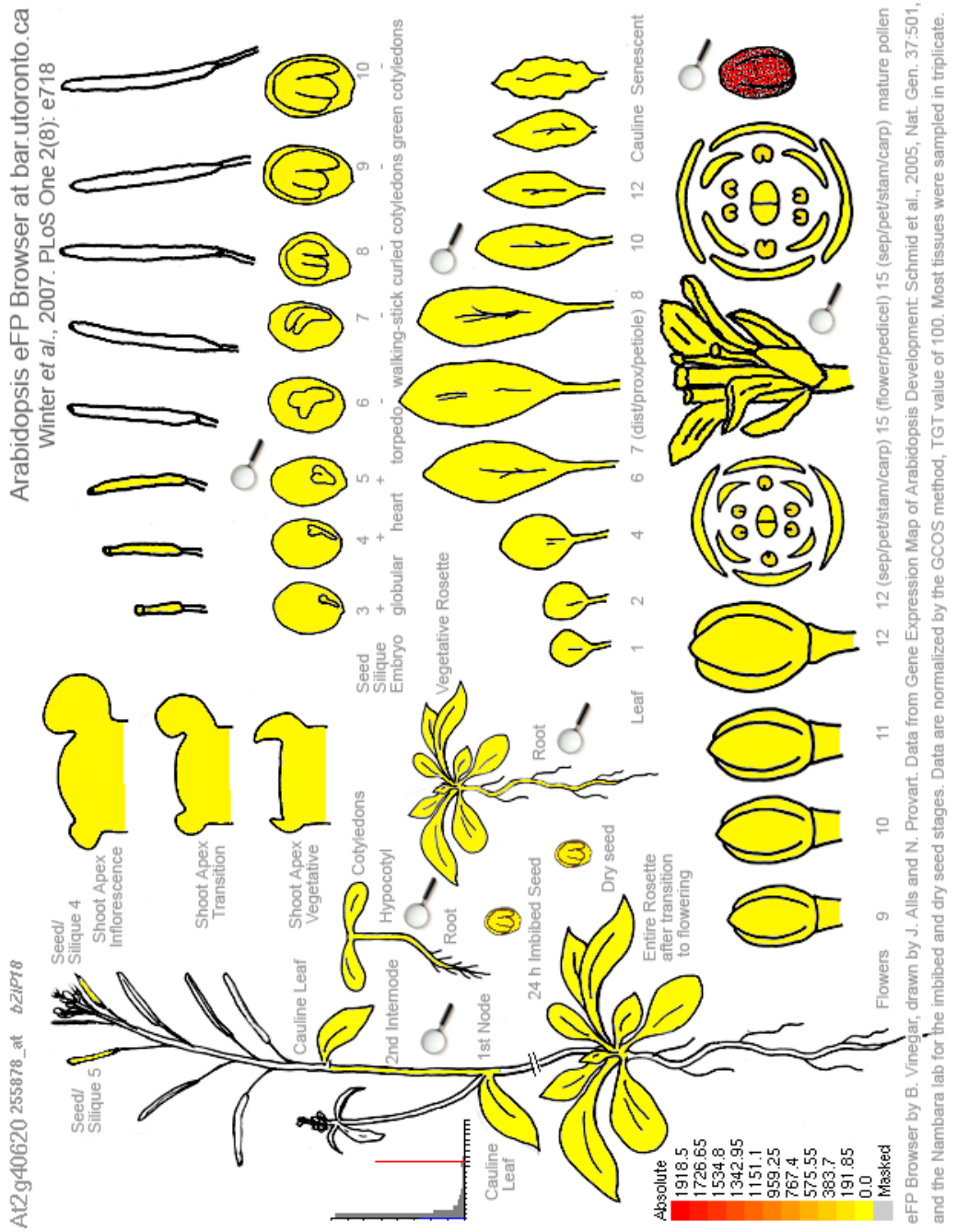

Figure 5-1: Transcription levels of AtbZIP18 mRNA in different tissues from *GeneVestigator*. AtbZIP18 is highly expressed in the mature pollen grain.

A finer analysis of nuclear morphology and chromatin organisation of mutant nuclei showed that chromocentres are more internal as the distance between chromocentres and the nuclear periphery is increased. Even if this experiment needs to be done other times with an increased number of nuclei in both guard and pavement cell populations, these preliminary results could indicate a defect in a putative physical tethering of the chromocentres at the nuclear periphery when AtNEAP proteins are absent. A similar result was obtained with the triple *Atsun1/4/5* mutant, which also shows a decompaction of chromocentres and a release of gene silencing at some repeated sequences (Poulet *et al*., 2016). However, no chromocentre decompaction was observed in the triple *Atneap1/2/3* mutant and preliminary RT-qPCR results using the same repeated sequences as for the triple *Atsun1/4/5* (180bp, TSI) failed to detect any defect in gene silencing. If AtNEAP proteins participate in the tethering of specific chromatin regions at the nuclear periphery, it does not seem to affect repeated sequences or chromocentre compaction. So far, how an alteration in chromocentre position affects genome expression or is linked to the phenotypical differences observed in *Atneap* mutant plants remains to be shown.

II – AtNEAP proteins interact with the transcription factor AtbZIP18

AtbZIP18 was identified in a MYTH screen using AtNEAP1 as bait (Pawar *et al*., 2016). AtbZIP18 is a transcription factor (TF) expressed everywhere in the plant but with a higher level of transcription in the mature pollen grain, (Gibalová *et al*., 2017), ***Figure 5-1***. Among *AtNEAP* genes, *AtNEAP1* and *AtNEAP2* are more highly transcribed compared to *AtNEAP3* in every tissue with a relative stronger transcription in seeds (***Appendix VII***, Pawar *et al*., 2016, Supplementary Fig4). In this work, interaction of AtNEAP proteins with AtbZIP18 has been confirmed *in vivo* by apFRET, ***Figure 4-6***. Note that during this experiment, AtbZIP18 localisation, ***Figure 4-5***, was significantly different from previous data

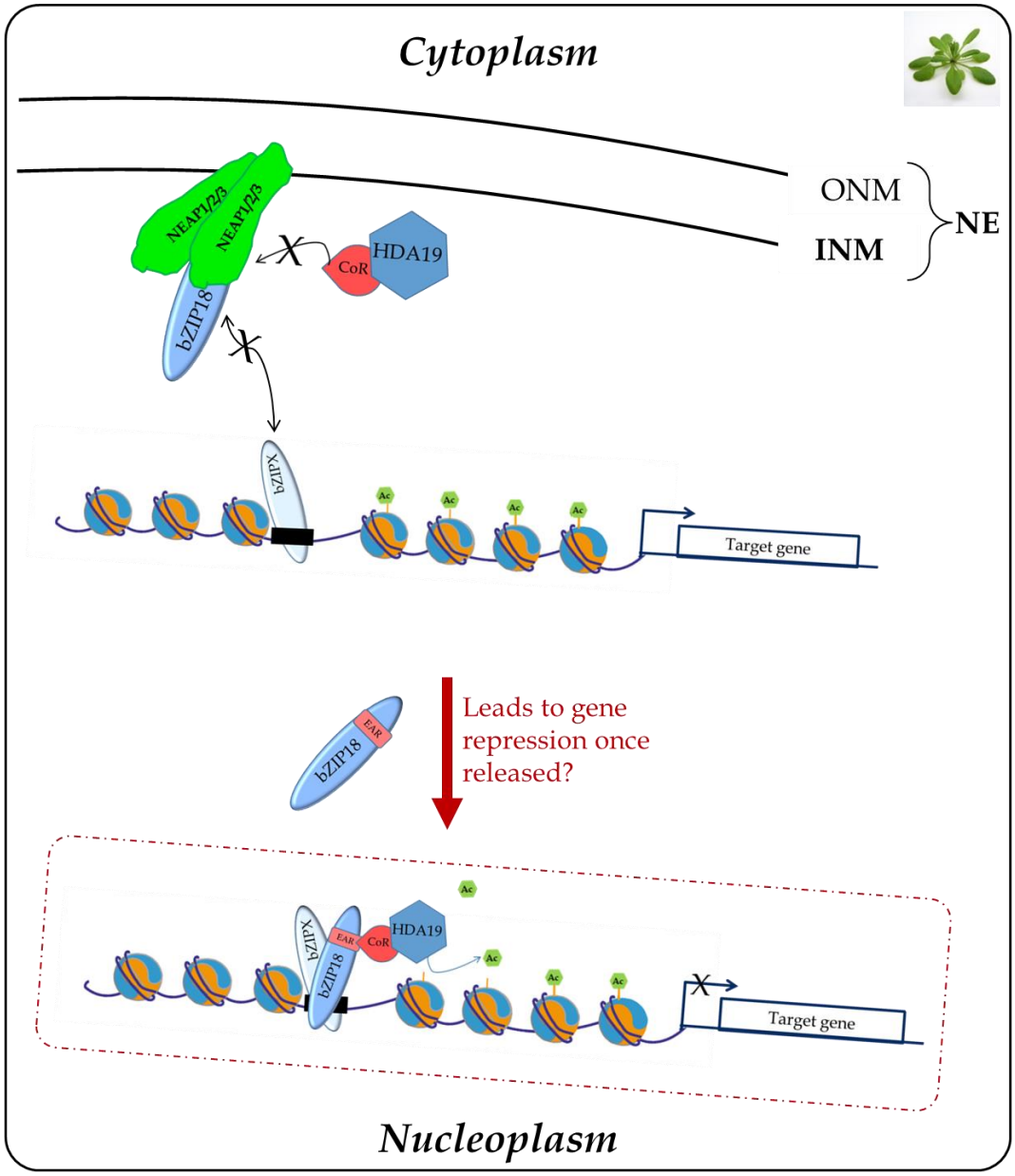

Figure 5-2: Proposed model of AtNEAP and AtbZIP18 function in gene repression in *A. thaliana*. AtbZIP18 would be sequestered by AtNEAP at the nuclear periphery, masking the EAR motif and blocking interactions with CoR and dimerisation with another bZIP. A loss of tethering by AtNEAP would lead to gene repression mediated by bZIP18 and other partners. bZIPX: AtbZIP34, 52 or 61. CoR: Co-repressors such as AtSIN3, AtSAP18 or TPL. Black rectangle represents the DNA motif for interaction with bZIP TFs.HDA19 is a histone deacetylase and leads to gene repression but the mechanism of the spreading remains to be elucidated.

(Pawar *et al*., 2016) where it was nucleoplasmic and not only restricted to the nuclear periphery. This could be due to different issues regarding the experiment in itself. Indeed, depending on the timing for observation, between two – to five days post-infiltration, as it is transient, the level of expression can drastically change and induce mis-localisation if proteins are too much over-expressed. In this case, it tends to leak into the nucleoplasm instead of being restricted to the nuclear periphery. This is probably the case in Pawar-Menon, PhD thesis, 2015, where AtNEAP1 on its own was sometimes peripheral, sometimes nucleoplasmic. Finally, it has been shown in Gibalova *et al.*, 2017, that AtbZIP18 on its own was enriched at the nuclear periphery. Therefore, it does make sense that the co-localisation and interaction of AtbZIP18/AtNEAP happen at the nuclear periphery as shown in this study, ***Figure 4-5 and Figure 4-6***, but if fusion proteins are too much over-expressed, this interaction may be seen into the nucleoplasm.

A recent analysis of the predicted domains of bZIP transcription factors including AtbZIP18 revealed the presence of CC domains overlapping the BRLZ domain implicated in its interaction with DNA and dimerization with other bZIP TFs (Dröge-Laser *et al*., 2018). CC domains are known to be important for Protein-Protein Interaction (PPI) and even if the CC domain is common to all bZIP TFs, (Dröge-Laser *et al*., 2018), in the case of AtbZIP18 it seems to be responsible for interaction with AtNEAP proteins according to Y2H experiments with AtbZIP18 domain deletions. This could raise the possibility that AtbZIP18 can either interact with AtNEAPs, and therefore be tethered at the NE, or at specific DNA target sites to regulate transcription, but would not be able to do both at the same time, ***Figure 5-2***. Indeed, by linking AtbZIP18 through its CC domain, AtNEAP could mask the Ethylene-responsive element binding factor-associated Amphiphilic Repression (EAR) motif (LxLxL) motif and prevent fixation of co-repressors on AtbZIP18, ***Figure 5-2***. Also, it is possible that AtNEAP/AtbZIP18 interaction inhibits AtbZIP18 dimerization and thus DNA binding. Then,

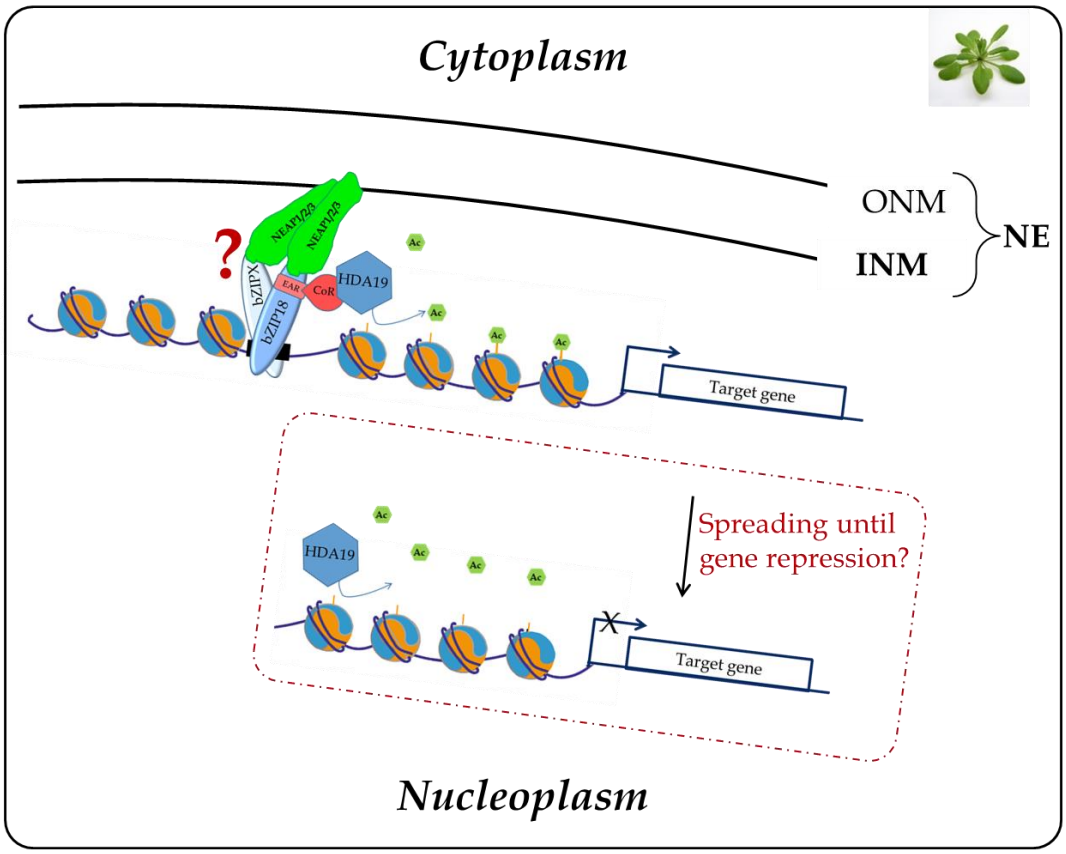

Figure 5-3: Alternative proposed model of AtNEAP and AtbZIP18 function in gene repression in *A. thaliana*. The TFs bZIP function as dimers and would be tethered by AtNEAP dimers, bZIPX: AtbZIP34, 52 or 61. CoR: Co-repressors such as AtSIN3, AtSAP18 or TPL. Black rectangle represents the DNA motif for interaction with bZIP TFs. HDA19 is a histone deacetylase and leads to gene repression but the mechanism of the spreading remains to be elucidated.

due to a stimuli or a stress from the environment, AtbZIP18 could be released from the NE tethering and would be able to trigger a gene repression pathway, ***Figure 5-2***. Therefore, it would be a matter of interest to investigate whether AtbZIP18 once bound to AtNEAP is still able to dimerize with another AtbZIP and to bind DNA or co-factors.

Alternatively, if the interaction of AtNEAP proteins with AtbZIP18 simultaneously bound to DNA is possible, it would suggest that AtNEAPs could be partially responsible for the tethering of chromatin domains at the nuclear periphery by linking TFs, ***Figure 5-3***. AtbZIP18 is a putative transcription repressor as its loss-of-function leads to the up-regulation of 117 genes out of 133 differentially expressed genes (Fold Change ≥2), (Gibalová *et al*., 2017). One possible explanation of this repressive activity is the presence of an EAR motif located at the 3' of the BRLZ domain within AtbZIP18. The EAR motif is a common motif found in TFs implicated in gene repression as this motif is known to be involved in transcriptional inhibition through chromatin modifications, (Gibalová *et al*., 2017; Kagale and Rozwadowski, 2010), ***Figure 5-3***. Indeed, the EAR motif is important for interaction of the TF with chromatin remodelling factors. These co-repressors are able to recruit AtHDA19, which is a histone deacetylase (HDAC), leading to gene repression, (Kagale and Rozwadowski, 2010, 2011).

AtbZIP18 was the only TF revealed by MYTH but recent experiments from the lab suggest that another transcription factor called AtMaMYB is also able to interact both with AtNEAP1 and AtbZIP18 in MYTH (Voisin and Vanrobays unpublished). Although these new interactions have to be confirmed *in vivo*, it suggests that other TFs interact with AtNEAPs.

III – Future work and perspectives

During the initial steps of this work, a Y2H screen was performed but failed to detect any new interactors. Also, neither AtbZIP18 nor AtMaMYB were identified in these screens. The failure to detect new partners could be explained by the fact that this system, compared to

the MYTH system, is not adapted for the specific requirements of TM proteins such as AtNEAPs, probably leading to a mis-localisation of AtNEAPs in yeast. Indeed, in Pawar-Menon, PhD thesis, 2015, a MYTH experiment revealed a weak interaction between AtSUN1/AtNEAP1 and AtSUN2/AtNEAP1 which was, nevertheless, confirmed by apFRET, (Pawar *et al*., 2016).

Thus, it would be interesting to perform these Y2H screens, this time with AtNEAPs having the TM domain deleted. The fact that results obtained so far to identify AtNEAP partners have resulted only in the identification of two TFs, AtbZIP18 and AtMaMYB, suggests that interaction between AtNEAP proteins and chromatin is indirect through TFs. If AtNEAP proteins interact with other components of the nuclear periphery, this will have to be identified by other strategies than Y2H.

One such strategy could be to apply immunoprecipitation (IP) of AtNEAP proteins followed by Mass-Spectrometry (MS) sequencing. The new generated antibodies successfully detected AtNEAP proteins on WB analysis, at least when over-expressed fusion proteins, ***Figure 4-9***, and it would be interesting to validate the absence of AtNEAP proteins in the triple *Atneap1/2/3*. In the future, IP protocols will have to be established, which have to be appropriate for the very hydrophobic AtNEAP proteins. This could first be tested on AtNEAP proteins expressed in yeast and then by using a line expressing c-Myc- or Flag-HA-tagged AtNEAP1 protein in a triple *Atneap1/2/3* background. Preliminary attempts to perform IP were tested but failed as AtNEAP proteins proved very challenging to extract, possibly remaining associated with the nuclear membrane and remaining in the insoluble fraction. Indeed, in the study presented in this thesis, a wide investigation of new AtNEAP interactants was initiated but was not successful due to failure at early steps of the protocol when preparing samples for IP due to the insolubility of the AtNEAPs.

It is striking to note that some early experiments to purify the putative plant lamina/nucleoskeleton by (Sakamoto and Takagi, 2013) also failed to detect AtNEAPs, AtbZIP18 or AtMaMYB. This could highlight the difficulties linked to the relative insolubility of AtNEAP proteins in standard buffers and explain their absence in the list of 660 proteins of the crude lamina (Sakamoto and Takagi, 2013). More recently, (Goto *et al*., 2019), performed a wide nuclear proteome investigation of *A. thaliana* with MS analysis. Of 1541 proteins identified, some nucleoskeleton proteins were found, such as AtCRWN1, AtCRWN4, AtKAKU4, AtSUN1, AtSUN2, but not AtNEAPs, AtbZIP18 or AtMaMYB. It seems that further protocol optimization is required in order to be able to do MS and define what the AtNEAP interactome *in vivo* exactly is.

The fact that the triple *Atneap1/2/3* mutant did not show an apparent phenotype either during the vegetative phase or in the shoot or root, suggests firstly that AtNEAP proteins may have a redundant function with other actors at the nuclear periphery. Alternatively, AtNEAP function could be related to stress response and therefore, mutants could show a stress-induced phenotype. Thus, this mutant, as well as all the single and double mutants could be challenged under different stress conditions like heat, cold, drought, salt or light duration and intensity. Indeed, plants have to adapt to changes of light and temperature between night and day and depending on weather. It has been shown that during photomorphogenesis in plants, heterochromatin organization is profoundly reorganized (Bourbousse *et al*., 2015) and a heat shock of 30h at 37°C induced heterochromatin decondensation, (Pecinka *et al*., 2010; Tittel-Elmer *et al*., 2010). Therefore, the plasticity of the genome is really important for plants during environment-dependent switches, which are particularly challenging. A defect in chromatin organization and positioning of the chromocentres could be deleterious at these critical steps in mutant plants. That is why a study of *Atneap* mutants under stress conditions could therefore reveal effects on growth conditions and nuclear morphology integrity. Also,

as proposed in models (***Figure 5-2 and 5-3***), AtNEAP proteins could be part of a signalling pathway; linking AtbZIP18 whose function is to repress specific target genes through the help of AtHDA19. Roles of this HDAC have been investigated and AtHDA19 was reported to control root cell elongation, modulate seed germination and to be implicated in salt- as well as abscisic acid stress-response, (Chen and Wu, 2010; Chen *et al*., 2015). Thus, the specific roles of HDA19 could be helpful in order to determine which kind of stresses could be applied to the triple *Atneap* mutant or the single *Atbzip18*.

So far, the triple *Atneap* mutant characterization has been mainly phenotypic. A deeper molecular characterization is required in order to get insight into the molecular roles of the AtNEAP protein family. Image analysis of the nuclear periphery in the triple *Atneap* mutant revealed mislocalisation of chromocentres as the distance from the nuclear periphery was increased. This was also visible in the triple *Atsun1/4/5* mutant, (Poulet *et al*., 2016) and in mammals presenting laminopathies, nuclear shape is also altered with lobulation of the NE, thickening of the nuclear lamina and loss of peripheral heterochromatin, (Mattout *et al*., 2006). An altered pattern of heterochromatin positioning leads to transcriptional alterations and for that purpose, RNAseq analysis might be relevant to reveal silencing release and sporadic transcription at the centromeric and pericentromeric regions or change in gene expression.

A rearrangement of heterochromatin would ultimately modify deeply the epigenome organization in the *Atneap* triple mutant. Therefore it could be interesting to perform whole genome bisulfite sequencing analysis as well as ChIP-seq on permissive and repressive histone marks such as, respectively, H3K4me3, H3K9Ac, and H3K9me2, H3K27me1, H3K27me3, to see which genes are affected by changes in this mutant. Also, to draw chromatin-chromatin interaction map at the whole genome level, Hi-C analyses could be carried out to look at potential modifications.

All those genome-wide analyses could also be carried out on stress-induced plants to exacerbate mutant effects on genome plasticity. In parallel, crossing the *Atneap1/2/3* mutant with the At*bZIP18* mutant would be worthwhile to investigate their interaction pattern and function in the protein network at the nuclear periphery. Indeed, *Atbzip18* single mutants, in addition to showing an increased number of aborted pollen grains and defects in living ones, shows a global gene up-regulation, (see ***paragraph II*** above). RNA-Seq experiments comparing the triple *Atneap1/2/3* with a quadruple *Atneap1/2/3, Atbzip18* could reveal which part of the transcriptome that might be altered in *Atneap1/2/3* mutants is mediated by AtbZIP18. In the same way, ChIP-Seq experiments could be designed to investigate these target sites if an AtbZIP18-GFP construct expressed under its own promoter is introduced into the *Atneap1/2/3* mutant line. A wide study using DAP-seq technology, (O'Malley *et al*., 2016), determined specific DNA-binding motives of multiple TFs including AtbZIP18 and some of its partners of TF group I, AtbZIP52 and 51. These motifs are -TGACAGCTGT- with a higher confidence for the core -CAGCT- and this information could be helpful for discovering AtbZIP18 target genes linked to the nuclear periphery. Indeed, from RNA-Seq results, the putative AtbZIP18 target genes can be identified and upstream regions can be screened for this common motif. Then, a co-expression analysis of these genes can be performed.

Altogether, these multiple approaches would be very promising to better define the impact of the nuclear periphery on gene expression and especially to further elucidate the role of AtNEAP proteins at the nuclear periphery, in anchoring chromatin and in the nucleoskeleton.

REFERENCES

REFERENCES

Alber, F., Dokudovskaya, S., Veenhoff, L.M., Zhang, W., Kipper, J., Devos, D., Suprapto, A., Karni-Schmidt, O., Williams, R., Chait, B.T., *et al*. (2007). The molecular architecture of the nuclear pore complex. Nature *450*, 695–701.

Bernard, P., and Couturier, M. (1992). Cell killing by the F plasmid CcdB protein involves poisoning of DNA-topoisomerase II complexes. J. Mol. Biol. *226*, 735–745.

Bharath, M.M.S., Chandra, N.R., and Rao, M.R.S. (2002). Prediction of an HMG-box fold in the C-terminal domain of histone H1: insights into its role in DNA condensation. Proteins *49*, 71–81.

Bi, X., Cheng, Y.-J., Hu, B., Ma, X., Wu, R., Wang, J.-W., and Liu, C. (2017). Nonrandom domain organization of the Arabidopsis genome at the nuclear periphery. Genome Res. *27*, 1162–1173.

Bourbousse, C., Mestiri, I., Zabulon, G., Bourge, M., Formiggini, F., Koini, M.A., Brown, S.C., Fransz, P., Bowler, C., and Barneche, F. (2015). Light signaling controls nuclear architecture reorganization during seedling establishment. Proc. Natl. Acad. Sci. U.S.A. *112*, E2836-2844.

Bradbury, E.M. (1992). Reversible histone modifications and the chromosome cell cycle. Bioessays *14*, 9–16.

Breyne, P., Van Montagu, M., and Gheysen, G. (1994). The role of scaffold attachment regions in the structural and functional organization of plant chromatin. Transgenic Res. *3*, 195–202.

Brohawn, S.G., Partridge, J.R., Whittle, J.R.R., and Schwartz, T.U. (2009). The nuclear pore complex has entered the atomic age. Structure *17*, 1156–1168.

Burke, B. (2012). It takes KASH to hitch to the SUN. Cell *149*, 961–963.

Burke, B., and Stewart, C.L. (2013). The nuclear lamins: flexibility in function. Nat. Rev. Mol. Cell Biol. *14*, 13–24.

Burns, L.T., and Wente, S.R. (2014). From hypothesis to mechanism: uncovering nuclear pore complex links to gene expression. Mol. Cell. Biol. *34*, 2114–2120.

Capelson, M., and Hetzer, M.W. (2009). The role of nuclear pores in gene regulation, development and disease. EMBO Rep. *10*, 697–705.

Chen, L.-T., and Wu, K. (2010). Role of histone deacetylases HDA6 and HDA19 in ABA and abiotic stress response. Plant Signal Behav. *5*, 1318–1320.

Chen, C.-Y., Wu, K., and Schmidt, W. (2015). The histone deacetylase HDA19 controls root cell elongation and modulates a subset of phosphate starvation responses in Arabidopsis. Sci. Rep. *5*, 15708.

Chodavarapu, R.K., Feng, S., Bernatavichute, Y.V., Chen, P.-Y., Stroud, H., Yu, Y., Hetzel, J.A., Kuo, F., Kim, J., Cokus, S.J., *et al*. (2010). Relationship between nucleosome positioning and DNA methylation. Nature *466*, 388–392.

Ciska, M., and Moreno Díaz de la Espina, S. (2014). The intriguing plant nuclear lamina. Front Plant Sci. *5*, 166.

Ciska, M., Masuda, K., and Moreno Díaz de la Espina, S. (2013). Lamin-like analogues in plants: the characterization of NMCP1 in Allium cepa. J. Exp. Bot. *64*, 1553–1564.

Clapier, C.R., and Cairns, B.R. (2009). The Biology of Chromatin Remodeling Complexes. Annual Review of Biochemistry *78*, 273–304.

Crisp, M., Liu, Q., Roux, K., Rattner, J.B., Shanahan, C., Burke, B., Stahl, P.D., and Hodzic, D. (2006). Coupling of the nucleus and cytoplasm: role of the LINC complex. J. Cell Biol. *172*, 41–53.

DeGrasse, J.A., DuBois, K.N., Devos, D., Siegel, T.N., Sali, A., Field, M.C., Rout, M.P., and Chait, B.T. (2009). Evidence for a shared nuclear pore complex architecture that is conserved from the last common eukaryotic ancestor. Mol. Cell Proteomics *8*, 2119–2130.

Desrosiers, R., and Tanguay, R.M. (1986). Further characterization of the posttranslational modifications of core histones in response to heat and arsenite stress in Drosophila. Biochem. Cell Biol. *64*, 750–757.

Desset, S., Poulet, A., and Tatout, C. (2018). Quantitative 3D Analysis of Nuclear Morphology and Heterochromatin Organization from Whole-Mount Plant Tissue Using NucleusJ. Methods Mol. Biol. *1675*, 615–632.

Dieppois, G., and Stutz, F. (2010). Connecting the transcription site to the nuclear pore: a multi-tether process that regulates gene expression. J. Cell. Sci. *123*, 1989–1999.

Dilsaver, M.R., Chen, P., Thompson, T.A., Reusser, T., Mukherjee, R.N., Oakey, J., and Levy, D.L. (2018). Emerin induces nuclear breakage in Xenopus extract and early embryos. Mol. Biol. Cell mbcE18050277.

Dittmer, T.A., Stacey, N.J., Sugimoto-Shirasu, K., and Richards, E.J. (2007). LITTLE NUCLEI genes affecting nuclear morphology in Arabidopsis thaliana. Plant Cell *19*, 2793–2803.

Dröge-Laser, W., Snoek, B.L., Snel, B., and Weiste, C. (2018). The Arabidopsis bZIP transcription factor family-an update. Curr. Opin. Plant Biol. *45*, 36–49.

Elgin, S.C.R., and Grewal, S.I.S. (2003). Heterochromatin: silence is golden. Curr. Biol. *13*, R895-898.

Evans, D.E., Pawar, V., Smith, S.J., and Graumann, K. (2014). Protein interactions at the higher plant nuclear envelope: evidence for a linker of nucleoskeleton and cytoskeleton complex. Front Plant Sci. *5*, 183.

Fauser, F., Schiml, S., and Puchta, H. (2014). Both CRISPR/Cas-based nucleases and nickases can be used efficiently for genome engineering in Arabidopsis thaliana. Plant J. *79*, 348–359.

Feng, S., Cokus, S.J., Schubert, V., Zhai, J., Pellegrini, M., and Jacobsen, S.E. (2014). Genome-wide Hi-C analyses in wild-type and mutants reveal high-resolution chromatin interactions in Arabidopsis. Mol. Cell *55*, 694–707.

Fields, S., and Song, O. (1989). A novel genetic system to detect protein-protein interactions. Nature *340*, 245–246.

Fiserova, J., and Goldberg, M.W. (2010). Relationships at the nuclear envelope: lamins and nuclear pore complexes in animals and plants. Biochem. Soc. Trans. *38*, 829–831.

Fiserova, J., Kiseleva, E., and Goldberg, M.W. (2009). Nuclear envelope and nuclear pore complex structure and organization in tobacco BY-2 cells. Plant J. *59*, 243–255.

Fransz, P., De Jong, J.H., Lysak, M., Castiglione, M.R., and Schubert, I. (2002). Interphase chromosomes in Arabidopsis are organized as well defined chromocenters from which euchromatin loops emanate. Proc. Natl. Acad. Sci. U.S.A. *99*, 14584–14589.

Fransz, P., Soppe, W., and Schubert, I. (2003). Heterochromatin in interphase nuclei of Arabidopsis thaliana. Chromosome Res. *11*, 227–240.

Fransz, P., ten Hoopen, R., and Tessadori, F. (2006). Composition and formation of heterochromatin in Arabidopsis thaliana. Chromosome Res. *14*, 71–82.

Gibalová, A., Steinbachová, L., Hafidh, S., Bláhová, V., Gadiou, Z., Michailidis, C., Műller, K., Pleskot, R., Dupľáková, N., and Honys, D. (2017). Characterization of pollen-expressed bZIP protein interactions and the role of ATbZIP18 in the male gametophyte. Plant Reprod. *30*, 1–17.

Goto, C., Tamura, K., Fukao, Y., Shimada, T., and Hara-Nishimura, I. (2014). The Novel Nuclear Envelope Protein KAKU4 Modulates Nuclear Morphology in Arabidopsis. Plant Cell *26*, 2143–2155.

Goto, C., Hashizume, S., Fukao, Y., Hara-Nishimura, I., and Tamura, K. (2019). Comprehensive nuclear proteome of Arabidopsis obtained by sequential extraction. Nucleus.

Graumann, K. (2014). Evidence for LINC1-SUN associations at the plant nuclear periphery. PLoS ONE *9*, e93406.

Graumann, K., Runions, J., and Evans, D.E. (2010). Characterization of SUN-domain proteins at the higher plant nuclear envelope. Plant J. *61*, 134–144.

Grob, S., Schmid, M.W., and Grossniklaus, U. (2014). Hi-C analysis in Arabidopsis identifies the KNOT, a structure with similarities to the flamenco locus of Drosophila. Mol. Cell *55*, 678–693.

Grossman, E., Medalia, O., and Zwerger, M. (2012). Functional architecture of the nuclear pore complex. Annu. Rev. Biophys. *41*, 557–584.

Gu, Y., Zebell, S.G., Liang, Z., Wang, S., Kang, B.-H., and Dong, X. (2016). Nuclear Pore Permeabilization Is a Convergent Signaling Event in Effector-Triggered Immunity. Cell *166*, 1526-1538.e11.

Guelen, L., Pagie, L., Brasset, E., Meuleman, W., Faza, M.B., Talhout, W., Eussen, B.H., de Klein, A., Wessels, L., de Laat, W., *et al*. (2008). Domain organization of human chromosomes revealed by mapping of nuclear lamina interactions. Nature *453*, 948–951.

Gumber, H.K., McKenna, J.F., Estrada, A.L., Tolmie, A.F., Graumann, K., and Bass, H.W. (2019). Identification and characterization of genes encoding the nuclear envelope LINC complex in the monocot species Zea mays. J. Cell. Sci. *132*.

Hagan, I., and Yanagida, M. (1995). The product of the spindle formation gene sad1+ associates with the fission yeast spindle pole body and is essential for viability. J. Cell Biol. *129*, 1033–1047.

Heitz, E. (1928). Das Heterochromatin der Moose. I Jahrb. Wiss. Bot. 69: 762–818.

Henikoff, S. (2008). Nucleosome destabilization in the epigenetic regulation of gene expression. Nat. Rev. Genet. *9*, 15–26.

Ho, R., and Hegele, R.A. (2018). Complex effects of laminopathy mutations on nuclear structure and function. Clin. Genet.

Huber, M.D., Guan, T., and Gerace, L. (2009). Overlapping functions of nuclear envelope proteins NET25 (Lem2) and emerin in regulation of extracellular signal-regulated kinase signaling in myoblast differentiation. Mol. Cell. Biol. *29*, 5718–5728.

Hutten, S., Flotho, A., Melchior, F., and Kehlenbach, R.H. (2008). The Nup358-RanGAP complex is required for efficient importin alpha/beta-dependent nuclear import. Mol. Biol. Cell *19*, 2300–2310.

Imhof, A., and Becker, P.B. (2001). Modifications of the histone N-terminal domains. Evidence for an “epigenetic code”? Mol. Biotechnol. *17*, 1–13.

Jenuwein, T., and Allis, C.D. (2001). Translating the histone code. Science *293*, 1074–1080.

Kagale, S., and Rozwadowski, K. (2010). Small yet effective: the ethylene responsive element binding factor-associated amphiphilic repression (EAR) motif. Plant Signal. Behav. *5*, 691–694.

Kagale, S., and Rozwadowski, K. (2011). EAR motif-mediated transcriptional repression in plants. Epigenetics *6*, 141–146.

Karpova, T., and McNally, J.G. (2006). Detecting protein-protein interactions with CFP-YFP FRET by acceptor photobleaching. Curr Protoc Cytom *Chapter 12*, Unit12.7.

Karpova, T.S., Baumann, C.T., He, L., Wu, X., Grammer, A., Lipsky, P., Hager, G.L., and McNally, J.G. (2003). Fluorescence resonance energy transfer from cyan to yellow fluorescent protein detected by acceptor photobleaching using confocal microscopy and a single laser. J Microsc *209*, 56–70.

Kind, J., Pagie, L., Ortabozkoyun, H., Boyle, S., de Vries, S.S., Janssen, H., Amendola, M., Nolen, L.D., Bickmore, W.A., and van Steensel, B. (2013). Single-cell dynamics of genome-nuclear lamina interactions. Cell *153*, 178–192.

van Koningsbruggen, S., Gierlinski, M., Schofield, P., Martin, D., Barton, G.J., Ariyurek, Y., den Dunnen, J.T., and Lamond, A.I. (2010). High-resolution whole-genome sequencing reveals that specific chromatin domains from most human chromosomes associate with nucleoli. Mol. Biol. Cell *21*, 3735–3748.

Laemmli, U.K. (1970). Cleavage of structural proteins during the assembly of the head of bacteriophage T4. Nature *227*, 680–685.

Law, M.J., Lower, K.M., Voon, H.P.J., Hughes, J.R., Garrick, D., Viprakasit, V., Mitson, M., De Gobbi, M., Marra, M., Morris, A., *et al*. (2010). ATR-X syndrome protein targets tandem repeats and influences allele-specific expression in a size-dependent manner. Cell *143*, 367–378.

Lewis, C.D., Lebkowski, J.S., Daly, A.K., and Laemmli, U.K. (1984). Interphase nuclear matrix and metaphase scaffolding structures. J. Cell Sci. Suppl. *1*, 103–122.

Li, J.-F., and Nebenführ, A. (2010). FAST technique for Agrobacterium-mediated transient gene expression in seedlings of Arabidopsis and other plant species. Cold Spring Harb Protoc *2010*, pdb.prot5428.

Link, J., Leubner, M., Schmitt, J., Göb, E., Benavente, R., Jeang, K.-T., Xu, R., and Alsheimer, M. (2014). Analysis of meiosis in SUN1 deficient mice reveals a distinct role of SUN2 in mammalian meiotic LINC complex formation and function. PLoS Genet. *10*, e1004099.

Luger, K., Mäder, A.W., Richmond, R.K., Sargent, D.F., and Richmond, T.J. (1997). Crystal structure of the nucleosome core particle at 2.8 A resolution. Nature *389*, 251–260.

Ma, X.M., and Blenis, J. (2009). Molecular mechanisms of mTOR-mediated translational control. Nat. Rev. Mol. Cell Biol. *10*, 307–318.

Macara, I.G. (2001). Transport into and out of the nucleus. Microbiol. Mol. Biol. Rev. *65*, 570–594, table of contents.

Maison, C., Bailly, D., Roche, D., Montes de Oca, R., Probst, A.V., Vassias, I., Dingli, F., Lombard, B., Loew, D., Quivy, J.-P., *et al*. (2011). SUMOylation promotes de novo targeting of HP1α to pericentric heterochromatin. Nat. Genet. *43*, 220–227.

Malone, C.J., Fixsen, W.D., Horvitz, H.R., and Han, M. (1999). UNC-84 localizes to the nuclear envelope and is required for nuclear migration and anchoring during C. elegans development. Development *126*, 3171–3181.

Marsischky, G., and LaBaer, J. (2004). Many paths to many clones: a comparative look at high-throughput cloning methods. Genome Res. *14*, 2020–2028.

Masuda, K., Xu, Z.J., Takahashi, S., Ito, A., Ono, M., Nomura, K., and Inoue, M. (1997). Peripheral framework of carrot cell nucleus contains a novel protein predicted to exhibit a long alpha-helical domain. Exp. Cell Res. *232*, 173–181.

Mattout, A., Dechat, T., Adam, S.A., Goldman, R.D., and Gruenbaum, Y. (2006). Nuclear lamins, diseases and aging. Current Opinion in Cell Biology *18*, 335–341.

Meier, I. (2001). The plant nuclear envelope. Cell. Mol. Life Sci. *58*, 1774–1780.

Meier, I. (2016). LINCing the eukaryotic tree of life - towards a broad evolutionary comparison of nucleocytoplasmic bridging complexes. J. Cell. Sci. *129*, 3523–3531.

Méjat, A., and Misteli, T. (2010). LINC complexes in health and disease. Nucleus *1*, 40.

Meng, J.-J., Rojas, M., Bacon, W., Stickney, J.T., and Ip, W. (2005). Methods to study protein-protein interactions. Methods Mol. Biol. *289*, 341–358.

Moreno Díaz de la Espina, S., Barthellemy, I., and Cerezuela, M.A. (1991). Isolation and ultrastructural characterization of the residual nuclear matrix in a plant cell system. Chromosoma *100*, 110–117.

Mounkes, L.C., and Stewart, C.L. (2004). Aging and nuclear organization: lamins and progeria. Current Opinion in Cell Biology *16*, 322–327.

Murphy, S.P., Simmons, C.R., and Bass, H.W. (2010). Structure and expression of the maize (Zea mays L.) SUN-domain protein gene family: evidence for the existence of two divergent classes of SUN proteins in plants. BMC Plant Biol. *10*, 269.

Németh, A., Conesa, A., Santoyo-Lopez, J., Medina, I., Montaner, D., Péterfia, B., Solovei, I., Cremer, T., Dopazo, J., and Längst, G. (2010). Initial genomics of the human nucleolus. PLoS Genet. *6*, e1000889.

Oda, Y., and Fukuda, H. (2011). Dynamics of Arabidopsis SUN proteins during mitosis and their involvement in nuclear shaping. Plant J. *66*, 629–641.

Okada, T., Endo, M., Singh, M.B., and Bhalla, P.L. (2005). Analysis of the histone H3 gene family in Arabidopsis and identification of the male-gamete-specific variant AtMGH3. Plant J. *44*, 557–568.

O'Malley, R.C., Huang, S.-S.C., Song, L., Lewsey, M.G., Bartlett, A., Nery, J.R., Galli, M., Gallavotti, A., and Ecker, J.R. (2016). Cistrome and Epicistrome Features Shape the Regulatory DNA Landscape. Cell *165*, 1280–1292.

Omarov, R., Sparks, K., Smith, L., Zindovic, J., and Scholthof, H.B. (2006). Biological relevance of a stable biochemical interaction between the tombusvirus-encoded P19 and short interfering RNAs. J. Virol. *80*, 3000–3008.

Pawar, V., Poulet, A., Détourné, G., Tatout, C., Vanrobays, E., Evans, D.E., and Graumann, K. (2016). A novel family of plant nuclear envelope-associated proteins. J. Exp. Bot. *67*, 5699–5710.

Pawar-Menon Vidya, 2015. PhD Thesis. Novel plant nuclear envelope-associated coiled-coil proteins. Oxford Brookes University.

Pecinka, A., Dinh, H.Q., Baubec, T., Rosa, M., Lettner, N., and Mittelsten Scheid, O. (2010). Epigenetic regulation of repetitive elements is attenuated by prolonged heat stress in Arabidopsis. Plant Cell *22*, 3118–3129.

Petesch, S.J., and Lis, J.T. (2012). Overcoming the nucleosome barrier during transcript elongation. Trends Genet. *28*, 285–294.

Picart-Picolo, A., Picault, N., and Pontvianne, F. (2019). Ribosomal RNA genes shape chromatin domains associating with the nucleolus. Nucleus 1–6.

Pombo, A., and Dillon, N. (2015). Three-dimensional genome architecture: players and mechanisms. Nat. Rev. Mol. Cell Biol. *16*, 245–257.

Pontvianne, F., Carpentier, M.-C., Durut, N., Pavlištová, V., Jaške, K., Schořová, Š., Parrinello, H., Rohmer, M., Pikaard, C.S., Fojtová, M., *et al*. (2016). Identification of Nucleolus-Associated Chromatin Domains Reveals a Role for the Nucleolus in 3D Organization of the A. thaliana Genome. Cell Rep. *16*, 1574–1587.

Poulet, A., Arganda-Carreras, I., Legland, D., Probst, A.V., Andrey, P., and Tatout, C. (2014). NucleusJ: an ImageJ plugin for quantifying 3D images of interphase nuclei. Bioinformatics.

Poulet, A., Probst, A.V., Graumann, K., Tatout, C., and Evans, D. (2016). Exploring the evolution of the proteins of the plant nuclear envelope. Nucleus *8*, 46–59.

Poulet, A., Duc, C., Voisin, M., Desset, S., Tutois, S., Vanrobays, E., Benoit, M., Evans, D.E., Probst, A.V., and Tatout, C. (2017). The LINC complex contributes to heterochromatin organisation and transcriptional gene silencing in plants. J. Cell. Sci. *130*, 590–601.

Probst, A.V., Dunleavy, E., and Almouzni, G. (2009). Epigenetic inheritance during the cell cycle. Nat. Rev. Mol. Cell Biol. *10*, 192–206.

Reddy, K.L., Zullo, J.M., Bertolino, E., and Singh, H. (2008). Transcriptional repression mediated by repositioning of genes to the nuclear lamina. Nature *452*, 243–247.

Ricci, M.A., Manzo, C., García-Parajo, M.F., Lakadamyali, M., and Cosma, M.P. (2015). Chromatin fibers are formed by heterogeneous groups of nucleosomes in vivo. Cell *160*, 1145–1158.

Rose, A., Patel, S., and Meier, I. (2004). The plant nuclear envelope. Planta *218*, 327–336.

Rothballer, A., and Kutay, U. (2013). The diverse functional LINCs of the nuclear envelope to the cytoskeleton and chromatin. Chromosoma *122*, 415–429.

Roudier, F., Teixeira, F.K., and Colot, V. (2009). Chromatin indexing in Arabidopsis: an epigenomic tale of tails and more. Trends Genet. *25*, 511–517.

Roudier, F., Ahmed, I., Bérard, C., Sarazin, A., Mary-Huard, T., Cortijo, S., Bouyer, D., Caillieux, E., Duvernois-Berthet, E., Al-Shikhley, L., *et al*. (2011). Integrative epigenomic mapping defines four main chromatin states in Arabidopsis. EMBO J. *30*, 1928–1938.

Rutowicz, K., Lirski, M., Mermaz, B., Schubert, J., Teano, G., Mestiri, I., Kroteń, M.A., Fabrice, T.N., Fritz, S., Grob, S., *et al*. (2018). Linker histones regulate fine-scale chromatin organization and modulate developmental decisions in Arabidopsis. BioRxiv 458364.

Sakamoto, Y., and Takagi, S. (2013). LITTLE NUCLEI 1 and 4 regulate nuclear morphology in Arabidopsis thaliana. Plant Cell Physiol. *54*, 622–633.

Samson, C., Petitalot, A., Celli, F., Herrada, I., Ropars, V., Le Du, M.-H., Nhiri, N., Jacquet, E., Arteni, A.-A., Buendia, B., *et al*. (2018). Structural analysis of the ternary complex between lamin A/C, BAF and emerin identifies an interface disrupted in autosomal recessive progeroid diseases. Nucleic Acids Res. *46*, 10460–10473.

Schiml, S., and Puchta, H. (2016). Revolutionizing plant biology: multiple ways of genome engineering by CRISPR/Cas. Plant Methods *12*, 8.

Schiml, S., Fauser, F., and Puchta, H. (2017). CRISPR/Cas-Mediated In Planta Gene Targeting. Methods Mol. Biol. *1610*, 3–11.

Sequeira-Mendes, J., Aragüez, I., Peiró, R., Mendez-Giraldez, R., Zhang, X., Jacobsen, S.E., Bastolla, U., and Gutierrez, C. (2014). The Functional Topography of the Arabidopsis Genome Is Organized in a Reduced Number of Linear Motifs of Chromatin States. Plant Cell *26*, 2351–2366.

Smith, S., Galinha, C., Desset, S., Tolmie, F., Evans, D., Tatout, C., and Graumann, K. (2015). Marker gene tethering by nucleoporins affects gene expression in plants. Nucleus *6*, 471–478.

Smoyer, C.J., and Jaspersen, S.L. (2014). Breaking down the wall: the nuclear envelope during mitosis. Curr. Opin. Cell Biol. *26*, 1–9.

Starr, D.A. (2009). A nuclear-envelope bridge positions nuclei and moves chromosomes. J. Cell. Sci. *122*, 577–586.

van Steensel, B., and Belmont, A.S. (2017). Lamina-Associated Domains: Links with Chromosome Architecture, Heterochromatin, and Gene Repression. Cell *169*, 780–791.

van Steensel, B., and Henikoff, S. (2000). Identification of in vivo DNA targets of chromatin proteins using tethered dam methyltransferase. Nat. Biotechnol. *18*, 424–428.

Strahl, B.D., and Allis, C.D. (2000). The language of covalent histone modifications. Nature *403*, 41–45.

Talbert, P.B., Ahmad, K., Almouzni, G., Ausió, J., Berger, F., Bhalla, P.L., Bonner, W.M., Cande, W.Z., Chadwick, B.P., Chan, S.W.L., *et al*. (2012). A unified phylogeny-based nomenclature for histone variants. Epigenetics Chromatin *5*, 7.

Tamura, K., and Hara-Nishimura, I. (2011). Involvement of the nuclear pore complex in morphology of the plant nucleus. Nucleus *2*, 168–172.

Tamura, K., and Hara-Nishimura, I. (2013). The molecular architecture of the plant nuclear pore complex. J. Exp. Bot. *64*, 823–832.

Tamura, K., Fukao, Y., Iwamoto, M., Haraguchi, T., and Hara-Nishimura, I. (2010). Identification and characterization of nuclear pore complex components in Arabidopsis thaliana. Plant Cell *22*, 4084–4097.

Tamura, K., Iwabuchi, K., Fukao, Y., Kondo, M., Okamoto, K., Ueda, H., Nishimura, M., and Hara-Nishimura, I. (2013). Myosin XI-i links the nuclear membrane to the cytoskeleton to control nuclear movement and shape in Arabidopsis. Curr. Biol. *23*, 1776–1781.

Tatout, C., Evans, D.E., Vanrobays, E., Probst, A.V., and Graumann, K. (2014). The plant LINC complex at the nuclear envelope. Chromosome Res. *22*, 241–252.

Tittel-Elmer, M., Bucher, E., Broger, L., Mathieu, O., Paszkowski, J., and Vaillant, I. (2010). Stress-induced activation of heterochromatic transcription. PLoS Genet. *6*, e1001175.

Tran, E.J., King, M.C., and Corbett, A.H. (2014). Macromolecular transport between the nucleus and the cytoplasm: Advances in mechanism and emerging links to disease. Biochim. Biophys. Acta *1843*, 2784–2795.

Turgay, Y., Eibauer, M., Goldman, A.E., Shimi, T., Khayat, M., Ben-Harush, K., Dubrovsky-Gaupp, A., Sapra, K.T., Goldman, R.D., and Medalia, O. (2017). The molecular architecture of lamins in somatic cells. Nature *543*, 261–264.

Tzur, Y.B., Wilson, K.L., and Gruenbaum, Y. (2006). SUN-domain proteins: "Velcro" that links the nucleoskeleton to the cytoskeleton. Nat. Rev. Mol. Cell Biol. *7*, 782–788.

Ungricht, R., and Kutay, U. (2017). Mechanisms and functions of nuclear envelope remodelling. Nat. Rev. Mol. Cell Biol. *18*, 229–245.

Wang, H., Dittmer, T.A., and Richards, E.J. (2013). Arabidopsis CROWDED NUCLEI (CRWN) proteins are required for nuclear size control and heterochromatin organization. BMC Plant Biol. *13*, 200.

Wilson, K.L., and Foisner, R. (2010). Lamin-binding Proteins. Cold Spring Harb Perspect Biol *2*, a000554.

Wu, R.S., Panusz, H.T., Hatch, C.L., and Bonner, W.M. (1986). Histones and their modifications. CRC Crit. Rev. Biochem. *20*, 201–263.

Xu, X.M., Meulia, T., and Meier, I. (2007). Anchorage of plant RanGAP to the nuclear envelope involves novel nuclear-pore-associated proteins. Curr. Biol. *17*, 1157–1163.

Yang, Y., Wang, W., Chu, Z., Zhu, J.-K., and Zhang, H. (2017). Roles of Nuclear Pores and Nucleo-cytoplasmic Trafficking in Plant Stress Responses. Front. Plant Sci. *8*, 574.

Zhao, Q., Leung, S., Corbett, A.H., and Meier, I. (2006). Identification and characterization of the Arabidopsis orthologs of nuclear transport factor 2, the nuclear import factor of ran. Plant Physiol. *140*, 869–878.

Zhou, X., and Meier, I. (2013). How plants LINC the SUN to KASH. Nucleus *4*, 206–215.

Zhou, X., and Meier, I. (2014). Efficient plant male fertility depends on vegetative nuclear movement mediated by two families of plant outer nuclear membrane proteins. Proc. Natl. Acad. Sci. U.S.A.

Zhou, X., Graumann, K., Evans, D.E., and Meier, I. (2012). Novel plant SUN-KASH bridges are involved in RanGAP anchoring and nuclear shape determination. J. Cell Biol. *196*, 203–211.

Zhou, X., Graumann, K., Wirthmueller, L., Jones, J.D.G., and Meier, I. (2014). Identification of unique SUN-interacting nuclear envelope proteins with diverse functions in plants. J. Cell Biol. *205*, 677–692.

Zhou, X., Graumann, K., and Meier, I. (2015). The plant nuclear envelope as a multifunctional platform LINCed by SUN and KASH. J. Exp. Bot. *66*, 1649–1659.

APPENDIX

APPENDIX

Appendix I: Primer table for genotyping and transcript analysis

Primer Description	Primer name	Forward/ Reverse	Tm (°C)	Sequence
NEAP1_SAIL846_B07	CT487	F	49	CTCTGCAGCTTTCTTGTCTGG
	CT488	R	47	AGCTTGAAGCTTCTGCATCTG
SAIL_T-DNA	AP9	F	67	TAGCATCTGAATTTCATAACCAATCTCGATACAC
NEAP2_GABI_589B02: insertion:chr5 9409811	CT497	F	45	AAAGGGCCATTGATTACCAAG
	CT498	R	45	AGAAATTCGGAAGGGAAAGAC
GABI_9474_T-DNA	CT491	R	50	ATAATAACGCTGCGGACATCTACATTTT
neap2_surroundingCRISPRmutation	CT740	F	58	AGTGGACGATCTGAGATCACA
	CT741	R	59	TCTGCTCTTCTTTGTCTCTCCA
NEAP3_WiscDsLoxHs086_02C	CT492	F	59	TTCCTACCAAACCCAGAAACC
	CT493	R	57	TCAGCCAATTCCTTCACAAAC
WiscDsLoxHs_T-DNA	CT494	F	55	TGATCCATGTAGATTTCCCGGACATGAAG
NEAP1.1_RT-PCR_avalTDNA_450-961	CT569	F	60	GCAGAGGCAAGTGCTGATTC
NEAP2.3_RT-PCR_autourTDNA_161-345	CT570	F	59	AAGATTTCCCCACATGCATTGAA
	CT571	R	60	AACGTTCCGCCTGAAACTCT
NEAP2.3_RT-PCR_5'CDS	CT572	F	59	GTCGGATTCCGTCAAAACGA
	CT573	R	60	CACTTGCTTTAACTCAGCTGCC
NEAP3_RT-PCR_autourTDNA_123-322	CT574	F	60	ATGTGGTGTCTTTGGCCACT
NEAP3_RT-PCR_avalTDNA_215-322	CT576	F	57	GAGGCAGAAACAAGAGTTAAGAG
actin_qPCR_ACT2_At3g18780	CT649	F	65	GAGAGATTCAGATGCCCAGAAGTC
	CT650	R	57	TGGATTCCAGCAGCTTCCA
NEAP1.1_qRT-PCR	CT554	F	58	GGGAAAGAAGGGACATGGAG
	CT555	R	59	CTTGAACCCTGAATTGTCCCAG
NEAP2.3_qRT-PCR	CT556	F	58	ATCGGTTTCAGGGGAGAAAC
	CT557	R	60	TGCAACTACTGCATTTACACACC
NEAP3_qRT-PCR	CT558	F	60	TGGGAGAGCGAAACGATGTG
	CT559	R	60	TCAACGCCTAGAAAACGCAAC

Appendix II: Primer table used for vector constructs

Primer Description	Primer name	Forward/ Reverse	Tm (°C)	Sequence
AttB1_NEAP1_5'	CT495	F	53	GGGG ACA AGT TTG TAC AAA AAA GCA GGC TTC ATGTCTTATTCTGAAAAAACGA
AttB2_NEAP1_3'	CT496	R	55	GGGG AC CAC TTT GTA CAA GAA AGC TGG GTG TCATCTCTTGGAGACTACC
AttB2_NEAP1ΔTM_3'_(Δ324-stop)	CT499	R	55	GGGG AC CAC TTT GTA CAA GAA AGC TGG GTG TTTATCCCAAGACTCATTGTTA
AttB1_NEAP2_5'	CT500	F	56	GGGG ACA AGT TTG TAC AAA AAA GCA GGC TTC ATGTCGGATTCCGTCAAAAC
AttB2_NEAP2ΔTM_3'_(Δ311-stop)	CT501	R	55	GGGG AC CAC TTT GTA CAA GAA AGC TGG GTG TTGTTTCTCCCCTGAAACC
AttB1_NEAP3_5'	CT502	F	54	GGGG ACA AGT TTG TAC AAA AAA GCA GGC TTC ATGCCAACTTCTGTTAGTCT
AttB2_NEAP3ΔTM_3'_(Δ314-stop)	CT503	R	55	GGGG AC CAC TTT GTA CAA GAA AGC TGG GTG CAAGTTTTGGTTGCTAGAATG
NEAP2_CRISPR_25_Exon3	CT577	F	58	ATTGAAGGCACAGAATGTGAGCTC
	CT578	R	58	AAACGAGCTCACATTCTGTGCCTT
NEAP2_CRISPR_56_Exon1	CT579	F	52	ATTGCGCTTTTGAAAGATTTGGAT
	CT580	R	52	AAACATCCAAATCTTTCAAAAGCG
CRISPR_M13_RP	AP198	R	18	CAGGAAACAGCTATGACC
CRISPR_ss42	AP619		22	TCCCAGGATTAGAATGATTAGG
CRISPR_ss43	AP620		22	CGACTAAGGGTTTCTTATATGC
CRISPR_ss61	AP621		24	GAGCTCCAGGCCTCCCAGCTTTCG

Appendix III: pDONR Gateway vectors constructed in this study

Table (**A**) and maps (**B** - **D**) of the different pDONR Gateway vectors.

A

Type of vector	Construct description	Bacterial resistance	Promoter
pDONR_207	AtNEAP2	Gentamycin	**UC origin**
pDONR_Zeo	Atneap2_CRISPRmutation	Zeocyn	**UC origin**
	AtNEAP1		
	AtNEAP3		
	AtNEAP1_ΔTM		
	AtNEAP2_ΔTM		
	AtNEAP3_ΔTM		
pEn-Chimera	**Exon1_NEAP2_CRISPR**	**Ampicillin**	**AtU6-26**
	Exon3_NEAP2_CRISPR		

B

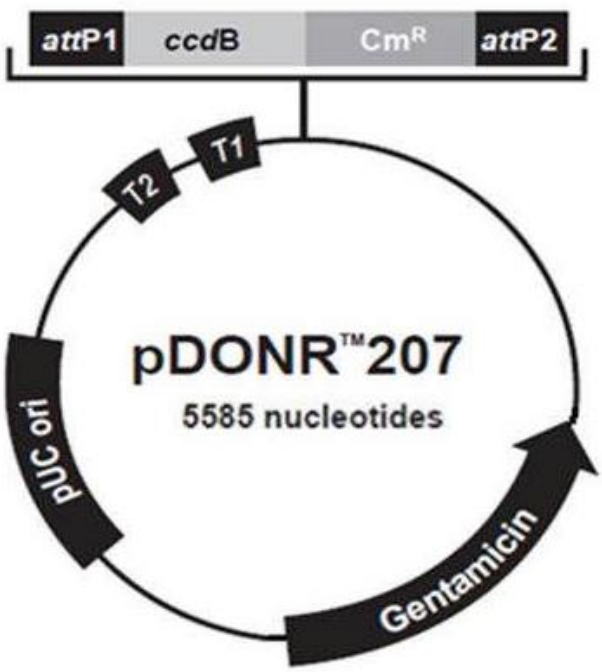

C

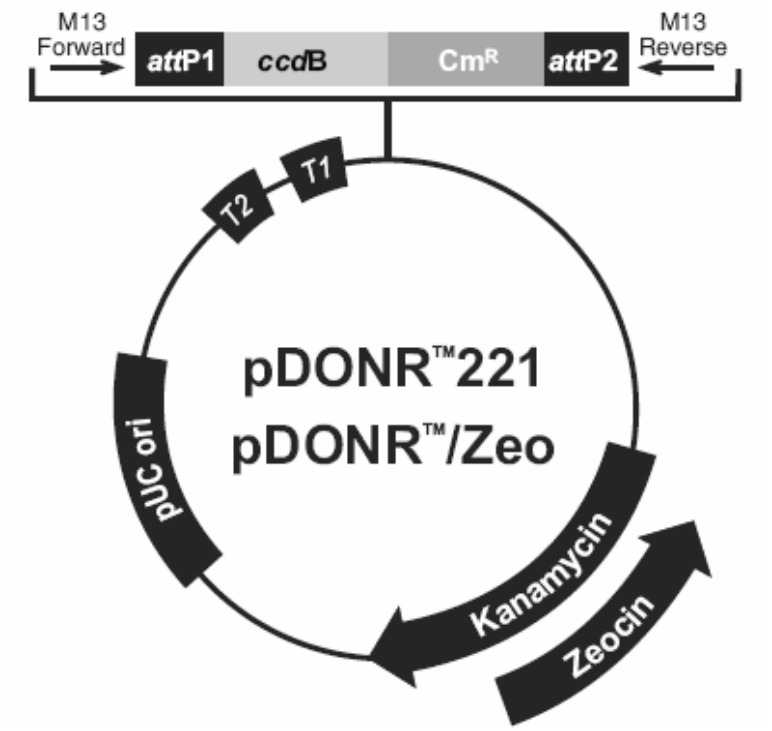
M13
Forward
attP1
ccdB
CmR
attP2
M13
Reverse
T2
T1
pDONR™221
pDONR™/Zeo
pUC ori
Kanamycin
Zeocin

D

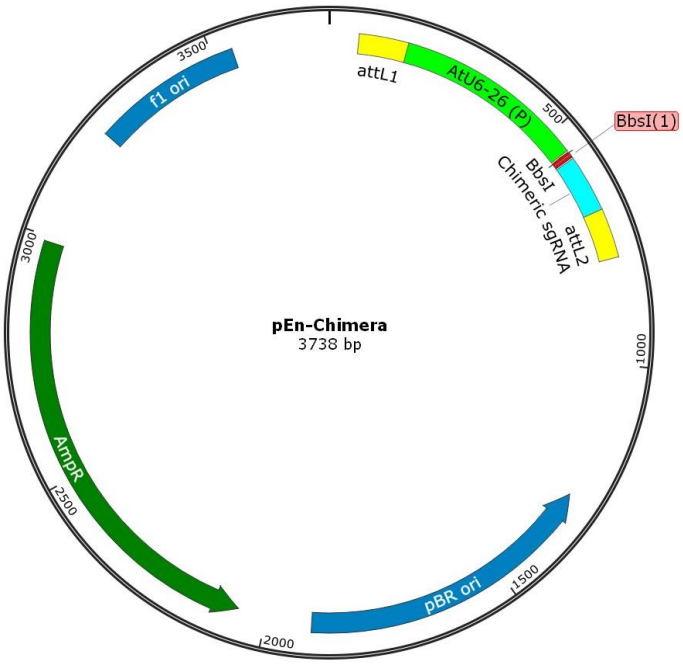
3500
f1 ori
attL1
AtU6-26 (P)
500
BbsI(1)
BbsI
Chimeric sgRNA
attL2
3000
pEn-Chimera
3738 bp
1000
AmpR
2500
pBR ori
1500
2000

Appendix IV: pDEST Gateway vectors constructed in this study for Y2H

Table (**A**) and maps (**B** and **C**) of the different pDEST Gateway vectors.

A

Type of vector	Construct description	Bacterial resistance	Promoter	Side of the fusion
pGADT7	AtNEAP1	Ampicillin	ADH1	N-ter
	AtNEAP2			
	AtNEAP3			
	AtNEAP1_ΔTM			
	AtNEAP2_ΔTM			
	AtNEAP3_ΔTM			
pGBKT7	AtNEAP1	Kanamycin		
	AtNEAP2			
	AtNEAP3			
	AtNEAP1_ΔTM			
	AtNEAP2_ΔTM			
	AtNEAP3_ΔTM			

B

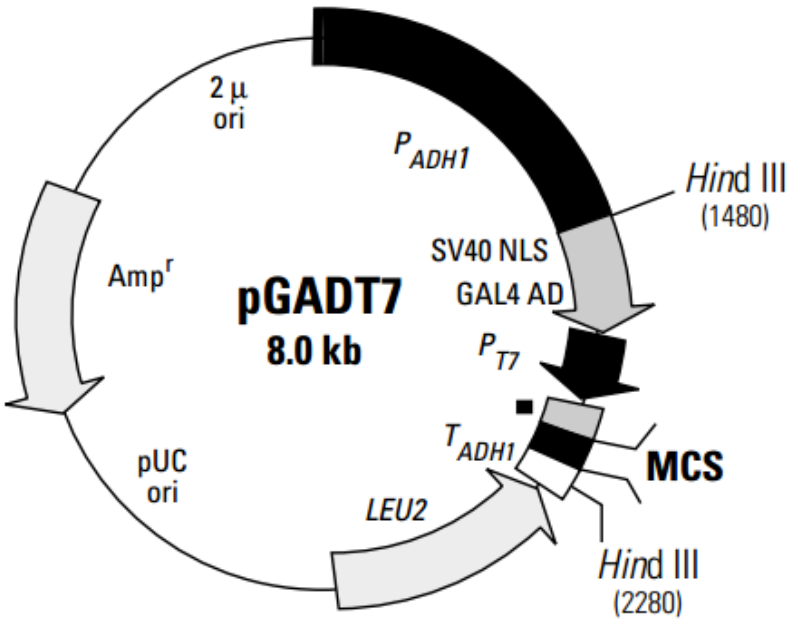
2 µ ori
P_{ADH1}
Hind III (1480)
SV40 NLS
GAL4 AD
Amp^r
pGADT7
8.0 kb
P_{T7}
T_{ADH1}
MCS
pUC ori
LEU2
Hind III (2280)
■ HA epitope tag

C

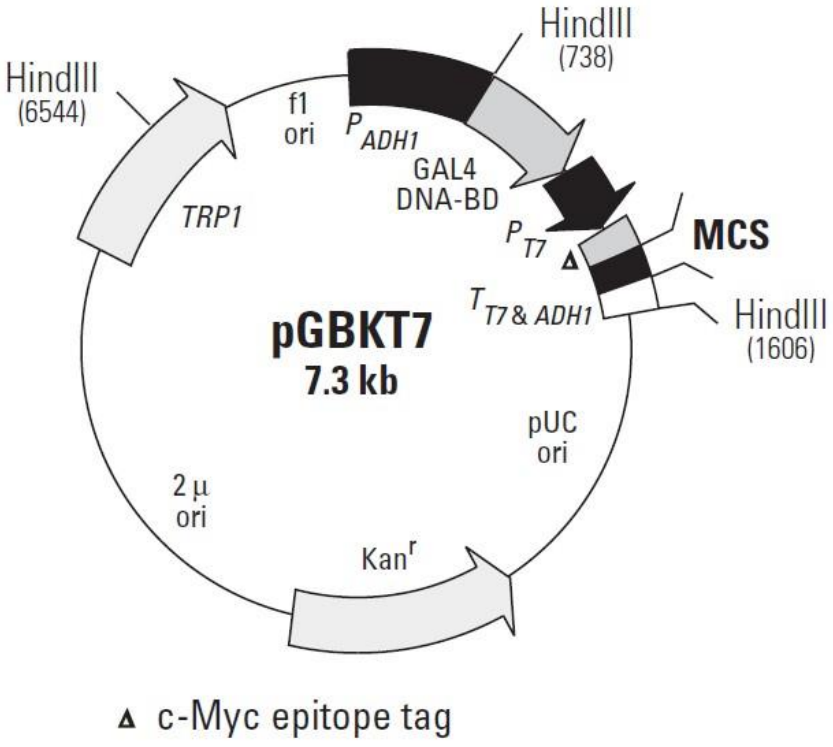
HindIII (738)
HindIII (6544)
f1 ori
P_{ADH1}
GAL4 DNA-BD
TRP1
P_{T7}
MCS
$T_{T7\ \&\ ADH1}$
HindIII (1606)
pGBKT7
7.3 kb
pUC ori
2 µ ori
Kan^r
▲ c-Myc epitope tag

Appendix V: pDEST Gateway vectors constructed in this study for plant transformation

Table (**A**) and maps (**B** - **E**) of the different pDEST Gateway vectors.

A

Type of vector	Construct description	Bacterial/Plant resistance	Promoter	Side of the fusion
pB7WGC2	CFP_AtNEAP1	Spectinomycin / Basta	35S	N-ter
	CFP_AtNEAP2			
	CFP_Atneap2_CRISPRmutation			
	CFP_AtNEAP3			
pB7WGY2	YFP_AtNEAP1			
	YFP_AtNEAP2			
	YFP_Atneap2_CRISPRmutation			
	YFP_AtNEAP3			
	YFP_AtNEAP1_ΔTM			
	YFP_AtNEAP2_ΔTM			
	YFP_AtNEAP3_ΔTM			
pGWB605	NLS_GFP			C-ter
pDe_Cas9	Exon1NEAP2_CRISPR		cUBI4-2	N/A
	Exon3NEAP2_CRISPR			

B

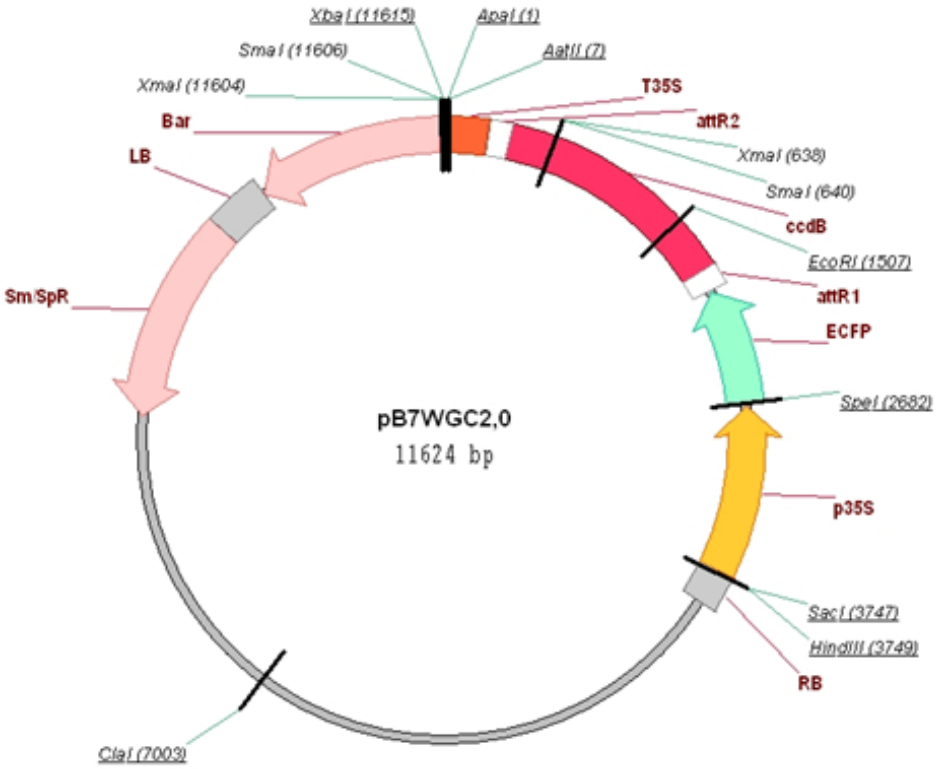
XbaI (11615)
ApaI (1)
SmaI (11606)
AatII (7)
XmaI (11604)
T35S
Bar
attR2
LB
XmaI (638)
SmaI (640)
ccdB
EcoRI (1507)
Sm/SpR
attR1
ECFP
SpeI (2682)
pB7WGC2,0
11624 bp
p35S
SacI (3747)
HindIII (3749)
RB
ClaI (7003)

C

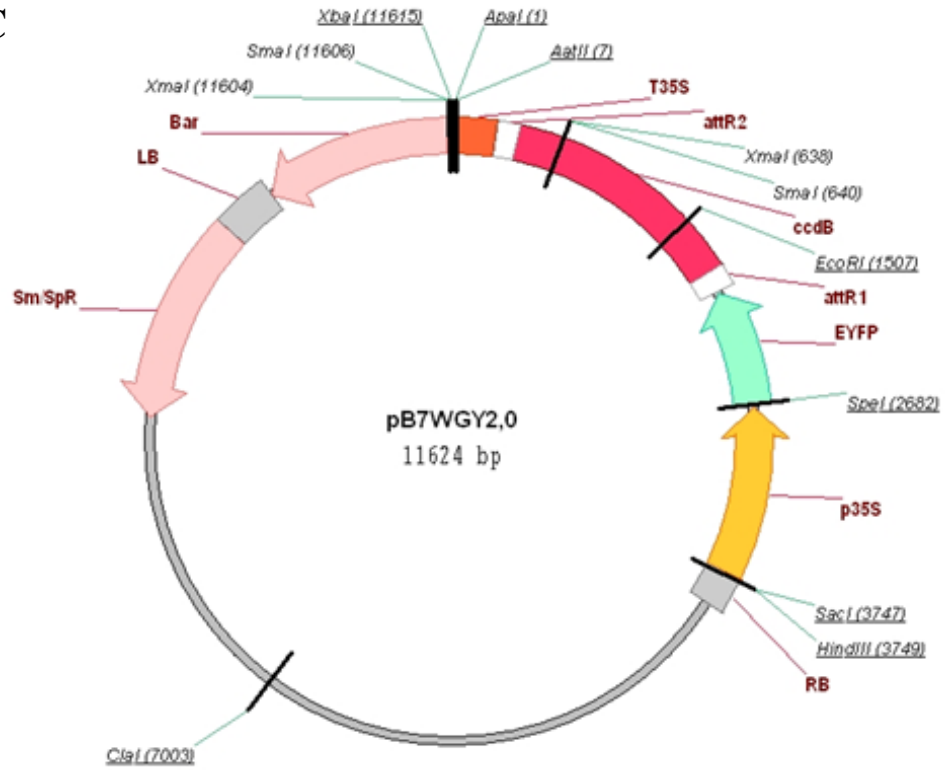
XbaI (11615)
ApaI (1)
SmaI (11606)
AatII (7)
XmaI (11604)
T35S
Bar
attR2
LB
XmaI (638)
SmaI (640)
ccdB
EcoRI (1507)
Sm/SpR
attR1
EYFP
SpeI (2682)
pB7WGY2,0
11624 bp
p35S
SacI (3747)
HindIII (3749)
RB
ClaI (7003)

D

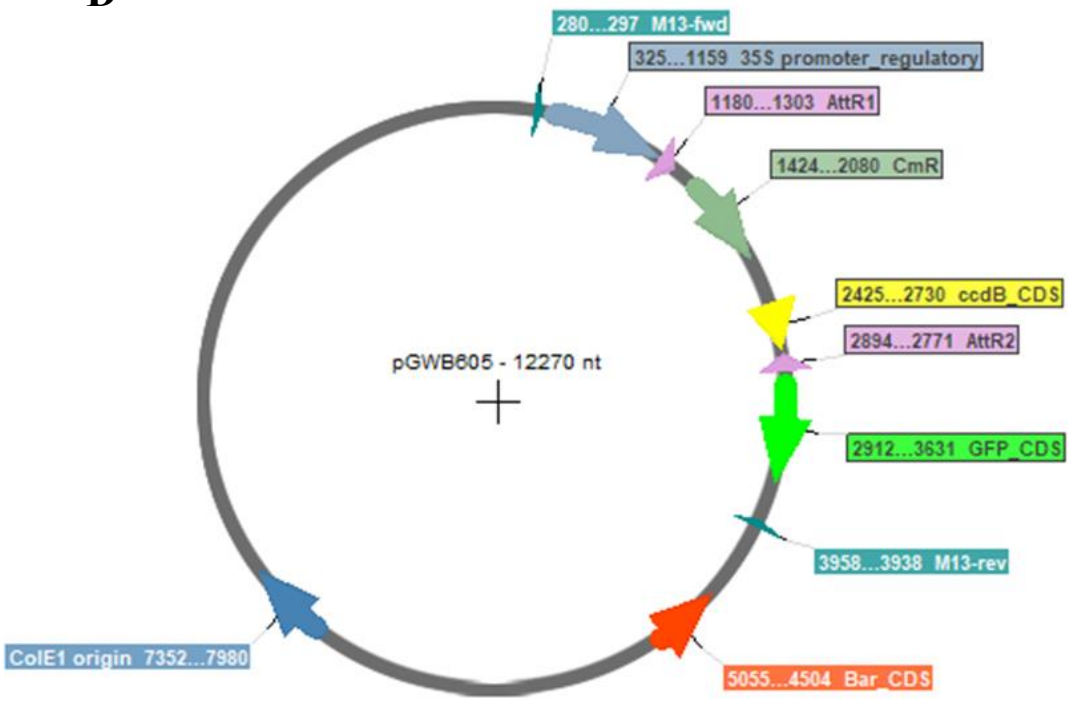
280...297 M13-fwd
325...1159 35S promoter_regulatory
1180...1303 AttR1
1424...2080 CmR
2425...2730 ccdB_CDS
2894...2771 AttR2
pGWB605 - 12270 nt
2912...3631 GFP_CDS
3958...3938 M13-rev
ColE1 origin 7352...7980
5055...4504 Bar_CDS

E

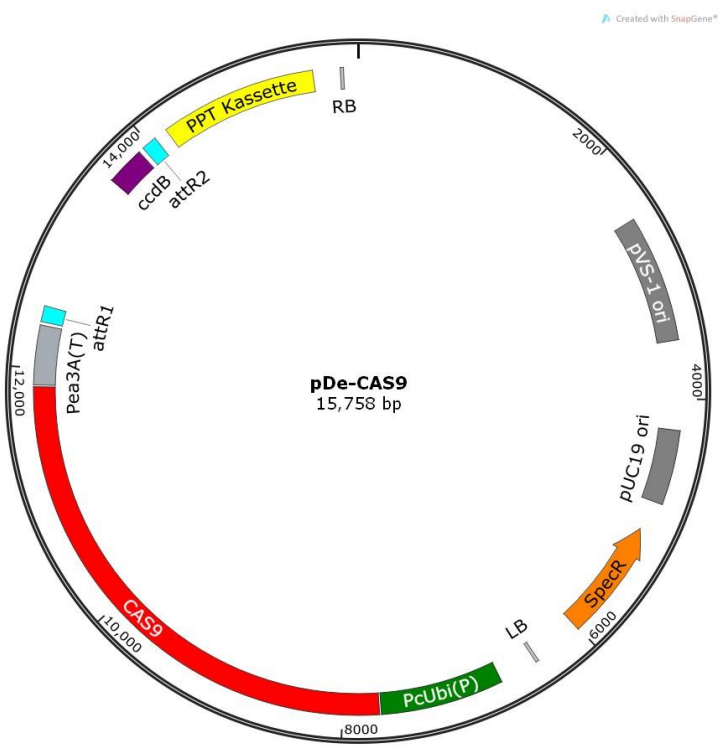
Created with SnapGene®
PPT Kassette
RB
14,000
2000
ccdB
attR2
pVS-1 ori
attR1
Pea3A(T)
12,000
pDe-CAS9
15,758 bp
4000
pUC19 ori
SpecR
LB
CAS9
10,000
6000
PcUbi(P)
8000

Appendix VI: In-silico WT and mutant transcripts and protein for AtNEAP2

A. *In-silico AtNEAP2* transcripts and prediction of AtNEAP2 protein. **B.** Potential *Atneap2* transcript and Atneap2 mutant protein. Wild type transcript (green), targeted site for CRIPSR (pink) and untranscribed region after an early stop codon (orange) are indicated. **Software:** Serial cloner.

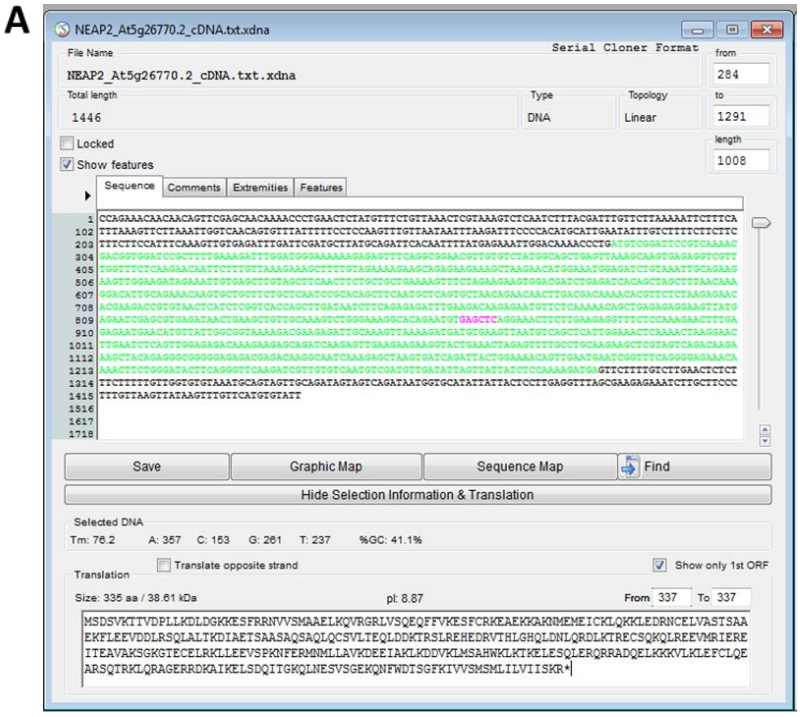

Appendix VII: Interaction of AtbZIP18 and AtMaMYB transcription factors with AtNEAP1

A. MYTH experiment carried out by Voisin, unpublished. Yeast strains were tested on permissive medium (upper panel) depleted in leucine and tryptophan to select diploïds only and on test medium (lower panel) depleted in leucine, tryptophan, histidine and adenine to select diploids with interacting proteins. Baits AtSUN3, AtMaMYB and AtNEAP1 were tested with pPOST and pPR3N respectively as positive and negative controls and with prey AtbZIP18. Bait AtNEAP1 was also tested with prey AtMaMYB. Data from Voisin, unpublished. **B.** Model of a potential network with transcription factors anchored at the nuclear periphery by AtSUN3 and AtNEAP1.

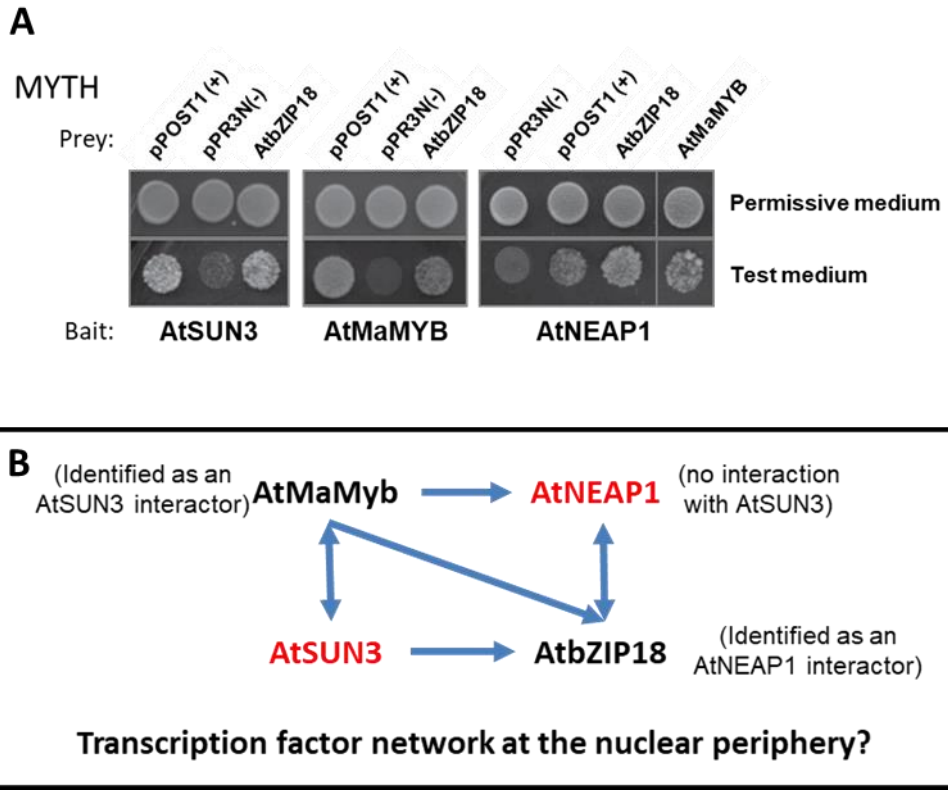

Appendix VIII: Scientific contribution during the PhD

Posters:

2016 – SEB meeting in Brighton, UK

2018 – JED Clermont-Ferrand, France

2019 – Post Graduate Symposium, Oxford, UK

Scientific papers:

Pawar, V., Poulet, A., **Détourné, G.**, Tatout, C., Vanrobays, E., Evans, D.E., and Graumann, K. (2016). A novel family of plant nuclear envelope-associated proteins. J. Exp. Bot. 67, 5699–5710

Duc, C., Benoit, M., **Détourné, G.**, Simon, L., Poulet, A., Jung, M., Veluchamy, A., Latrasse, D., Le Goff, S., Cotterel, S., Tatout, C., Benhamed, M., and Probst, AV. (2017). Arabidopsis ATRX Modulates H3.3 Occupancy and Fine-Tunes Gene Expression. Plant Cell 29, 1773–1793

Characterisation of a novel family of plant nuclear envelope associated proteins (NEAP) in *Arabidopsis thaliana*

Gwénaëlle DETOURNE[1,2], Vidya PAWAR[2], Axel POULET[1,2], Emmanuel VANROBAYS[1], Katja GRAUMANN[2], Christophe TATOUT[1] and David EVANS[2]

[1] CNRS UMR6293 INSERM U1103, Génétique Reproduction et Développement (GReD), Université Clermont Auvergne, Clermont-Ferrand, France
[2]Department of Biological and Medical Sciences, Faculty of Health and Life Sciences, Oxford Brookes University, Oxford, United-Kingdom

Animals and fungi contain a meshwork structure beneath the inner nuclear membrane (INM) which is called, in animals, the lamina, and composed of lamins, Lamin B Receptor and LEM (LAP2β, Emerin and Man1) protein families. The lamina interacts with chromatin and lamina mutations affect chromatin organisation, modify gene expression and are associated with severe human diseases. Much less is known about the plant lamina and this project aims to characterize new components of the INM and their possible interactions with chromatin.

Screening for new proteins with nuclear membrane properties

NEAPs contain coiled-coil domains , a transmembrane domain and a nuclear localisation signal

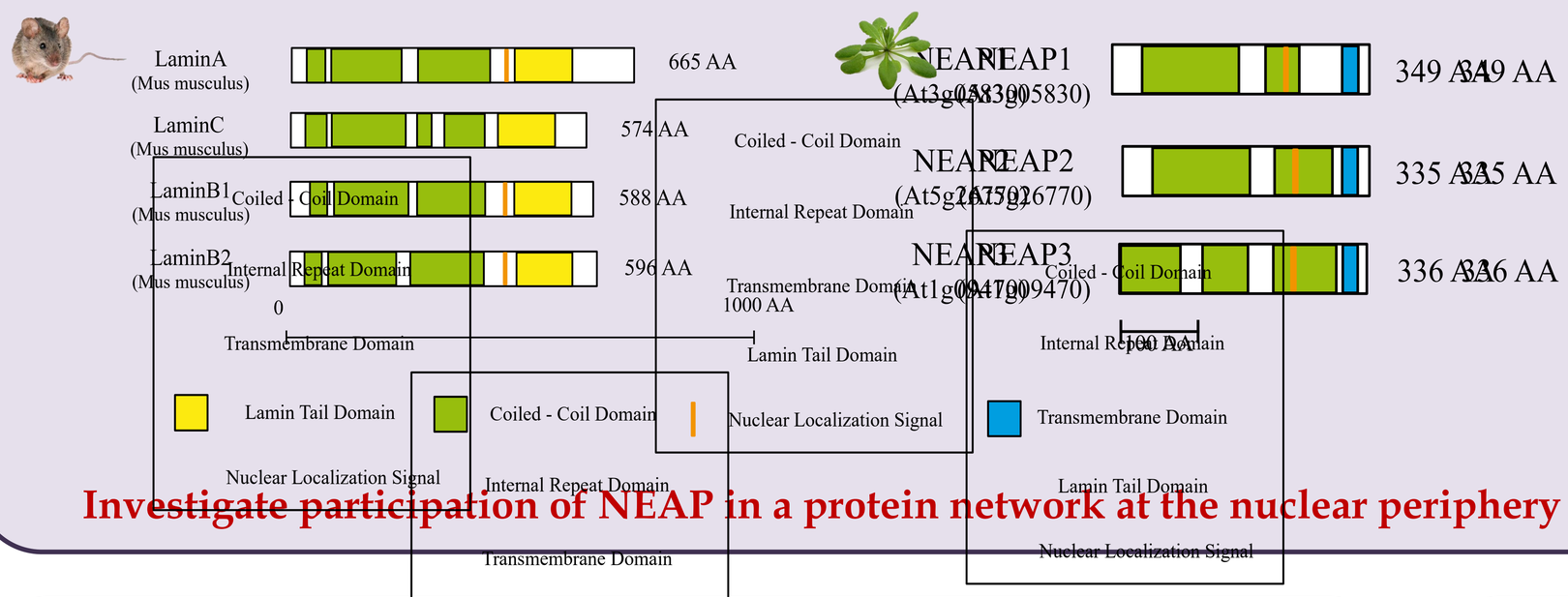

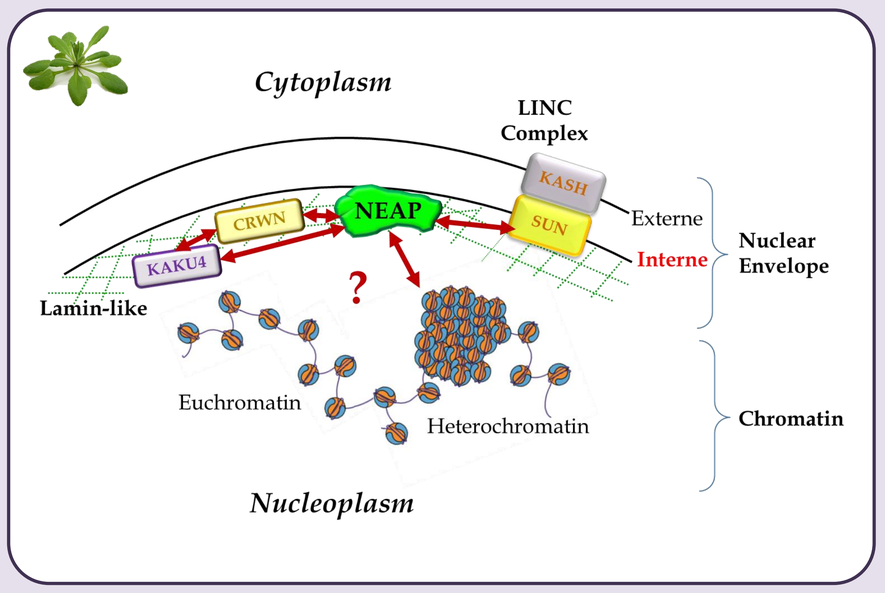

Investigate participation of NEAP in a protein network at the nuclear periphery and potential interactions with chromatin

NEAP *in vivo* localisation by transient expression in *A. thaliana*

Transient expression with fluorescent fusion proteins

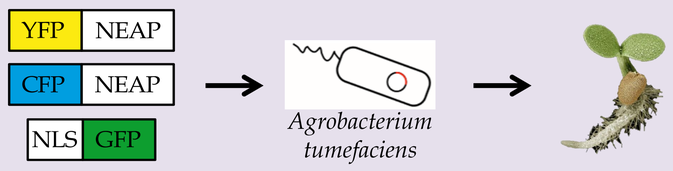

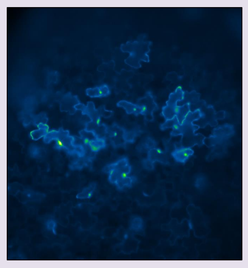

Patches of « expressing cells »

Protocol details:

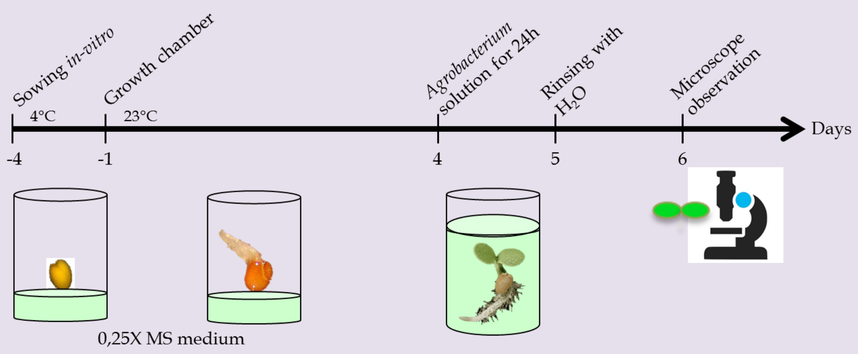

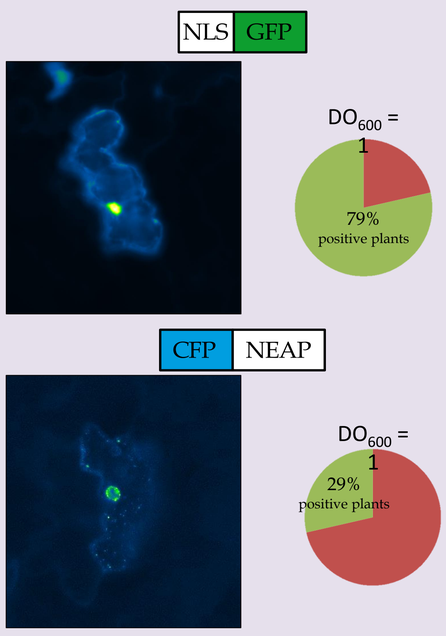

- **Investigate NEAP nuclear localisation in lamina mutants *(neap, crwn, kaku4, etc…)***
- **Investigate NEAP interaction *in planta* (FRET experiments)**

NEAPs form homo- and hetero- dimers

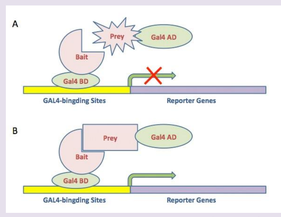

Yeast Two Hybrid system

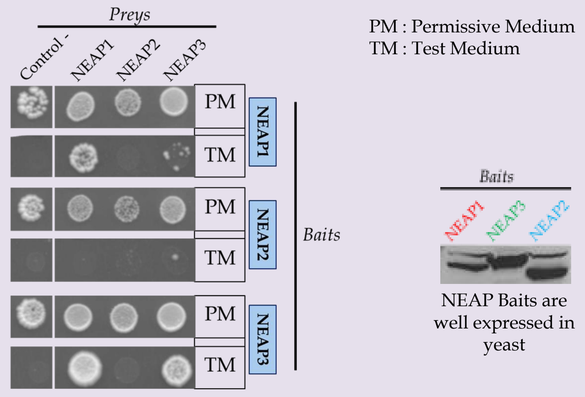

NEAP Baits are well expressed in yeast

- **Screening of cDNA library (Clontech) using each NEAP as bait**
- **Investigate NEAP interaction with other proteins of the nuclear periphery**

neap triple mutant impacts nuclear morphology and chromatin organisation

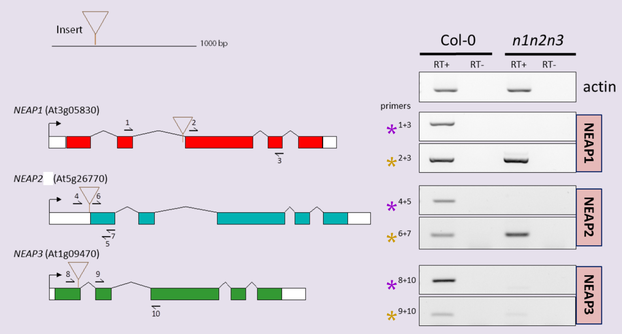

* Primers surrounding insertion site

* Primers downstream of T-DNA insertion

GC : Guard cells PC : Pavement cells

***NucleusJ* analysis**

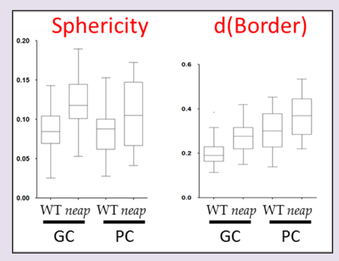

- **Generate CRISPR-Cas9 mutant for NEAP2**
- **Characterisation of *neap* triple mutant**

Interaction of NEAPs with chromatin

Stable transformation of NEAP fluorescent fusion proteins

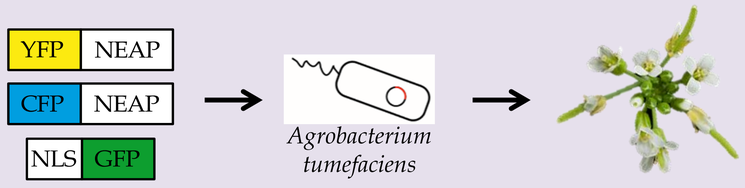

- **ChIP using GFP antibody: identification of sequences or chromatin domains interacting with NEAPs**
- **GFP-trap using GFP antibody: identification of new NEAP protein partners**

Conclusions and Perspectives

→ New family of nuclear envelope proteins (NEAPs) identified
- ✓ NEAPs interact with each other
- ✓ They are localised at the nuclear periphery

→ Developing tools and methods to identify:
- ❖ new NEAP-interacting proteins
- ❖ NEAP-associated chromatin domains

Gwénaëlle DETOURNE, first year PhD student
Co-tutelle between Oxford (UK) and Clermont-Ferrand (F)
Contact: gwenaelle_detourne@hotmail.com

Characterisation of a novel family of plant nuclear envelope associated proteins (NEAP) in *Arabidopsis thaliana*

Gwénaëlle DETOURNE[1,2], Emmanuel VANROBAYS[1], Katja GRAUMANN[2], Aline V. Probst[1], Christophe TATOUT[1] and David EVANS[2]

[1] CNRS UMR6293 INSERM U1103, Génétique Reproduction et Développement (GReD), Université Clermont Auvergne, Clermont-Ferrand, France

[2]Department of Biological and Medical Sciences, Faculty of Health and Life Sciences, Oxford Brookes University, Oxford, United-Kingdom

The nucleoskeleton underneath the nuclear envelope is needed to transmit signals to the nucleus and induce changes in chromatin organisation and ultimately gene expression. A novel family of Nuclear Envelope Associated Proteins (NEAPs) proposed to be new components of the plant nucleoskeleton has been recently evidenced in the model plant *Arabidopsis thaliana*. They are anchored at the inner nuclear membrane (INM) and results suggest they are part of a protein network responsible for maintaining nuclear morphology and chromatin organisation.

The Nuclear Periphery organisation and the NEAPs

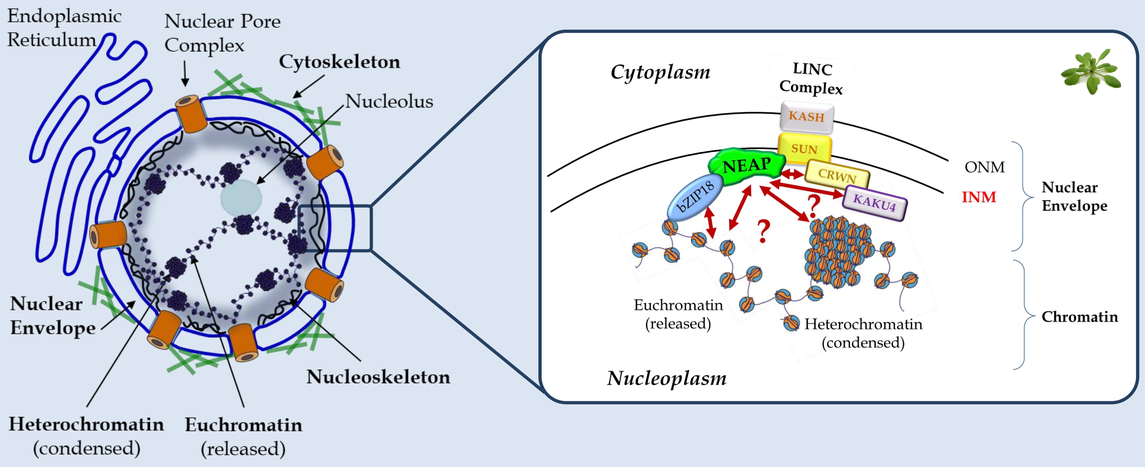

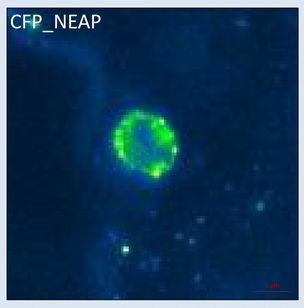

Transient expression in *Arabidopsis thaliana*

NEAPs are localised at the **Nuclear Periphery**

NEAP proteins contain

Coiled-Coil domains

a **TransMembrane Domain**

and a **Nuclear Localisation Signal**

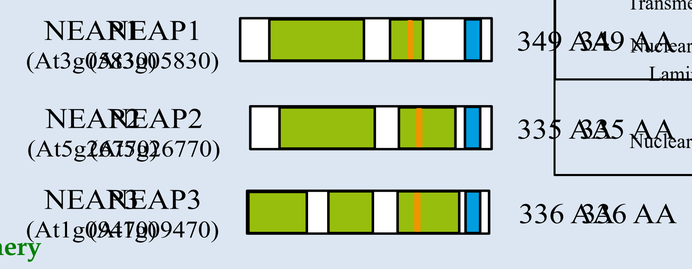

Investigate participation of NEAP in a protein network at the nuclear periphery and potential interactions with chromatin

Study of the NEAP interactome

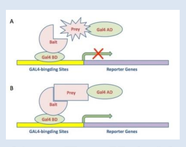

Yeast Two Hybrid system

Full length NEAPs

NEAPs without TM domain

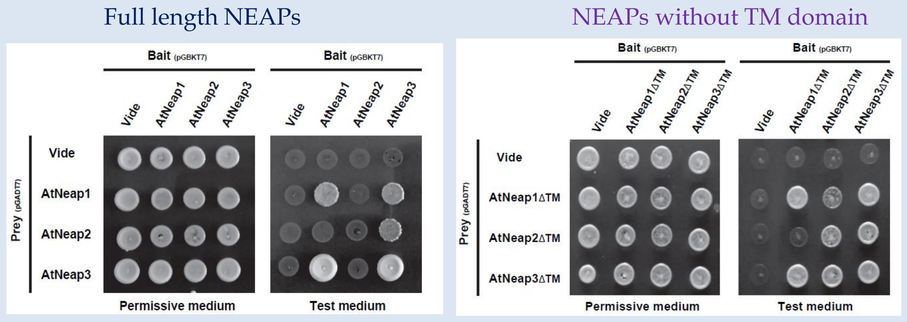

NEAP proteins are able to interact with each other
No interactions with other NE proteins found in Y2H nor with new interactors

But Interaction of Transcription Factor **bZIP18** with **NEAP1** found by Membrane Y2H (Pawar et al, 2016)

→Investigate bZIP18/NEAP interaction *in planta* by apFRET experiment
(acceptor photobleaching Fluorescence Resonance Energy Transfer)

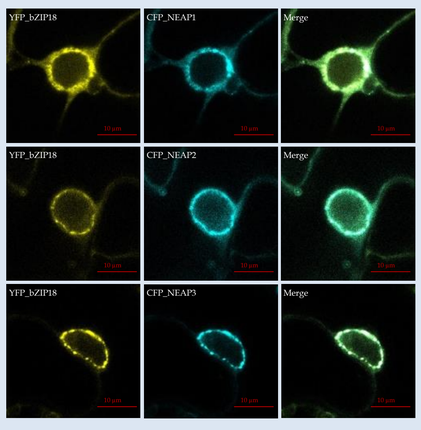

Transient expression in *Nicotiana benthamiana* leaf epidermal cells

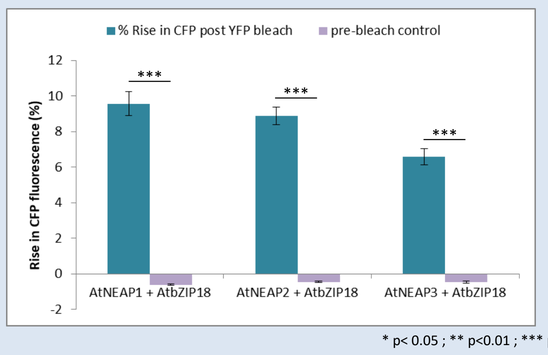

* p< 0.05 ; ** p<0.01 ; *** p<0.001

Interactions confirmed for **AtbZIP18** and **AtNEAPs**

Functional analysis of *neap* mutants

A ***neap1neap3* double mutant**

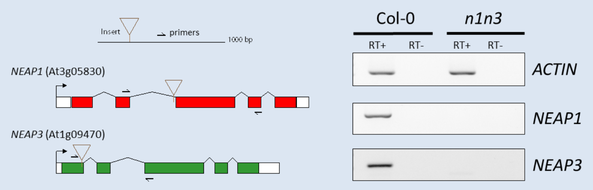

neap1neap3 is a double knock-out mutant

3D Image analysis

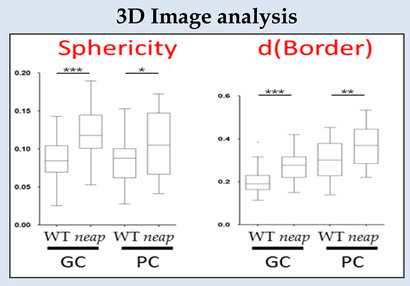

GC : Guard cells
PC : Pavement cells

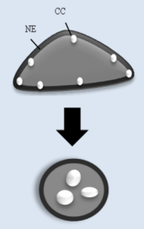

Double *neap* mutant alters **nucleus shape** and **chromocentre position**

B ***neap2* mutant created by CRISPR/Cas9**

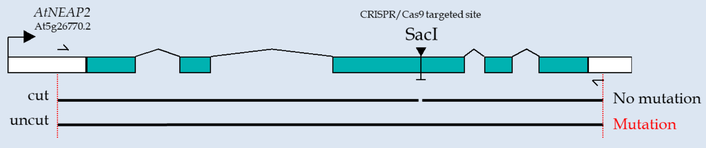

SacI
5′…G AGCT C…3′
3′…C TCGA G…5′

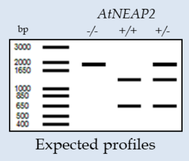

Expected profiles

Single nucleotide insertion

AtNEAP2	TCCTGAG – CTCACAT
Atneap2-1	TCCTGAG**T**CTCACAT
Atneap2-2	TCCTGAG**C**CTCACAT

Early stop codon after insertion site leads to a truncated protein missing NLS, one CC and TM domains

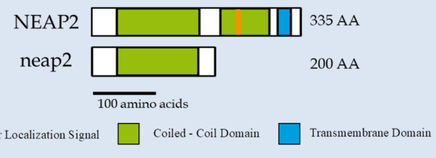

C **Obtaining triple *neap* mutant**

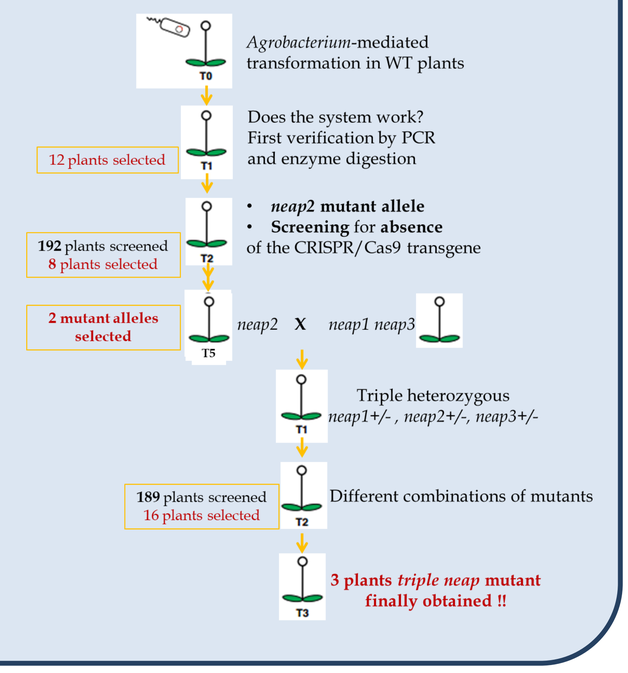

Designing AtNEAP antibodies

anti-NEAP1/2 (QLDDKTRSLRE)

anti-NEAP wobble (H-DL-D/G-E/H-KK-E/H-SFRRNVVS-C-NH_2)

Targeting N-terminus of NEAPs

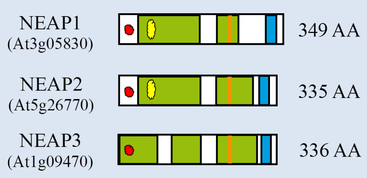

Antibodies work for Western blotting

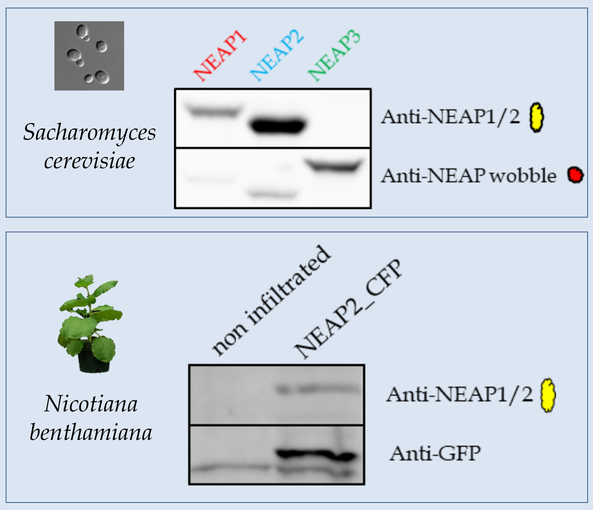

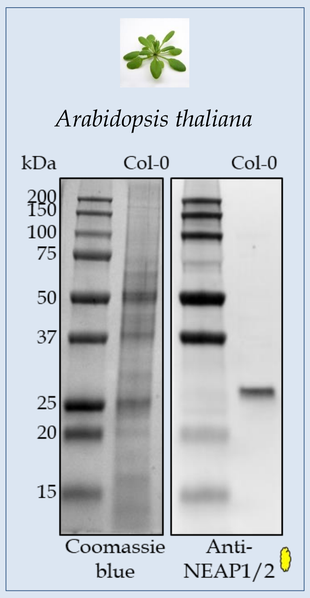

→ **Characterize *neap* single, double and triple mutants concerning protein synthesis**

→ **Use them for ImmunoPrecipitation (and co-IP) in order to look for new NEAP interactors by Mass Spectrometry**

Conclusions and Perspectives

- Characterize single *neap2* and triple *neap* mutants
  - 3D image analysis for nuclear morphology
  - Identify NEAPs-regulated genes (RNAseq)
- Look for new NEAP partners by different techniques
  - IP/co-IP followed by Mass Spectrometry
  - apFRET analysis with known NE proteins

Gwénaëlle DETOURNE, third year PhD student
Co-tutelle between Oxford (UK) and Clermont-Ferrand (F)
Contact: 15059427@brookes.ac.uk

Nigel Groome Studentship

Characterisation of a novel family of plant nuclear envelope associated proteins (NEAP) in *Arabidopsis thaliana*

Gwénaëlle DETOURNE[1,2], Emmanuel VANROBAYS[1], Katja GRAUMANN[2], Aline V. Probst[1], Christophe TATOUT[1] and David EVANS[2]

[1] CNRS UMR6293 INSERM U1103, Génétique Reproduction et Développement (GReD), Université Clermont Auvergne, Clermont-Ferrand, France
[2]Department of Biological and Medical Sciences, Faculty of Health and Life Sciences, Oxford Brookes University, Oxford, United-Kingdom

The nucleoskeleton underneath the nuclear envelope is needed to transmit signals to the nucleus and induce changes in chromatin organization and ultimately gene expression. A novel family of Nuclear Envelope Associated Proteins (NEAPs) proposed to be new components of the plant nucleoskeleton has been recently evidenced in the model plant *Arabidopsis thaliana*. They are anchored at the inner nuclear membrane (INM) and results suggest they are part of a protein network responsible for maintaining nuclear morphology and chromatin organization.

The Nuclear Periphery organisation and the NEAPs

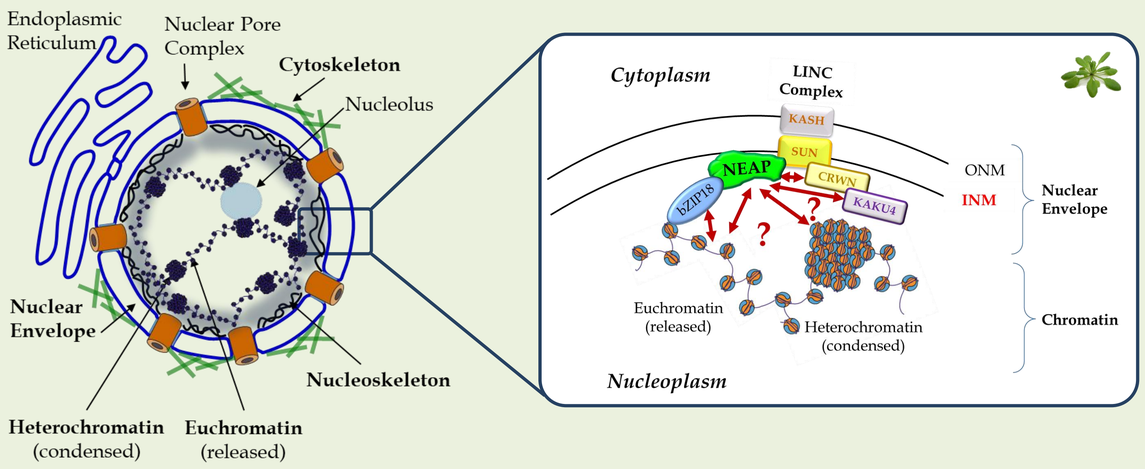

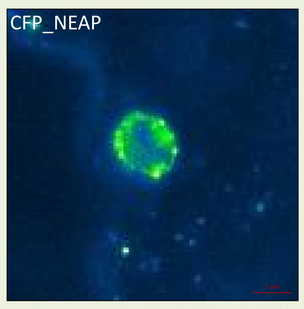

Transient expression in *Arabidopsis thaliana*

NEAPs are localised at the **Nuclear Periphery**

NEAP proteins contain

Coiled-Coil domains

a **TransMembrane Domain**

and a **Nuclear Localisation Signal**

Investigate participation of NEAP in a protein network at the nuclear periphery and potential interactions with chromatin

Study of the NEAP interactome

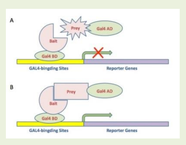

Yeast Two Hybrid system

Full length NEAPs

NEAPs without TM domain

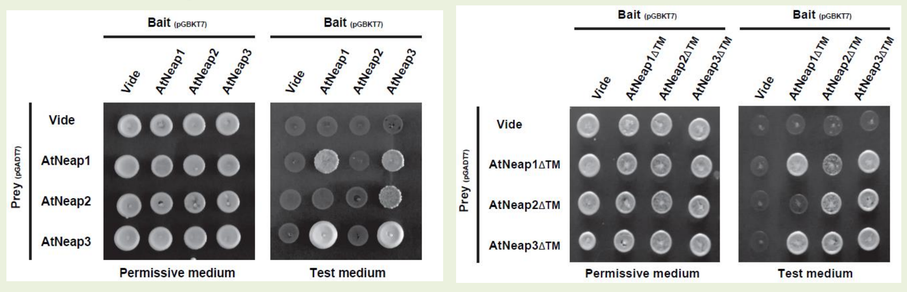

NEAP proteins are able to interact with each other
Other interactors of NEAP are difficult to identify by classical Y2H

Interaction of Transcription Factor **bZIP18** with **NEAP1** found by Membrane Y2H
(Pawar et al, 2016)

→Investigate bZIP18/NEAP interaction *in planta* by apFRET experiment
(acceptor photobleaching Fluorescence Resonance Energy Transfer)

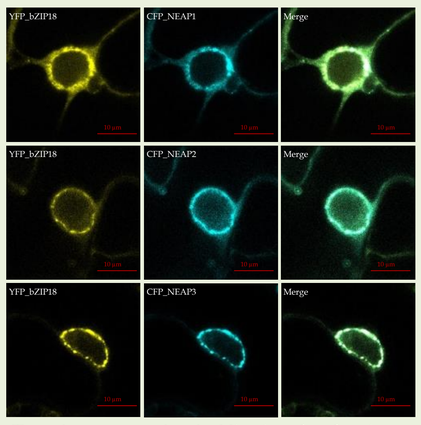

Transient expression in *Nicotiana benthamiana* leaf epidermal cells

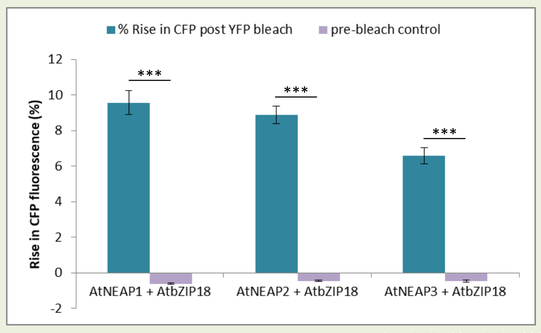

* p< 0.05 ; ** p<0.01 ; *** p<0.001

Interactions confirmed between **AtbZIP18** and **AtNEAPs**

Functional analysis of *neap* mutants

A ***neap1neap3* double mutant**

Nucleus shape and **chromocentre position** are **altered** in double *neap1neap3* mutant

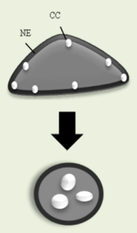

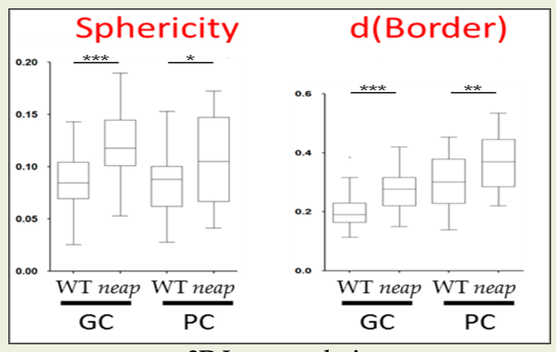

GC : Guard cells
PC : Pavement cells

3D Image analysis

B **New mutants obtained: *neap2* mutant (by CRISPR/Cas9) and triple *neap* mutant, « *neap1/2/3* »**

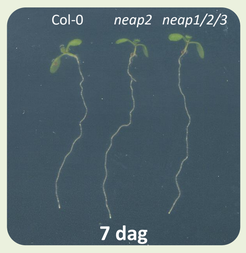

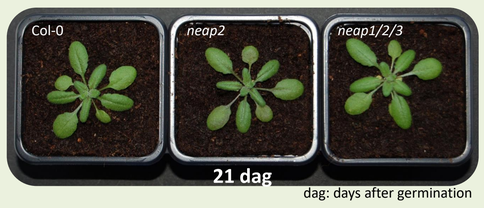

dag: days after germination

General growth is **not** altered

Silique size (mm) is **reduced**

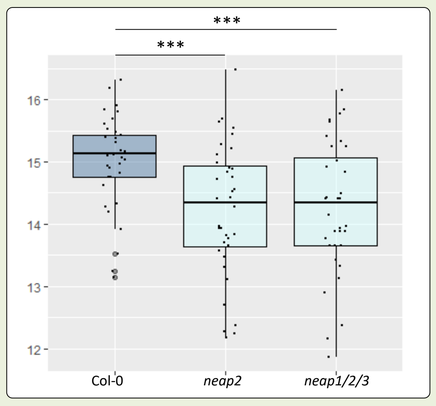

Weak effects on seed production

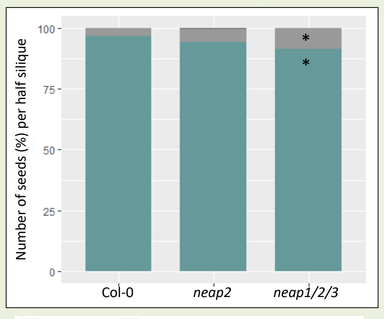

→ Look at nuclear morphology with 3D image analysis
→ Look at meiosis and embryo formation in mutants

Designing AtNEAP antibodies

anti-NEAP1/2 (QLDDKTRSLRE)

anti-NEAP wobble (H-DL-D/G-E/H-KK-E/H-SFRRNVVS-C-NH_2)

Targeting N-terminus of NEAPs

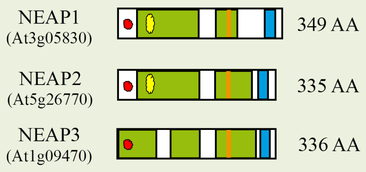

Antibodies detect proteins with expected MW in Western blotting

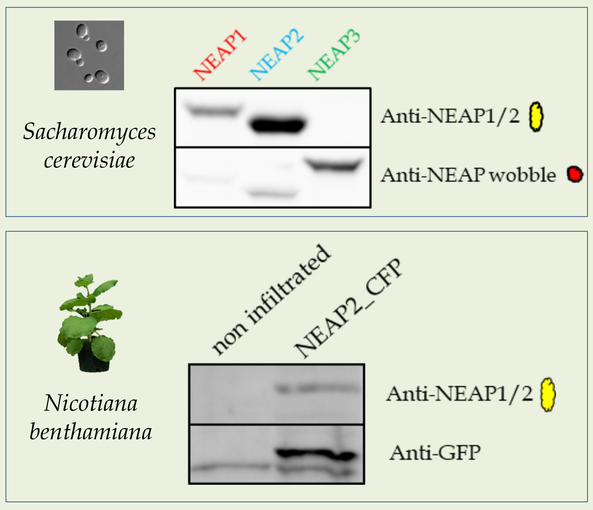

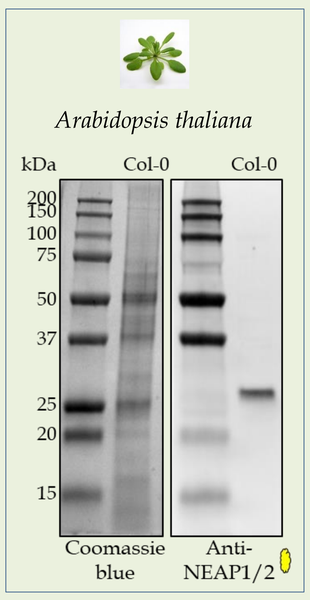

→ Characterization of protein synthesis in *neap* single, double and triple mutants
→ Available for immunoprecipitation and Co-IP to detect new NEAP interactors

Conclusions and Perspectives

- Transcription factor AtbZIP18 interact with AtNEAPs
- New mutants obtained showing a reduced silique size
- Antibodies generated, suitable for protein detection

Future work:

- 3D image analysis for nuclear morphology in *neap1/2/3*, single *bZIP18* and *neap1/2/3;bzip18* mutants
- Immunoprecipitation of AtNEAPs to identify new partners by Mass Spectrometry

Gwénaëlle DETOURNE, third year PhD student
Co-tutelle between Oxford (UK) and Clermont-Ferrand (F)
Contact: 15059427@brookes.ac.uk

Nigel Groome Studentship

Figure **S1**

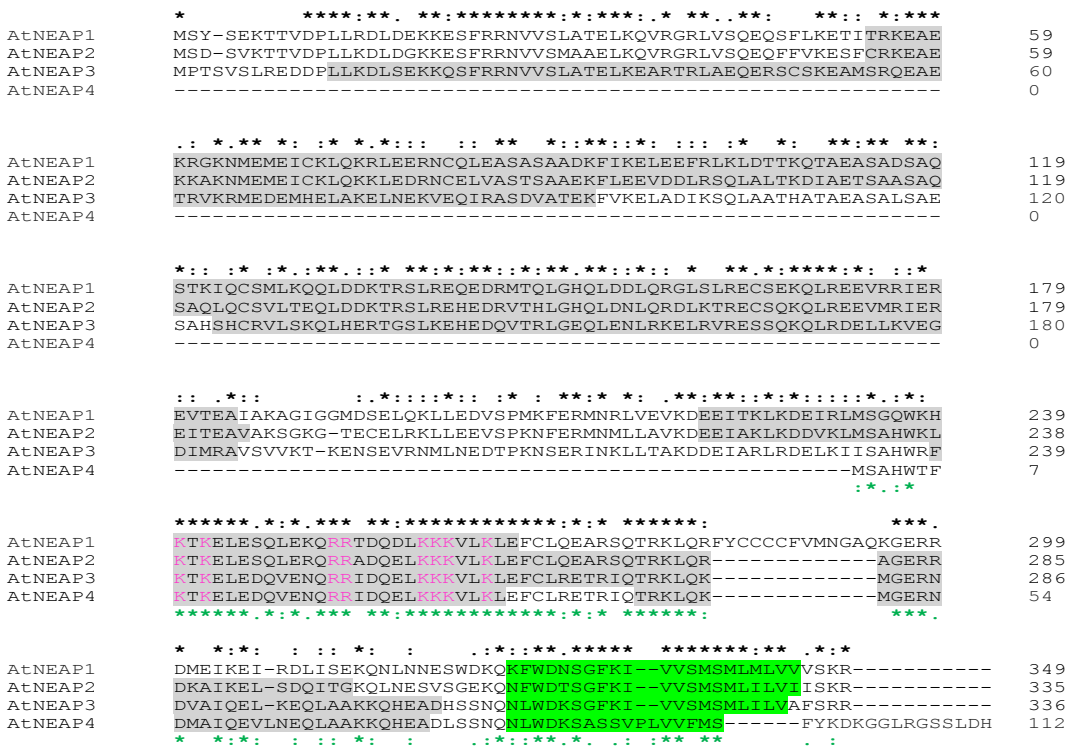

Figure S1 Clustal Omega (1,2.1) multiple sequence alignment of AtNEAPs 1-4 and prediction of functional domains. * donates consensus sequence between AtNEAPs 1-3; green * represents consensus between AtNEAPs 1-4. Coiled coil domains highlighted in grey, NLS pink and TM domains in green. Coiled coil domains were predicted using SMART, COILS, PairCoil2 and Marcoil (Lupas et al, 1991; Dolerenzi and Speed, 2002; McDonnell et al., 2006, Letunic et al., 2012). NLS predicted using cNLS mapper and NLSstradamus (Kosugi et al., 2009; Nguyen Ba at al., 2009_. TM domains were predicted using ARAMEMNON and DAS (Cserzo et al., 1997; Schwacke et al., 2003).

Figure S2

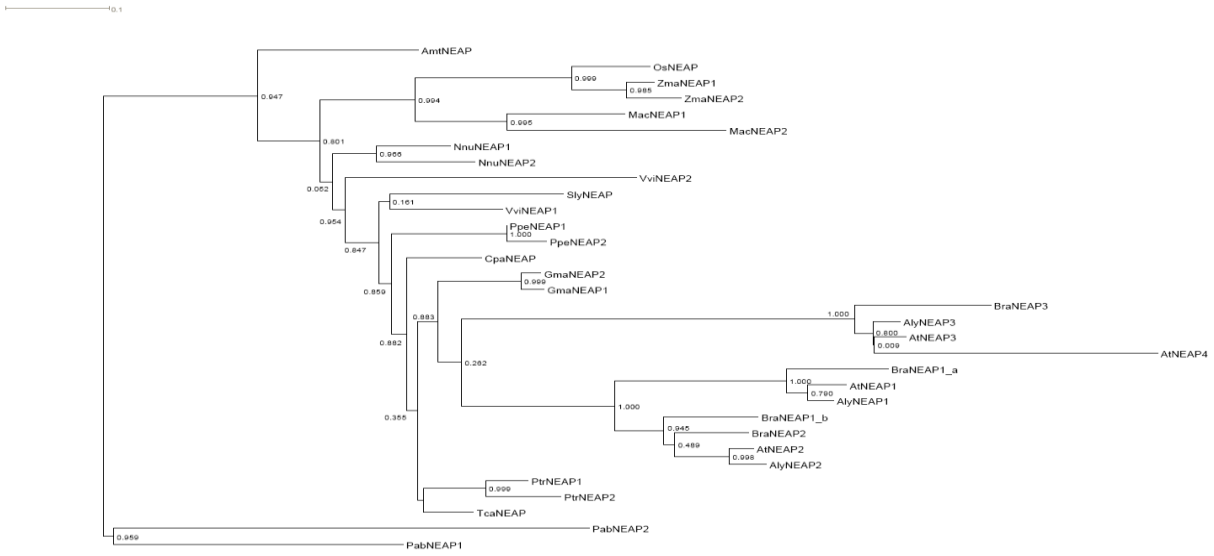

Figure S2 Maximum likelihood (ML) phylogenetic tree. The ML tree was inferred using proteins sequences from dicot species including *Arabidopsis thaliana* (AtNEAP1, AtNEAP2, AtNEAP3 and AtNEAP4 respectively [GenBank: NP_001189818, NP_568487, NP_172418 and NP_683289]), *Arabidopsis lyrata* (AlyNEAP1, AlyNEAP2 and AlyNEAP3 respectively [GenBank: XP_002882437, XP_002874325 and XP_002892507]) *Brassica rapa* (BraNEAP1_a, BraNEAP1_b, BraNEAP2 and BraNEAP3 respectively [GenBank: CDY27738, CDY19756, XP_009151160 and XP_00914824]), *Carica papaya* (CpaNEAP [ldPlaza: CP00048G02160]), *Glycine max* (GmaNEAP1 and GmaNEAP2 respectively [GenBank: XP_003555780 and XP_003536028]), *Nelumbo nuciferagi* (NnuNEAP1 and NnuNEAP2 respectively [GenBank: XP_010276551 and XP_010270974]), *Prunus persica* (PpeNEAP1 and PpeNEAP2 respectively [Genbank: XP_007205454 and XP_007205455]), *Populus trichocarpa* (PtrNEAP1 and PtrNEAP2 respectively [Genbank: XP_006382272 and XP_002318927], *Solanum lycopersicum* (SlyNEAP: [GenBank: XP_004230355]), *Theobroma cacao* (TcaNEAP: [Genbank: XP_007031253]), *Vitis vinifera* (VviNEAP1 and VviNEAP2 respectively [GenBank: CBI39661 and XP_002280405]), monocot species including *Zea mays* (ZmaNEAP1 and ZmaNEAP2 respectively [GenBank: NP_001149106 and XP_008661538]), *Oryza sativa* (OsNEAP: [Genbank NP_001054577]), *Musa acuminata* (MacNEAP1 and MacNEAP2 respectively [Genbank: XP_009382460 and XP_009411597), basal angiosperm species including *Amborella trichopoda* (AmtNEAP :[Genbank : XP_006840319]), and gymnosperm species including *Picea abies* (PabNEAP1 and PabNEAP2 respectively [congenie: MA_136804g0010 MA_902507g0010]) . Numbers above branches indicate bootstrap values.

Figure S3

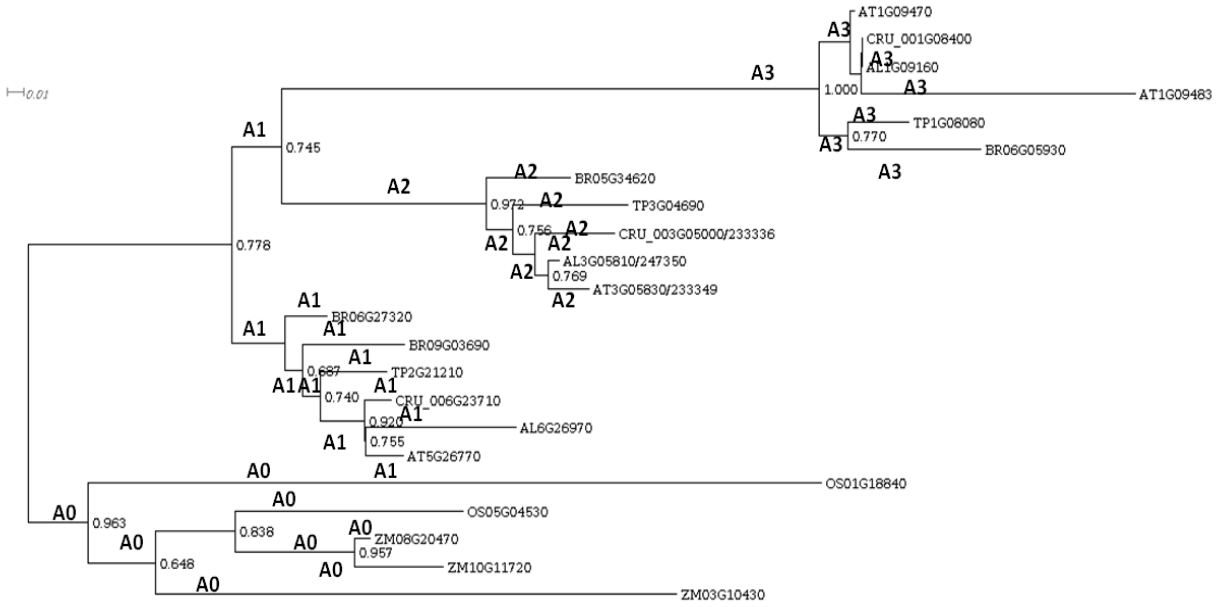

	hypothesis	ωA0	ωa1	ωa2	ωa3	ωa4	l		2Δl	p value
h0	H0: ωA0 = ωA1 = ωA2 = ωA3 = ωA4	0.17489	= ωA0	= ωA0	= ωA0	= ωA0	-6495.969814	Na	NA	
h1	H1: ωA0 = ωA1 = ωA2 ≠ ωA3 = ωA4	0.17049	= ωA0	= ωA0	0.20053	= ωA3	-6495.767548	H0 vs H1	0.202266	0.6528
h2	H2: ωA0 = ωA1 = ωA2 ≠ ωA3 ≠ ωA4	0.17025	= ωA0	= ωA0	0.09985	0.84655	-6487.539788	H0 vs H1	8.430026	0.0036
h3	H3: ωA0 ≠ ωA1 ≠ ωA2 ≠ ωA3 = ωA4	0.16185	0.16890	0.20727	0.20171	= ωA3	-6495.379931	H0 vs H1	0.589883	0.4424
h4	H4: ωA0 ≠ ωA1 ≠ ωA2 ≠ ωA3 ≠ ωA4	0.1617	0.1686	0.2078	0.1002	0.8515	-6487.137043	H0 vs H1	8.832771	0.0029
h5	H5: ωA0 = ωA1 = ωA2 =ωA3 ≠ ωA4	0.16116	= ωA0	= ωA0	= ωA0	0.84888	-6488.941673	H0 vs H5	7.028141	0.0080

Figure S3 NEAP coding sequences were used for phylogenic reconstruction and substitution rate calculation. Selected protein sequences were aligned with MUSCLE multiple sequence alignment and maximum likelihood analysis was performed with FastTree using default parameters. ω (the ratio of nonsynonymous/synonymous substitution rates) was determined using Codeml from the PaML package NEAP4 has an rate evolution rate (0.8) higher than the other NEAPs, which have rates equal or equivalent to expressed genes.
This shows an accumulation of non synonymous mutations in the *AtNEAP4* sequence, which implies a possible decrease in selection pressure, and a pseudogeneisation of *AtNEAP4*

Figure S4

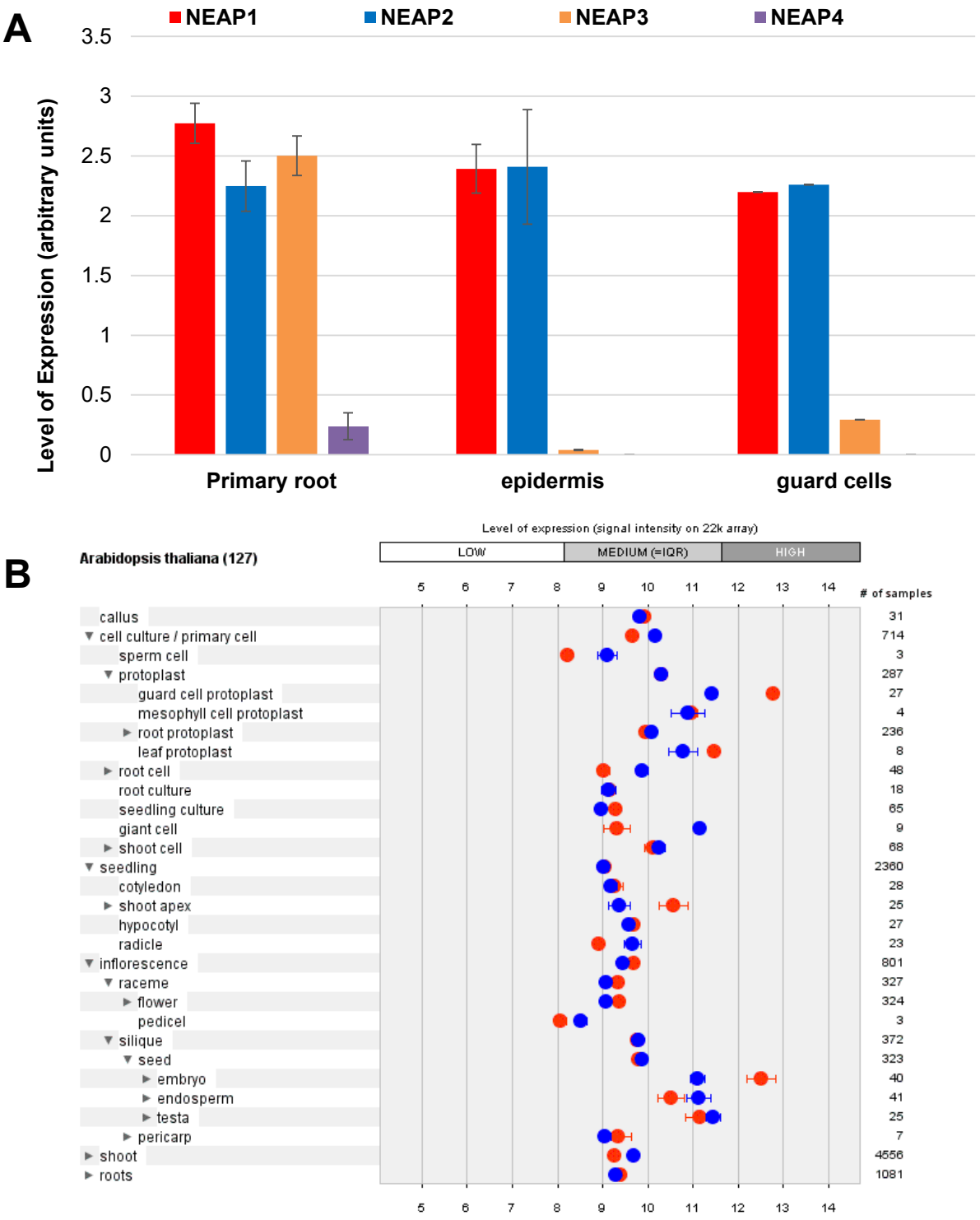

Figure S4 Expression profile of *AtNEAP1, 2, 3* and *4* mRNA obtained from RNA-Seq and Genevestigator (http://www.ncbi.nlm.nih.gov/geo/browse/; Toufighi et al., 2005). A) RNA-Seq data shows that *AtNEAP1* and *AtNEAP2* are expressed at higher levels in all three tissues while *AtNEAP3* is also highly expressed in root but not in episermis and guard cells. No or low expression of *AtNEAP4* suggests it may be a pseudogene. B) Genevestigator microarray data shows *AtNEAP1* (red) and *AtNEAP2* (blue) expressed at medium levels in all tissues with higher levels of AtNEAP1 expression in guard cells and embryos.

Figure S5

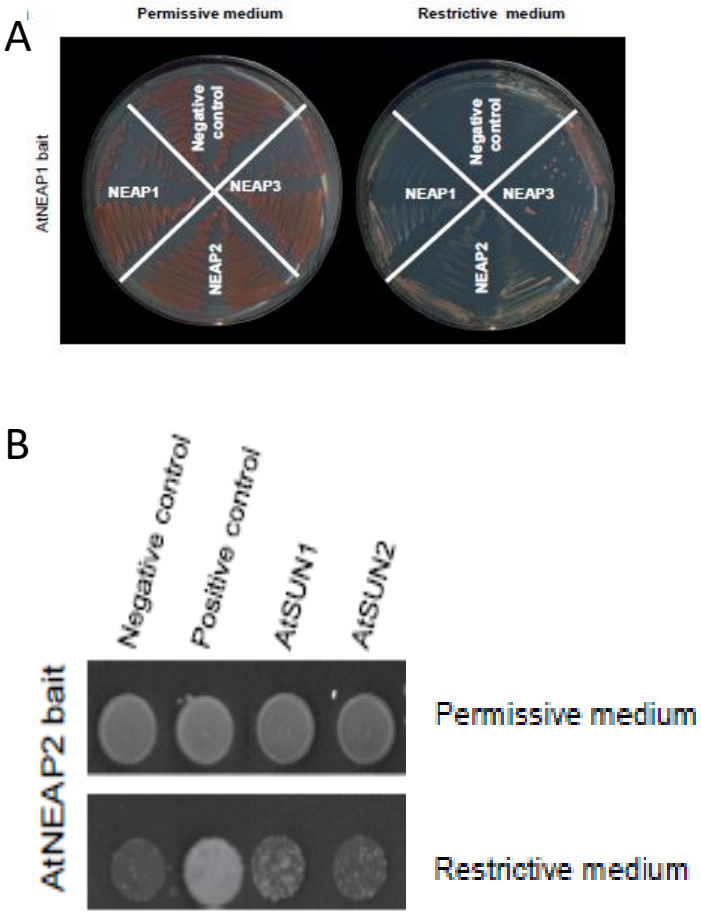

Figure S5 Split ubiquitin membrane yeast two hybrid (MYTH) assay. A) Colonies of yeast showing transformed yeast cells grown on permissive and restrictive medium indicating successful bait prey interaction for AtNEAPs 1-3. B) Yeast colonies containing AtNEAP2 bait transformed with AtSUN1 and AtSUN2 prey vectors grown on permissive and restrictive medium. Transformation with empty prey vector was used as a negative control; the positive control was an ER protein fused to the N-terminus of the split ubiquitin molecule.

Table S1 lists all primers used to genotype *Atneap* and *Atbzip18* insertion mutants

Primer name	Forward/ Reverse	Primer description	Tm (˚C)	Sequence
LPNEAP1	F	NEAP1_SAIL846_B07	49	CTCTGCAGCTTTCTTGTCTGG
RPNEAP1	R	NEAP1_SAIL846_B07	47	AGCTTGAAGCTTCTGCATCTG
LB3_SAIL	F	SAIL left border	55	TAGCATCTGAATTTCATAACCAATCTCGATACAC
LPNEAP2	F	NEAP2_SALK_012087	43	TTTGATTCGATGCTTATGCAG
RPNEAP2	R	NEAP2_SALK_012087	47	AGAAGCAGCACTTGTTTCTGC
LBb1.3_SALK	F	SALK left border	42	ATTTTGCCGATTTCGGAAC
Wisc_LPNEAP2	F	WiscDsLoxHs194_12D	47	TACCATATCAGAGCGGGATTG
Wisc_RPNEAP2	R	WiscDsLoxHs194_12D	45	TTGTTGCTCGAACTGTTGTTG
WiscHS_LB	F	WiscDsLoxHs left border	55	TGATCCATGTAGATTTCCCGGACATGAAG
178C02_LPN2a	F	NEAP2_GABI178C02: insertion:chr5 9409102	47	TGCACCTGAGATTCAAGTTCC
178C02_RPN2a	R	NEAP2_GABI178C02: insertion:chr5 9409102	48	TGCTTTGGTAGGGTCAGAAATC
178C02_LPN2b	F	NEAP2_GABI178C02: insertion:chr5 9409081	43	CGCTTTTGAAAGATTTGGATG
178C02_RPN2b	R	NEAP2_GABI178C02: insertion:chr5 9409081	49	GCTTCAGTTATCTCACGCTCG
589B02_LPN2a	F	NEAP2_GABI_589B02: insertion:chr5 9409811	45	AAAGGGCCATTGATTACCAAG
589B02_RPN2a	R	NEAP2_GABI_589B02: insertion:chr5 9409811	45	AGAAATTCGGAAGGGAAAGAC
589B02_LPN2b	F	NEAP2_GABI_589B02: insertion:chr5 9409738	47	AGCGAGGTTTTAGACTTTCCG
589B02_RPN2b	R	NEAP2_GABI_589B02: insertion:chr5 9409738	47	CCTTTTCAGCAGCAGAAGTTG
GABI_8474	F	GABI right border	50	ATAATAACGCTGCGGACATCTACATTTT
LPNEAP3	F	NEAP3_WiscDsLoxHs086_02C	50	TTCCTACCAAACCCAGAAACC
RPNEAP3	R	NEAP3_WiscDsLoxHs086_02C	50	TCAGCCAATTCCTTCACAAAC
LPNEAP4	F	NEAP4_SAIL_1239_G02	50	TTCACTCCAATGAAATCGAGC
RPNEAP4	R	NEAP4_SAIL_1239_G02	50	TTGTTCTTCTGGATCAGGTGG

Table S2 lists all primers used to clone *AtNEAP* and *AtbZIP18* coding DNAs

Primer name	Forward/ Reverse	Primer description	Tm (˚C)	Sequence
FNEAP1 (FTL5)	F	binds first 24 bp of AtNEAP1	63	ATGTCTTATTCTGAAAAAACGACG
RNEAP1(RTL5)	R	binds last 24 bp of AtNEAP1 (minus stop)	56	TCTCTTGGAGACTACCACTAACAT
RT_FNEAP1	F	binds bp 150-177 spanning the first intron of AtNEAP1	54	GAGACCATTACTAGAAAAGAAGCAGAG
RT_RNEAP1	R	binds bp 834-857 spanning the last intron of AtNEAP1	54	CAACAACAATAAAACCTCTGCAGC
FNEAP2	F	binds first 25bp of AtNEAP2	63	ATGTCGGATTCCGTCAAAACGACGG
RNEAP2	R	binds last 25bp of AtNEAP2 (minus STOP)	56	TCTTTTGGAGATAATAACTAATATC
FNEAP3	F	binds first 20bp of AtNEAP3	48	ATGCCAACTTCTGTTAGTCT
RNEAP3	R	binds last 19bp of AtNEAP3 (minus STOP)	47	ACGCCTAGAAAACGCAACT
FN3dCC1a	F	binds bp 280 to 299 of NEAP3, CC1 ends at 279	47	TTTGTGAAGGAATTGGCTG
FN3dCC1b	F	same as FN3dCC1a but adds beginning of NEAP3 as overhang	47	ATGCCAACTTCTGTTAGTCTAAGAGAGGATGATCCT-TTTGTGAAGGAATTGGCTG
RN3dCC2a	R	binds bp 351 to 369 of NEAP3, CC2 starts at 370	49	ATGTGCTGATTCAGCTGAC
RN3dCC2b	R	same as RN3dCC2a, but adds region after CC2 as overhang	49	GGTCTTGACCACTGATAC-ATGTGCTGATTCAGCTGAC
FN3dCC2a	F	binds bp 556 to 574 of NEAP3, CC2 ends at 555	48	GTATCAGTGGTCAAGACC
FN3dCC2b	F	same as FN3dCC2a, but adds region before CC2 as overhang	48	GTCAGCTGAATCAGCACAT-GTATCAGTGGTCAAGACC
RN3dNLSa	R	binds bp 701 to 718, NLS starts at 719	49	AAACCTCCAGTGAGCCG
RN3dNLSb	R	same as RN3dNLSa, but adds region after NLS as overhang	49	CTTGTATTGCCACATCGTT-AAACCTCCAGTGAGCCG
FN3dNLSa	F	binds bp 856 to 875 of NEAP3, NLS ends at 855	47	AACGATGTGGCAATACAAG
FN3dNLSb	F	same as FN3dNLSa, but adds region before NLS as overhang	47	CGGCTCACTGGAGGTTT-AACGATGTGGCAATACAAG
RN3dTMa	R	binds bp 913 to 933 of NEAP3, TM domain starts at 934	50	TTGGTTGCTAGAATGATCAGC
RN3dTMb	R	same as RN3dTMa, but adds last 12 bp after TM as overhang	50	ACGCCTAGAAAA-TTGGTTGCTAGAATGATCAGC
GWRN3dTM	R	GW primer binds end of delTM sequence cloned using RN3dTMa &b, addsattB2 sequence	50	GGGGACCACTTTGTACAAGAAAGCTGGGTC-ACGCCTAGAAAATTGGTTGC
FNEAP4	F	binds bp 1 - 18 of AtNEAP4	57	ATGTCGGCTCATTGGACG
RNEAP4	R	binds bp 316 - 336 of AtNEAP4	56	ATGATCAAGACTTGAACCACG
RNEAP4a	R	binds bp 308 - 329 of AtNEAP4	58	AGACTTGAACCACGTAATCCAC
attL1_FNEAP4	F	gateway primer, binds bp1 to 20 of AtNEAP4 with attB1 sequence	60	GGGGACAAGTTTGTACAAAAAAGCAGGCTTCCCGCCA-ATGTCGGCTCATTGGACGTT
RNEAP4_attL2	R	gateway primer, binds last 27 of AtNEAP4 with attB2 sequence	60	GGGGACCACTTTGTACAAGAAAGCTGGGTC-ATGATCAAGACTTGAACCACGTAATCC
FbZIP18	F	binds bp 1 to 21 of bZIP18	60	ATGGAGGATCCTTCTAACCCACA
RbZIP18	R	binds last 23 bp of bZIP18 (minus STOP)	57	AGTGCTGCTGCTTTCACTGAC
attL1_FbZIP	F	gateway primer, binds bp1 to 23 of AtbZIP18 with attB1 sequence	61	GGGGACAAGTTTGTACAAAAAAGCAGGCTTCCCGCCA-ATGGAGGATCCTTCTAACCCACA
RbZIP_attL2	R	gateway primer, binds last 20 bp of AtbZIP18 with attB2 sequence	61	GGGGACCACTTTGTACAAGAAAGCTGGGTC-CATAGTGCTGCTGCTTTCAC

Table S3 lists all fluorescent protein fusions constructed in this study

Construct	Gateway destination Vector	Bacterial resistance*
35S-YFP-NEAP2	pB7WGY2	spectinomycin
35S-NEAP2-CFP	pK7CWG2	spectinomycin
35S-CFP-NEAP2	pK7WGC2	spectinomycin
35S-YFP-NEAP3	pB7WGY2	spectinomycin
35S-NEAP3-CFP	pK7CWG2	spectinomycin
35S-CFP-NEAP3	pK7WGC2	spectinomycin
35S-NEAP3ΔCC1-CFP	pK7CWG2	spectinomycin
35S-NEAP3ΔCC2-CFP	pK7CWG2	spectinomycin
35S-NEAP3ΔNLS-CFP	pK7CWG2	spectinomycin
35S-NEAP3ΔTM-CFP	pK7CWG2	spectinomycin
35S-YFP-NEAP3ΔCC1	pCambia1300-casetteA	kanamycin
35S-YFP-NEAP3ΔCC2	pCambia1300-casetteA	kanamycin
35S-YFP-NEAP3ΔNLS	pCambia1300-casetteA	kanamycin
35S-YFP-NEAP3ΔTM	pCambia1300-casetteA	kanamycin
35S-SUN2ΔSUN-YFP	pCambia1300-casetteB	kanamycin
35S-SUN2ΔCC-YFP	pCambia1300-casetteB	kanamycin
35S-SUN2ΔN-YFP	pCambia1300-casetteB	kanamycin
35S-YFP-bZIP18	pCambia1300-casetteA	Kanamycin

Duc, C., Benoit, M., Détourné,, G. (2017) Arabidopsis ATRX Modulates H3.3 Occupancy and Fine-Tunes Gene Expression, *The Plant Cell* 29, 1773-1793
doi: 10.1105/tpc.16.00877

ABSTRACT

During evolution, eukaryotic cells have acquired a nuclear envelope (NE) enclosing and protecting the genome, which is organized in chromatin, a structure wrapping DNA around histone proteins. The NE is composed of two membranes: on the nucleoplasmic side, the Inner Nuclear Membrane (INM) and on the cytoplasmic side, the Outer Nuclear Membrane. The NE allows communication between both compartments through Nuclear Pore Complexes and bridges the cytoskeleton to the nucleoskeleton through the LInker of Nucleoskeleton to Cytoskeleton complex. Thus, the nucleoskeleton associated with the INM is needed to transmit signals to the nucleus and induce changes in chromatin organisation and ultimately gene expression.

A novel family of NUCLEAR ENVELOPE ASSOCIATED PROTEINS (NEAPs) proposed to be new components of the plant nucleoskeleton has been recently evidenced in the model plant *Arabidopsis thaliana*. AtNEAP proteins are encoded by a small gene family composed of three genes and are targeted through a nuclear localisation signal to the nucleus where they are anchored at the INM through their C-terminal transmembrane domain. AtNEAPs also possess several long coiled-coil domains reminiscent of the lamin structure in animals. This thesis aimed at performing a functional analysis of AtNEAPs using T-DNA insertion and CRISPR/Cas9 mutant lines. The AtNEAP interactome was investigated by molecular approaches (Yeast Two Hybrid), which indicated AtNEAP interactions with each other to form homo or hetero-dimers; as well as *in vivo* localisation and co-localisation coupled to image analyses (apFRET, acceptor photobleaching Fluorescence Resonance Energy Transfer), which confirmed interactions with the transcription factor (TF) AtbZIP18. AtNEAP specific antibodies generated during this study were used to confirm expression *in vivo*. Altogether, results indicated that AtNEAPs are part of the nucleoskeleton, with a role in anchoring TFs at the INM to maintain nuclear morphology and chromatin organisation.